

# Oil & Natural Gas Technology

DOE Award No.: DE-FE0001243

## Topical Report

# RATES AND MECHANISMS OF OIL SHALE PYROLYSIS: A CHEMICAL STRUCTURE APPROACH

Submitted by:  
University of Utah  
Institute for Clean and Secure Energy  
155 South 1452 East, Room 380  
Salt Lake City, Utah 84112

Prepared for:  
United States Department of Energy  
National Energy Technology Laboratory

November 2014



Office of Fossil Energy

# **Rates and Mechanisms of Oil Shale Pyrolysis: A Chemical Structure Approach**

Topical Report

Reporting Period: October 1, 2010 through September 30, 2014

Principal Authors:

Thomas H. Fletcher  
Chemical Engineering Department  
Brigham Young University

Ronald J. Pugmire  
Chemical Engineering Department  
University of Utah

Contributing Authors:

U of U: Mark S. Solum, Charles L. Mayne, Anita M. Orendt

BYU: Ryan Gillis, Jacob Adams, Trent Hall, Drew Gillespie, Daniel Barfuss

University of Utah  
Institute for Clean and Secure Energy  
155 South 1452 East, Room 380  
Salt Lake City, Utah 84112

## **DISCLAIMER**

This report was prepared as an account of work sponsored by an agency of the United States Government. Neither the United States Government nor any agency thereof, nor any of their employees, makes any warranty, express or implied, or assumes any legal liability or responsibility for the accuracy, completeness, or usefulness of any information, apparatus, product, or process disclosed, or represents that its use would not infringe privately owned rights. Reference herein to any specific commercial product, process, or service by trade name, trademark, manufacturer, or otherwise does not necessarily constitute or imply its endorsement, recommendation, or favoring by the United States Government or any agency thereof. The views and opinions of authors expressed herein do not necessarily state or reflect those of the United States Government or any agency thereof.

## **ACKNOWLEDGEMENT**

This material is based upon work supported by the Department of Energy under Award Number DE-NT0001243.

## ABSTRACT

Three pristine Utah Green River oil shale samples were obtained and used for analysis by the combined research groups at the University of Utah and Brigham Young University. Oil shale samples were first demineralized and the separated kerogen and extracted bitumen samples were then studied by a host of techniques including high resolution liquid-state carbon-13 NMR, solid-state magic angle sample spinning  $^{13}\text{C}$  NMR, GC/MS, FTIR, and pyrolysis. Bitumen was extracted from the shale using methanol/dichloromethane and analyzed using high resolution  $^{13}\text{C}$  NMR liquid state spectroscopy, showing carbon aromaticities of 7 to 11%. The three parent shales and the demineralized kerogens were each analyzed with solid-state  $^{13}\text{C}$  NMR spectroscopy. Carbon aromaticity of the kerogen was 23-24%, with 10-12 aromatic carbons per cluster. Crushed samples of Green River oil shale and its kerogen extract were pyrolyzed at heating rates from 1 to 10 K/min at pressures of 1 and 40 bar and temperatures up to 1000°C. The transient pyrolysis data were fit with a first-order model and a Distributed Activation Energy Model (DAEM). The demineralized kerogen was pyrolyzed at 10 K/min in nitrogen at atmospheric pressure at temperatures up to 525°C, and the pyrolysis products (light gas, tar, and char) were analyzed using  $^{13}\text{C}$  NMR, GC/MS, and FTIR. Details of the kerogen pyrolysis have been modeled by a modified version of the chemical percolation devolatilization (CPD) model that has been widely used to model coal combustion/pyrolysis. This refined CPD model has been successful in predicting the char, tar, and gas yields of the three shale samples during pyrolysis. This set of experiments and associated modeling represents the most sophisticated and complete analysis available for a given set of oil shale samples.

## EXECUTIVE SUMMARY

In 2010 a research effort was initiated to obtain new structural data on carefully selected Green River oil shale deposits. While a great deal of chemical structure information was already available, much of the existing data came from narrowly selected samples and analytical techniques. It was recognized that both geological information and a diversity of analytical techniques on well characterized samples could bring new light to details of carefully selected representative samples of the Green River oil shale resources. To obtain these representative samples, the Institute for Clean and Secure Energy (ICSE) at the University of Utah and the Utah Geological Survey selected a site to drill a 1,000 foot, 4-inch core which was carefully taken and preserved. Three one foot-sections of this core from three different depths were then prepared for analysis by a wide range of chemical analytical techniques. The analytical work was carried out at ICSE and at the Department of Chemical Engineering at Brigham Young University. The analytical samples were first demineralized and the separated kerogen and extracted bitumen samples were then studied by a host of techniques including high resolution carbon-13 nuclear magnetic resonance ( $^{13}\text{C}$  NMR) spectroscopy, magic angle sample spinning  $^{13}\text{C}$  NMR, gas chromatography/mass spectrometry (GC/MS), Fourier transform infrared spectroscopy (FTIR), and pyrolysis.

Bitumen was extracted from the shale using methanol/dichloromethane. Kerogen was isolated from the shale using a nine-step extraction procedure employing hydrochloric and hydrofluoric acids. Bitumen samples from the three cores were analyzed using high resolution  $^{13}\text{C}$  NMR liquid state spectroscopy, showing carbon aromaticities of 7 to 11%. Aliphatic carbons were dominated by methylene structures, with average aliphatic chain lengths of 24 carbons.

The three parent shales and the demineralized kerogens were each analyzed with solid-state  $^{13}\text{C}$  NMR spectroscopy. The solid-state  $^{13}\text{C}$  NMR data contain new information on 14 structural and 8 lattice parameters that describe the skeletal structures of the shale, the unreacted kerogen, and the pyrolysis chars. This type of data has not been previously available. Analysis of the carbon structure in the shale was hindered by the large amount of carbonates present, but the organic structure of the shale was shown to be almost identical to the structure of the demineralized kerogen. Carbon aromaticity of the kerogen was 23-24%, with 10-12 aromatic carbons per cluster and estimated molecular weights of 776 to 946, side chain molecular weights of 131 to 148, and side chain lengths of 11-13 carbons.

Crushed samples of Green River oil shale and its kerogen extract were pyrolyzed at heating rates from 1 to 10 K/min at pressures of 1 and 40 bar and temperatures up to 1000°C. Two to four mass release peaks were observed, with the two major peaks corresponding to kerogen pyrolysis and carbonate decomposition. The transient pyrolysis data were fit with a first-order model and a Distributed Activation Energy Model (DAEM).

The demineralized kerogen was pyrolyzed at 10 K/min in nitrogen at atmospheric pressure at temperatures up to 525°C. The pyrolysis products (light gas, tar, and char) were analyzed using <sup>13</sup>C NMR, GC/MS, and FTIR. Pyrolysis yields of 80% on a dry, ash-free (daf) basis were achieved at these conditions, with 60% daf tar yield at the highest temperature. The solid-state NMR results indicate that the aromaticity of the kerogen char increased from 20% (before reaction) to 80% during pyrolysis with a corresponding decrease in the average aliphatic carbon chain length from 12 to less than 1. The average number of aromatic carbons per cluster increased from 12 to 20 in a narrow temperature window between 425° and 525°C with an increase in the number of attachments per cluster from 6 to 8 in that same temperature window. Liquid-state NMR results of the condensed tars showed predominance of n-alkyl chains with similar carbon aromaticities at each temperature. The alkyl chains were also observed in the GC/MS data. The light gases determined by FTIR were primarily methane, carbon monoxide, and carbon dioxide. The combination of gas, tar, and char yields and chemical structure analyses are valuable for modeling of oil shale processes based on chemical structure rather than empiricism.

Details of the kerogen pyrolysis have been modeled by a modified version of the chemical percolation model (CPD) that has been widely used to model coal pyrolysis. This refined CPD model has been successful in predicting the char, tar, and gas yields of the three shale samples during pyrolysis.

## TABLE OF CONTENTS

	Page
Acknowledgement .....	ii
Abstract .....	iii
Executive Summary .....	iv
List of Figures .....	viii
List of Tables .....	x
Chapters	
1. Introduction .....	1
2. Characterization of Bitumen and Kerogen .....	2
Background .....	2
Sample Characterization .....	3
<sup>13</sup> C NMR Analysis of Bitumen Samples .....	8
Quantitative High Resolution Carbon-13 data .....	9
DEPT .....	9
NMR analysis of GR1, GR2, and GR3, bitumens. ....	9
Solid State NMR Techniques on Shale and Kerogen .....	15
Measurement of <sup>13</sup> C solid state NMR: .....	15
Solid State NMR Spectra of Shales and Kerogen Samples .....	15
Conclusions .....	25
References .....	25
3. Thermogravimetric Analysis .....	29
Modeling of Data .....	30
Comparision of Oil Shale Pyrolysis Models .....	32
References .....	33
4. Products of Kerogen Pyrolysis .....	34
Background .....	34
Experiment Descriptions .....	35
Kerogen Retort .....	35
Elemental Analysis .....	37
<sup>13</sup> C NMR Analysis .....	37
GC/MS Analysis .....	38
FTIR Analysis .....	39
Results .....	39
Kerogen Retort Data .....	39
NMR Analysis of Char from Kerogen Retort .....	42
Solution-state <sup>13</sup> C NMR Analysis of Tars from the Kerogen Retort .....	49
GC/MS Analysis .....	56
FTIR Analysis of Light Gases .....	57
Discussion .....	60
Summary and Conclusion .....	61
References .....	62
5. Modeling Kerogen Pyrolysis with the CPD Model .....	64
Conclusion .....	70
References .....	70
6. Analysis of Changes in Char Aromaticity .....	72

References.....	75
7. Summary and Conclusions.....	76
Recommendations.....	77
Publications and Presentations.....	77

## LIST OF FIGURES

	Page
<b>Chapter 2</b>	
Figure 2-1. Outline of demineralization procedure to separate kerogen and bitumen from oil shale.....	6
Figure 2-2. SEM/EDAX analysis of ash from demineralized kerogen samples of (a, top) GR2.9 and (b, bottom) GR3.9.....	7
Figure 2-3. QuantC spectrum of GR2 bitumen dissolved in CD <sub>2</sub> Cl <sub>2</sub> showing the aliphatic (91.05) to aromatic carbon (8.95) ratio. ....	10
Figure 2-4. Expanded aliphatic region (with height cropped for the peak at 30.1 ppm) of the quantC spectrum of GR2 bitumen dissolved in CD <sub>2</sub> Cl <sub>2</sub> . ....	12
Figure 2-5. Aliphatic region of the DEPT spectrum of GR2 bitumen dissolved in CD <sub>2</sub> Cl <sub>2</sub> . ....	13
Figure 2-6. Aromatic region of the DEPT spectrum of the GR2 bitumen dissolved CD <sub>2</sub> Cl <sub>2</sub> .....	14
Figure 2-7. Definition and source of information for determining 14 structural and 8 lattice parameters used to define critical structural components of carbonaceous materials including oil shale kerogens.....	16
Figure 2-8. Single pulse experiments on the three shale samples.....	19
Figure 2-9. CPMAS spectra of the three shales.....	20
Figure 2-10. SPMAS spectrum of the three kerogen concentrates.....	21
Figure 2-11. CPMAS spectra of the three kerogen concentrates.....	22
Figure 2-12. Dipolar dephasing ( $\tau=42$ ms) spectra of the kerogen concentrates.....	24
<b>Chapter 3</b>	
Figure 3-1. GR1 raw sample at 10 K/min and 1 atm.....	29
Figure 3-2. Method to correct for buoyancy.....	30
Figure 3-3. TGA pyrolysis data and best-fit model calculations for GR1 oil shale crushed and sieved to 60 $\mu$ m mass mean diameter, heated at 5 K/min. ....	31
Figure 3-4. Comparison of BYU vs. U. of Utah pyrolysis data from the GR2 sample at atmospheric pressure, heating rates of 1, 5, and 10 K/min.....	33
<b>Chapter 4</b>	
Figure 4-1. Schematic of the kerogen retort used for generating chars and tars. ....	36
Figure 4-2. Yields of char, tar, and light gas from pyrolysis of (a) GR1, (b) GR2, and (c) GR3 in the kerogen retort in N <sub>2</sub> at a heating rate of 10 K/min.....	41
Figure 4-3. CPMAS spectra of the GR3.9 kerogen concentrate and chars made from the concentrate.....	46
Figure 4-4. CPMAS dipolar dephased spectra of the GR3.9 kerogen concentrate and chars made from the concentrate. ....	47
Figure 4-5. Aromatic and aliphatic carbon fractions for the kerogen chars formed at 10°C/min in the kerogen retort.....	48
Figure 4-6. Aromatic carbons per cluster (C), attachments per cluster ( $\sigma+1$ ), and estimated carbons per side chain in kerogen chars.....	49
Figure 4-7. <sup>13</sup> C spectra of tar from GR2 kerogen pyrolyzed at 445°C dissolved in CD <sub>2</sub> Cl <sub>2</sub> . (A) quantC and (B) quantD experiments.....	50
Figure 4-8. Aliphatic region of the DEPT spectrum of GR2.9 tar dissolved in CD <sub>2</sub> Cl <sub>2</sub> . ....	52

Figure 4-9. QuantD spectra of GR3 kerogen pyrolysis tars pyrolyzed at various maximum temperatures. ....	54
Figure 4-10. Aromatic region of the DEPT spectrum of tar from GR2 kerogen pyrolyzed at 445°C. ....	55
Figure 4-11. Gas chromatogram of components of GR 3.9 tar collected at various temperatures during pyrolysis (10°C/min). ....	56
Figure 4-12. FTIR spectra of light gas collected from pyrolysis of the GR1.9 kerogen sample in the kerogen retort at the listed temperatures. ....	58
Figure 4-13. Composition of light gases evolved over different temperatures ranges from (a) GR1.9 kerogen and (b) GR3.9 kerogen determined by quantitative FTIR analysis. ....	59

## Chapter 5

Figure 5-1. Bridge-breaking scheme used in the CPD model. ....	65
Figure 5-2. Intial CPD predictions of tar and char yields for GR3.9 kerogen pyrolysis at 10 K/min. ....	66
Figure 5-3. CPD model calculations of tar and char yields for kerogen pyrolysis at 10 K/min using rate coefficients from Table 5-2 and counting 80% of the “light gas” as tar. ....	67
Figure 5-4. CPD model calculations of tar and char yields for kerogen pyrolysis at 10 K/min using rate coefficients from Table 5-3 and assigning $g_2$ as the “light gas” and $g_1$ as the condensable “heavy gas”. ....	70

## Chapter 6

Figure 6-1. Two possible path ways to increase the aromaticity of the shale oil char. ....	73
Figure 6-2. Carbon and hydrogen contents of the chars from the kerogen retort collected at different temperatures. The heating rate was 10 K/min for these experiments. ....	74
Figure 6-3. Hydrogen to carbon ratios of the chars from the kerogen retort collected at different temperatures. The heating rate was 10 K/min for these experiments. ....	75

## LIST OF TABLES

	Page
<b>Chapter 2</b>	
Table 2-1. Definitions of the Structural and Lattice Parameters from the Standard 1-D Analysis Procedure.....	4
Table 2-2. Moisture and Ash Analyses of the GR1, GR2, and GR3 Samples.....	5
Table 2-3. SEM/EDAX Analysis of the Residual Matter in the Demineralized Kerogen Samples. ....	8
Table 2-4. Ultimate Analysis of GR1, GR2, and GR3 Samples by Huffman Laboratories. ....	8
Table 2-5. Green River Shales and Their Kerogens from Three Cores.....	17
<b>Chapter 3</b>	
Table 3-1. Experimental Conditions for Each of the 3 Samples.....	29
Table 3-2. Kinetic Coefficients Determined from TGA Pyrolysis of GR Oil Shale Samples. ....	31
<b>Chapter 4</b>	
Table 4-1. Elemental Analysis of the Chars from the Kerogen Retort.....	37
Table 4-2. Yields of Char, Tar, and Light Gas from the Kerogen Retort.....	40
Table 4-3. Carbon Structural Parameters Determined from <sup>13</sup> C NMR Spectroscopy for Demineralized Kerogen (GR1.9) and Resulting Chars Collected at Different Temperatures.....	43
Table 4-4. Carbon Structural Parameters Determined from <sup>13</sup> C NMR Spectroscopy for Demineralized Kerogen (GR2.9) and Resulting Chars Collected at Different Temperatures.....	44
Table 4-5. Carbon Structural Parameters Determined from <sup>13</sup> C NMR Spectroscopy for Demineralized Kerogen (GR3.9) and Resulting Chars Collected at Different Temperatures.....	45
Table 4-6. Explanation of Peak Labels in Figures 4-8 and 4-9. ....	53
Table 4-7. Selected Identified Peaks from Gas Chromatography Data in Figure 4-11.....	57
<b>Chapter 5</b>	
Table 5-1. Chemical Structure Parameters Measured for the GR1.9, GR2.9, and GR3.9 Kerogen Samples.....	64
Table 5-2. Rate Coefficients Determined for a First-Order DAEM Model for the GR1, GR2, and GR3 Oil Shale Samples from TGA Data at Three Heating Rates.....	65
Table 5-3. Rate Coefficients Determined for Bridge Breaking in the CPD Model for the GR1.9, GR2.9, and GR3.9 Kerogen Samples to Fit the Kerogen Retort Data of Fletcher et al. ....	69
<b>Chapter 6</b>	
Table 6-1. Elemental Compositions of Shale Oil and Pyrolysis Products.....	72
Table 6-2. Final Yields of the Pyrolysis of Shale Oil.....	72

## CHAPTER 1.INTRODUCTION

---

There is renewed interest in unconventional fuel resources whenever oil prices climb. Unconventional oil resources are defined as extra heavy oils and bitumens associated with oil sand deposits and as kerogen associated with oil shale resources. Most of the world's known oil sand and oil shale deposits are in North America, and the combined potential from these resources far exceeds the world's known conventional oil reserves. The most significant oil shale deposits are in the Green River Formation of Colorado, Utah, and Wyoming, with an estimated resource size as high as 4.3 trillion barrels.<sup>1</sup> These oil shale resources will be used primarily for producing transportation fuels. In a carbon-constrained world, transportation fuel production from these resources will require an understanding of processes that occur over a wide range of length and time scales from the structure of kerogen and how it binds to an inorganic matrix to the fluid flow resulting from in-situ processing of an oil shale interval that covers hundreds of acres. In this regard, parameters which are important for the analysis of the in-situ pyrolysis processing of oil shale include:

1. Kerogen conversion to oil, gas and coke
2. Nature of the pore space before and after pyrolysis
3. Porous media characteristics after pyrolysis
4. Permeabilities, and
5. Relative permeabilities.

In this report, we describe approaches to address the very challenging characterization problems of item one. In addition to the standard approach of empirical fitting of mass release data from pyrolysis experiments, we have characterized the chemical structure of the kerogen and related the chemical structure to the pyrolysis behavior. The chemical structure of the parent kerogen and the subsequent pyrolysis products (termed gas, tar, and char) are analyzed by Fourier transform infrared spectroscopy (FTIR), gas chromatography/ mass spectrometry (GC/MS), and nuclear magnetic resonance spectroscopy (NMR).

The main parts of this report have appeared in the two publications listed below. We anticipate one more publication regarding the chemical structure-based modeling of kerogen pyrolysis based on Chapters 5 and 6.

1. Solum, M. S., C. L. Mayne, A. M. Orendt, R. J. Pugmire, J. Adams, T. H. Fletcher, "Characterization of Macromolecular Structure Elements from a Green River Oil Shale, I. Extracts," *Energy and Fuels*, **28**, 453-465 (2014). [dx.doi.org/10.1021/ef401918u](https://doi.org/10.1021/ef401918u)
2. Fletcher, T. H., R. Gillis, J. Adams, T. Hall, C. L. Mayne, M. S. Solum, and R. J. Pugmire, "Characterization of Macromolecular Structure Elements from a Green River Oil Shale, II. Characterization of Pyrolysis Products by <sup>13</sup>C NMR, GC/MS, and FTIR," *Energy & Fuels*, **28**, 2959–2970 (2014). [dx.doi.org/10.1021/ef500095j](https://doi.org/10.1021/ef500095j)

### References

1. Oil Shale: Energy to Fuel Our Future, 2013 Update, National Oil Shale Association, pp. 1-24 (2013).

## CHAPTER 2. CHARACTERIZATION OF BITUMEN AND KEROGEN

---

### Background

Oil shales are fine-grained sedimentary rocks that contain organic matter which, upon heating, can be converted to liquid shale oil. The shale oil can then be refined into a slate of products that are similar to those obtained from refining of petroleum crude oil. There are two fractions of organic matter in oil shale: (i) bitumen, which is the fraction that is soluble in organic solvents, and (ii) kerogen, which constitutes approximately 90% of the organic matter and is insoluble in common organic solvents.<sup>1</sup> Source rock in the Green River formation, one of the most extensive oil shale reserves in the world, contain hydrogen-rich algal kerogen (type I) with up to ~20 weight percent (wt%) organic matter in the form of amorphous kerogen solid integrated in a silicate- and carbonate-based mineral matrix.<sup>2</sup> The Green River oil shale formation spans parts of eastern Utah, southern Wyoming, and western Colorado. It contains approximately 60 % of the known world reserves of oil shale, with estimates as high as 4.3 trillion barrels of oil equivalent.<sup>3-5</sup>

Vandenbroucke has provided a general description of the major oil shale deposits found world-wide, including the Green River formation from the Uinta Basin in Utah. “The Green River shale is an organic-rich formation that was deposited in two Paleocene/Eocene alkaline palaeolakes, Lake Gosiute in Wyoming, and Lake Uinta in Utah and Colorado...” The highly paraffinic nature of oils and extracts created problems “because C<sub>25+</sub> hydrocarbons reprecipitated during compound separation with usual solvents.”<sup>6</sup>

The work of Siskin et al.<sup>7</sup> in development of a two-dimensional model of the Green River Oil Shale (GROS) structure has been a major step forward in understanding the chemical structure of GROS. Orendt et al.<sup>8</sup>, using a combination of ab initio and molecular mechanics calculations, have more recently developed three-dimensional (3D) structural models of the Green River kerogen based on the two-dimensional (2D) structure proposed by Siskin.

Solution state proton (<sup>1</sup>H)-NMR has been used to characterize oil shale extracts since the early 1960's. As carbon-13 (<sup>13</sup>C) NMR became routine in the 1970's, NMR has become a mainstay of research in this area. Netzel et al.<sup>9</sup> provided an extensive study of shale oil distillates. Burnham et al.<sup>10-12</sup> have published a number of studies elucidating the extraction of shale oil from various oil bearing shale formations. Using model compounds, Dalling et al.<sup>13</sup> showed how assignments can be made in these complex mixtures even when multiple chiral centers complicate the spectra.

Likewise, solid-state NMR spectroscopy has been widely used to characterize oil shale related materials. Early experiments combining cross-polarization (CP) with magic angle spinning (MAS) provided a technique that gave higher sensitivity and greater resolution than static samples provided. This combined technique of CP/MAS has been used to study the structural characteristics of many types of carbonaceous materials including oil shale and kerogen concentrates derived from many oil shales, including samples from the Green River formation. Bartuska et al.<sup>14</sup> presented static CP spectra of a shale and kerogen and demonstrated the improvement in resolution upon spinning over that from static (CP) spectra. Resing et al.<sup>15</sup> used CP/MAS to determine the aromaticity of a Green River shale and kerogen, but the kerogen appeared to be derived from a different shale sample source. Maciel et al.<sup>16</sup> studied the correlation between the aliphatic resonances and oil yields in various shales and kerogen concentrates, including Green River samples. Miknis et al.<sup>17</sup> provided CP/MAS spectra of ten shale samples (including the Green River shale). They also analyzed several sets of shales and

pyrolyzed shales (chars) using the CP/MAS technique, thus determining oil yields and aromaticities.<sup>18</sup> Maciel et al.<sup>2</sup> used CP/MAS to study the aromatic structures of six shales and their kerogen concentrates including the Green River formation. They analyzed the spectra in terms of integrals of various carbon-13 chemical shift ranges corresponding to various functional groups and pointed out that great care must be taken in the phasing of the spectra. Hagan et al.<sup>19</sup> studied Green River shales from the Mahogany zone at different depths and related the integrals of the aliphatic carbon chemical shift range using an internal standard to the likely oil yield. Petsch et al.<sup>20</sup> studied weathered kerogens, including a Green River sample, and found that polymethylenic, highly aliphatic kerogens were not altered, but aromatic and branched aliphatic kerogens were. Recently, Salmon et al.<sup>21</sup> used liquid state NMR to study extracts from a Green River kerogen using various solvents and high resolution MAS on a deuterated dimethyl sulfoxide (DMSO-d<sub>6</sub>) swollen kerogen sample. These data displayed liquid-like resolution in 2D H-C chemical shift correlation spectra of the swollen solid.

Solum et al.<sup>22</sup> were successful in differentiating the basic structural features of all eight coals available from the Argonne Premium Coal Sample Bank and were able to define 14 parameters that are useful in defining macromolecular structures as well as 8 other lattice parameters that are applicable to fossil fuels. These NMR parameters can be used in conjunction with the elemental compositions to determine several other chemical structure parameters such as the number of aromatic carbons per cluster and the molecular weight of clusters and side chains. The procedure followed in obtaining the functional group components as well as the lattice parameters found wide application not only in coal structures<sup>22, 23</sup> but also in modeling devolatilization of coal structures<sup>24-27</sup> char structure<sup>28, 29</sup>, soot formation<sup>30-33</sup>, and combustion deposits.<sup>34, 35</sup> The definitions of these functional groups and lattice parameters are found in the appendix of Jiang et al.<sup>30</sup> as well as in Table 2-1. This technique was previously applied to a demineralized Green River oil shale from Colorado, as well as to the solid residue from pyrolysis of that demineralized kerogen.<sup>36, 37</sup> All of these studies exploit the power of solid and solution state NMR combined with GC/MS for increased understanding of oil shale as an important potential energy source.

This chapter presents data on the macromolecular structure of the parent shale, demineralized kerogen, and bitumen from three sections of a core, Skyline 16, drilled in eastern Utah's Uinta Basin. The NMR analysis presented here is the most advanced technique available for analyzing macromolecular structure. For the first time, lattice parameters have been calculated for the demineralized kerogen, providing further insight into the macromolecular structure.

## **Sample Characterization**

Oil shale samples were taken from a 1000-foot long, 4-inch diameter core at the Uinta Skyline 16 location, as provided by the Utah Geological Survey (UGS) and the University of Utah's Institute for Clean and Secure Energy (ICSE). Three one-foot segments of this core were studied and are identified as: GR1 (462-463 feet), GR2 (486-487 feet), and GR3 (548-549 feet). Samples were powdered with a Reutsch automated agate mortar and pestle in air until the resulting powder passed through a 100 mesh (149 microns) screen. Sized particles were stored under dry nitrogen (N<sub>2</sub>) until used.

**Table 2-1. Definitions of the Structural and Lattice Parameters from the Standard 1-D Analysis Procedure.**

**Structural Parameters**

- $f_a$  = The fraction of carbon atoms that are  $sp^2$  hybridized (aromaticity).  
 $f_a^C$  = The fraction of carbon atoms that are in carboxyl or carbonyl groups.  
 $f_a^O$  = The fraction of carbon atoms that are in a carbonyl group (aldehydes and ketones).  
 $f_a^{OO}$  = The fraction of carbon atoms that are in a carboxyl group (acids, esters, amides).  
 $f_{a'}$  = The fraction of carbon atoms that are  $sp^2$  hybridized excluding  $f_a^C$  (corrected aromaticity).  
 $f_a^H$  = The fraction of carbon atoms that are protonated aromatics.  
 $f_a^N$  = The fraction of carbon atoms that are non-protonated aromatics.  
 $f_a^P$  = The fraction of carbon atoms that are aromatic with an oxygen atom attached.  
 $f_a^S$  = The fraction of carbon atoms that are aromatic with a carbon chain attached (also includes bi-aryl carbons).  
 $f_a^B$  = The fraction of carbon atoms that are aromatic and a bridgehead carbon.  
 $f_{al}$  = The fraction of carbon atoms that are  $sp^3$  hybridized (aliphatic).  
 $f_{al}^H$  = The fraction of carbon atoms that are aliphatic but not methyls.  
 $f_{al}^*$  = The fraction of carbons that are aliphatic and methyls.  
 $f_{al}^O$  = The fraction of carbon atoms that are aliphatic and attached to an oxygen atom.

**Lattice Parameters.**

- $\chi_b$  = The mole fraction of bridgehead carbon atoms.  
 $C$  = The average aromatic cluster size.  
 $\sigma+1$  = The average number of attachments on an aromatic cluster.  
 $P_0$  = The fraction of attachments that don't end in a side chain (methyl group).  
B.L.= The average number of attachments on an aromatic cluster that are bridges or loops (a loop is a bridge back to the same cluster).  
S.C.= The average number of side chains on an aromatic cluster.  
MW = The average molecular weight of an aromatic cluster including side-chains and bridges.  
 $M_\delta$  = The average mass of a side-chain or one-half of a bridge.

Moisture and ash analyses of the powdered oil shale samples were performed at Brigham Young University (BYU) using American Society for Testing and Materials (ASTM) procedures, except that ashing was performed for ~80 hours at 505°C in air to prevent CO<sub>2</sub> release from the carbonates in the shale. The analysis was performed twice, and the average moisture, ash, and organic content of the oil shales are presented in Table 2-2. The GR1 shale was the richest in organic content (almost 26 wt%), followed by the GR3 (20.5 wt%), and then GR2 (~16 wt%). The moisture content of all samples was less than 0.5 wt%.

**Table 2-2. Moisture and Ash Analyses of the GR1, GR2, and GR3 Samples.**

Wt% of parent shale	GR1	GR2	GR3	Avg. Standard Deviation
<b>Moisture</b>	0.415	0.265	0.38	0.066
<b>Ash</b>	73.64	85.44	79.11	0.038
<b>Organic</b>	25.95	15.80	20.51	0.71
<b>Oil Yield (gal/ton)<sup>a</sup></b>	60	28	22	
<b>Wt% oil from shale<sup>b</sup></b>	23%	11%	8%	

<sup>a</sup>Results of Fischer oil assay reported by UGS

<sup>b</sup>Based on a specific gravity of 0.9 for the organic material

A portion of the shale core was demineralized at the University of Utah using procedures similar to those of Vandegraft et al.<sup>38</sup> except that 4:1 dichloromethane(DCM)/methanol was used instead of benzene for some of the extraction steps and additional washings with boric acid and hydrochloric acid were performed. The nine-step demineralization procedure is outlined in Figure 2-1. The three demineralized kerogen samples are referred to as GR1.9, GR2.9, and GR3.9. Ash tests were performed on the three kerogen samples to determine the residual mineral matter not removed by the procedure. The three demineralized kerogen samples (GR1.9, GR2.9, and GR3.9) had ash contents of 5.0%, 4.1%, and 4.7% respectively. Scanning Electron Spectroscopy/Energy-dispersive X-ray spectroscopy (SEM/EDAX) analysis was performed on the ash from the fully burned GR2.9 and GR3.9 demineralized kerogens. Figure 2-2 shows the spectra from this analysis, and Table 2-3 shows the quantitative ash analysis. As expected, the ash from both samples is high in iron and sulfur, as well as calcium. The iron peak was particularly high in the GR3.9 sample. It seems likely that pyrite was not eliminated from the sample during the demineralization process.

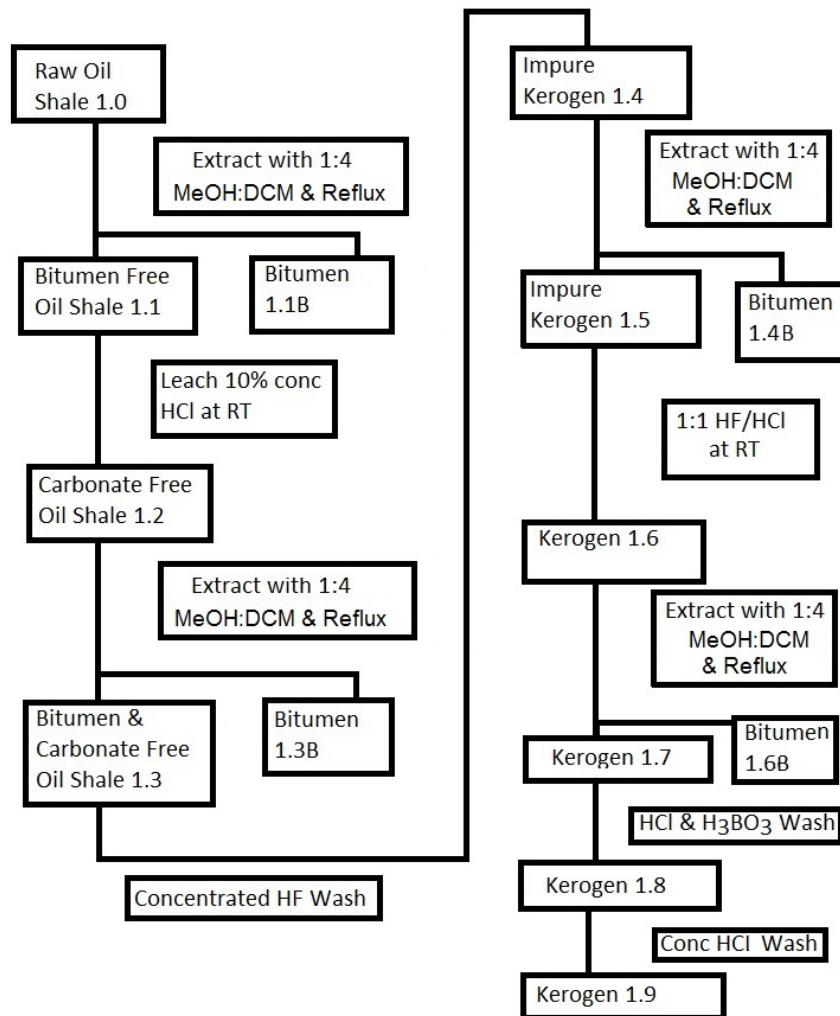


**Figure 2-1. Outline of demineralization procedure to separate kerogen and bitumen from oil shale.**

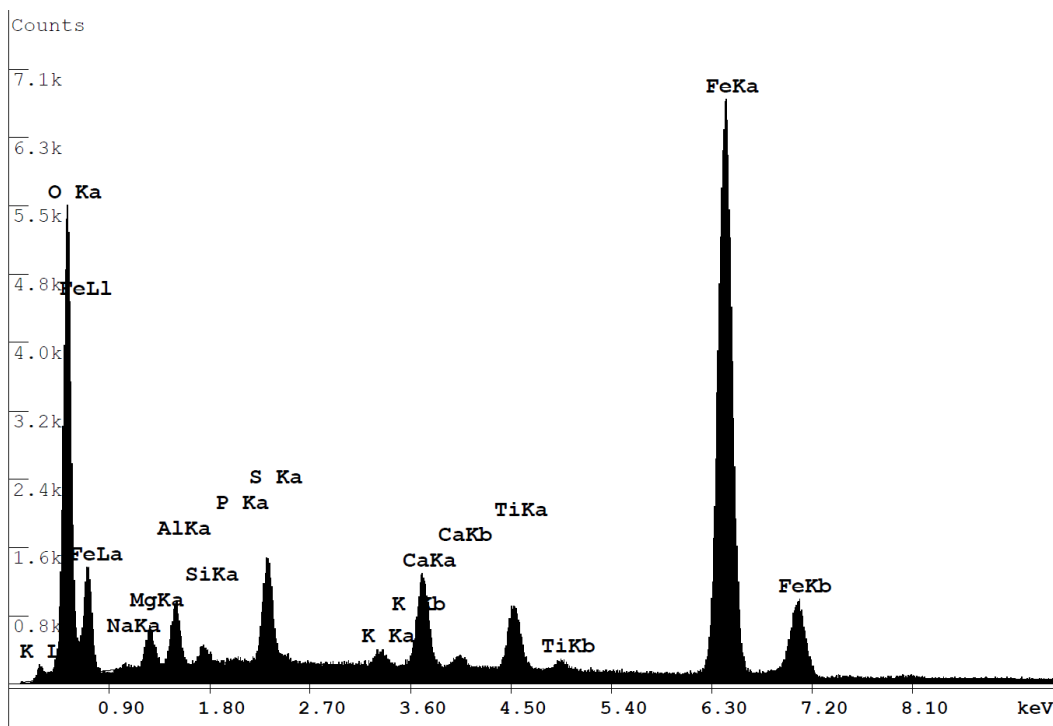
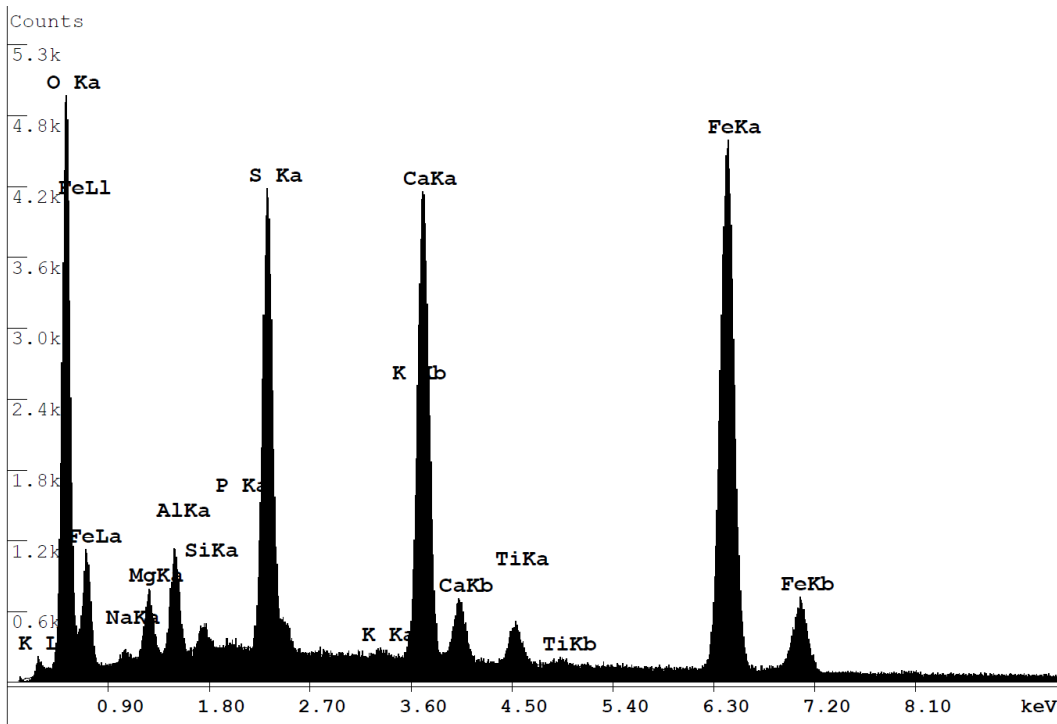


Figure 2-2. SEM/EDAX analysis of ash from demineralized kerogen samples of (top) GR2.9 and (bottom) GR3.9.

**Table 2-3. SEM/EDAX Analysis of the Residual Matter in the Demineralized Kerogen Samples.**

<b>Element</b>	<b>GR2.9 Wt%</b>	<b>GR3.9 Wt%</b>
O	31.5	26.0
Na	0.5	0.3
Mg	2.2	2.2
Al	2.7	2.6
Si	0.6	0.7
P	0.1	0.2
S	9.3	3.2
K	0.2	0.6
Ca	12.7	3.4
Ti	1.5	3.2
Fe	38.7	57.6
<b>Total</b>	<b>100.0</b>	<b>100.0</b>

The demineralized kerogen samples were also sent to Huffman Laboratories (4630 Indiana Street, Golden CO; [www.huffmanlabs.com](http://www.huffmanlabs.com)) for ultimate analysis (see Table 2-4). The ash analyses reported by Huffman laboratories were similar to those obtained at BYU. All three kerogen samples showed a carbon content of approximately 77 wt% on a dry, ash-free (daf) basis; hydrogen, nitrogen and oxygen contents are also similar. The GR3.9 sample had nearly twice the sulfur content as the other samples.

**Table 2-4. Ultimate Analysis of GR1, GR2, and GR3 Samples by Huffman Laboratories.**

	<b>GR1.9</b>	<b>GR2.9</b>	<b>GR3.9</b>
Moisture (Wt% as rec'd)	0.77	0.39	0.54
C (Wt% daf)	77.4	77.5	76.2
H	9.8	10.0	9.5
N	2.8	2.6	2.5
O (diff)	8.2	8.0	8.1
S	2.0	2.0	3.7
Ash (Wt% dry)	5.30	4.60	3.87

### **<sup>13</sup>C NMR Analysis of Bitumen Samples**

The bitumen samples obtained from the kerogen isolation procedure for GR1, GR2, and GR3 were prepared at 150 mg/mL in methylene chloride-d<sub>2</sub>; 0.7 mL of the solution was transferred to a 5 mm NMR tube with a screw cap and polytetrafluoroethylene (PTFE)-lined septum to prevent solvent loss during data acquisition. All high resolution NMR data were acquired using an Agilent Technologies Direct Drive 500 MHz spectrometer with a 5 mm

switchable broadband probe equipped with z-axis pulsed field gradient coil and sample temperature control. The sample temperature was controlled at 26°C using a stream of dry N<sub>2</sub> flowing at 10 L/min.

### ***Quantitative High Resolution Carbon-13 Data***

Two methods were used to acquire quantitative <sup>13</sup>C spectra. The first method (called quantC in what follows) used the classical gated decoupling method to obtain decoupled spectra with the nuclear Overhauser effect (NOE) suppressed. Typical acquisition parameters were: relaxation delay of 20 s, acquisition time of 2 s, 45 degree tip angle, 67,500 complex samples of the flame ionization detector (FID), and 22 hours total acquisition time. This method retains both protonated and non-protonated carbon resonances but sacrifices considerable sensitivity due to suppression of the NOE.

The second method (called quantD in what follows) used the Agilent-supplied QDEPT pulse sequence and quantdept macro.<sup>39</sup> The technique involves a double array of the width of the final proton read pulse and the evolution time delay. The sum of all the members of the array yields a quantitative carbon spectrum with non-protonated carbons suppressed, however, it retains the proton to carbon magnetization transfer enhancement inherent in the Distortionless Enhancement by Polarization Transfer (DEPT) technique.<sup>40</sup> Typical acquisition parameters were: relaxation delay of 10 s, acquisition time of 4 s, 125,000 complex samples of the FID, 22 hours total acquisition time. These spectra were integrated using the standard Agilent VNMRJ software integration tools.

### ***DEPT***

DEPT spectra were obtained using the standard Agilent QDEPT pulse sequence to differentiate among non-protonated CH, CH<sub>2</sub>, and CH<sub>3</sub> carbons. The QDEPT sequence incorporates shaped broadband inversion pulses to obtain more uniform inversion of the carbon magnetization across the entire carbon chemical shift range. This sequence also retains resonances from non-protonated carbons, in contrast to the classical DEPT technique that suppresses non-protonated carbon resonances.

### ***NMR Analysis of GR1, GR2, and GR3 Bitumens***

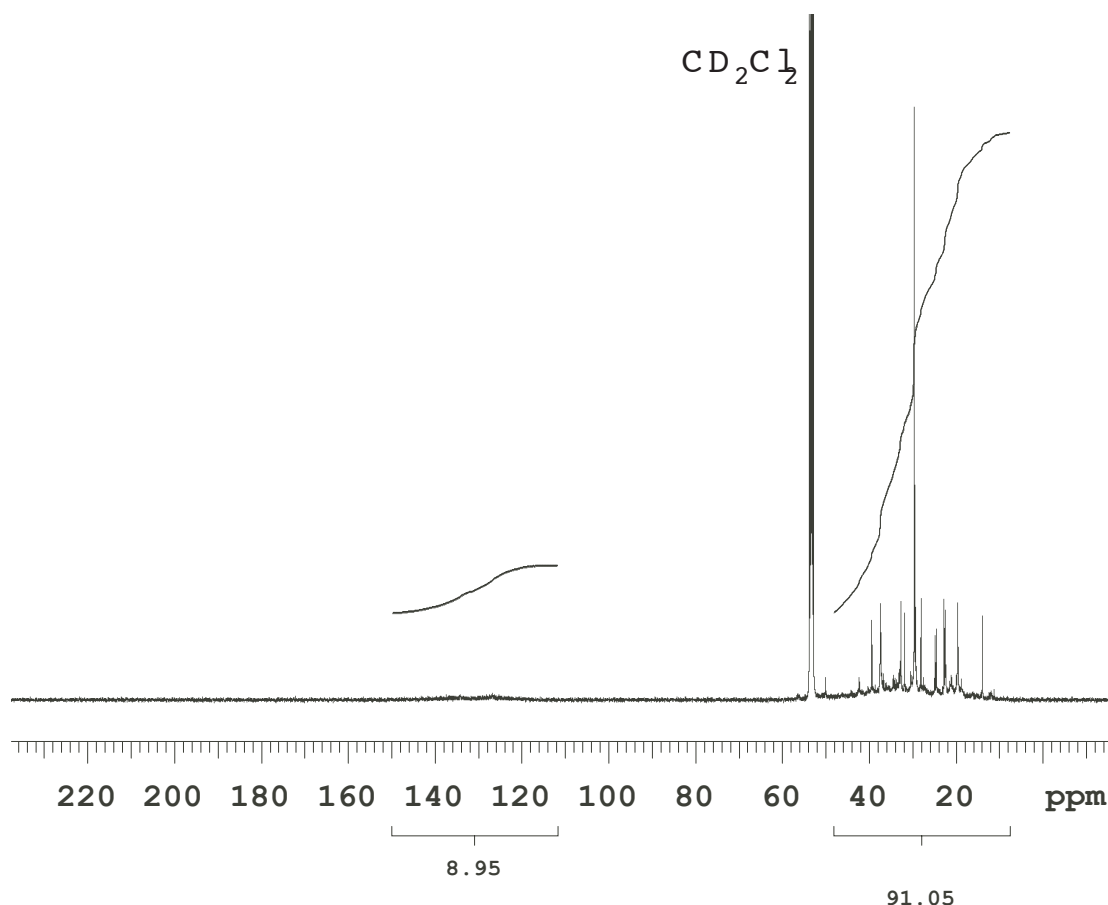
All three of the bitumen samples show essentially the same <sup>13</sup>C resonances with small differences in intensity, likely within experimental error, even though the GR1 and GR3 core segments were separated by 86 feet. These spectra are also substantially similar to spectra published previously on similar materials.<sup>9-13</sup> Assignment of the lower intensity resonances to the numerous minor components of the bitumen consists mainly of branched (i.e., isopranes) and, to a lesser extent, cyclic hydrocarbons.

Using the quantC method, the fraction of aromatic carbons measured 11.2%, 9.3%, and 7.4% for bitumen isolated from core segments GR1 through GR3, respectively. The signal-to-noise (S/N) in the aromatic region of the spectra is quite low, and these results should be interpreted to mean that the differences in aromatic content among the three bitumen samples is barely outside experimental error. However, the aromatic content of the bitumens is substantially lower than that of the corresponding kerogens (24%, 23% and 24%) from these shale samples.

Although the S/N in the aromatic region is low and the spectra are too complex to assign individual resonances to particular compounds, comparing the quantC (all aromatic carbons) and quantD (only protonated aromatic carbons) results, it is possible to separate protonated from non-protonated carbons in the aromatic region, even though the ranges of carbon chemical shifts

involved overlap for these two types of aromatic carbons. Since non-protonated carbons contribute a negligible amount to the integrals of the aliphatic region of the spectra, this integral represents the same number of carbons in either the quantC or quantD spectra and can be used to normalize the integrals of the aromatic region in each case. For the GR1, GR2, and GR3 bitumens, this treatment yields 30%, 46% and 47% of the aromatic carbons as protonated carbons, respectively. Again, the errors in these estimates are large due to low S/N ratios and should be interpreted to mean that a little less than half of the aromatic carbons are protonated in each of the three bitumen samples.

Since all three bitumen samples exhibit essentially the same results by NMR, the GR2 bitumen will be discussed in detail below as an example. Figure 2-3 shows a quantC spectrum with integrals. Aliphatic carbon dominates the sample with only 9% aromatic carbon.



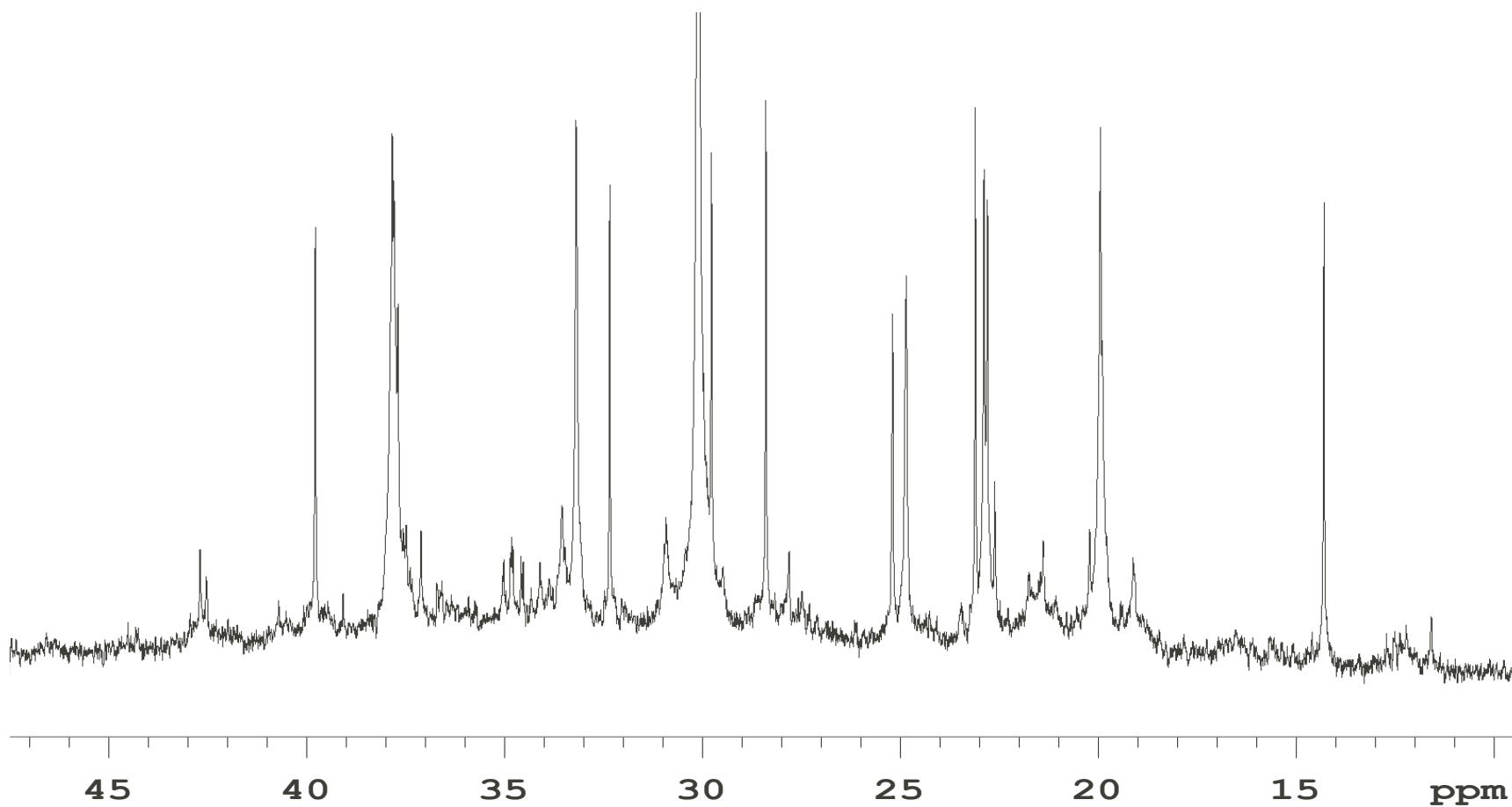
**Figure 2-3. QuantC spectrum of GR2 bitumen dissolved in CD<sub>2</sub>Cl<sub>2</sub> showing the aliphatic (91.05) to aromatic carbon (8.95) ratio.**

Figure 2-4 shows the aliphatic region of the spectrum from 10 to 45 parts per million (ppm) expanded. The intense resonance near 30.1 ppm arises from the carbons located at least five carbons from the methyl end of a normal hydrocarbon chain. The high intensity of this resonance shows that the GR2 bitumen contains a significant amount of long chain normal hydrocarbons. The corresponding methyl is located at 14.3 ppm with carbons 2, 3, and 4 located at 23.1, 32.3, and 29.8 ppm respectively. Note that the peaks for carbons 1-4 have similar

intensities and, in a long n-alkyl chain, each would represent two carbons (one from each end of the chain). Since the ratio of the intensity of the peak at 30.1 ppm to the average intensity of the first four peaks in the chain is about 8 (i.e., 16 carbons), one can assert that the average length of these normal chains is about 24 carbons. Of course, these n-alkyl chains can be attached to aromatic centers, cyclic alkyl groups,<sup>12</sup> or have alkyl side-chains at either or both ends of the chain. However, as long as the n-alkyl chain is C10 or longer, the resonances from the carbons far from the substituent will contribute to the resonance at 30.1 ppm, and this can produce a systematic error increasing the estimate of the chain length. However, the low abundance of these moieties would indicate that this error is small compared to other sources of error in the determination of peak areas.

The other spectral lines in Figure 2-4 indicate that the bitumen also contains branched alkanes that can be readily identified. If one carefully compares the chemical shifts of isoprenoid structures with the bitumen spectra it is possible to identify chiral centers in isoprenes in addition to the n-alkanes that are present, e.g., structures like pristane, phytane, farnesane, squalane, etc.<sup>9,13</sup> The structures of these isoprenes are superimposed on the spectrum and the appropriate structural lines are identified for 6 isoprenes. While these branched alkanes are not unique to this study, they represent candidate structural forms that are found in steranes/isoprenoids. The complexity of the spectrum contains much information that is just above the noise level; thus, it is not possible to estimate the relative abundance of n-alkanes from the highly branched components. We searched the chemical shift data for any indications of the presence of cyclic alkyl (as well as aromatic) components that could serve as terminal structures for the alkyl chains/cross links. We were not able to clearly identify any such components.

Figure 2-5 shows the expanded aliphatic region of a set of DEPT spectra showing separately the resonances of various carbons according to the number of attached protons. This spectrum adds additional evidence of the presence of isoprenoids due to the presence of peaks identified as CH and CH<sub>2</sub> groups. Note that the vertical scale has been adjusted so that the intense methylene resonance at 30.1 ppm is off-scale to permit closer examination of the other resonances. Due to various instrumental limitations, cancellation of one carbon type from the spectrum of another carbon type is not perfect. Note, for example, that the methyl resonance at 14.5 ppm appears at diminished intensity in the methylene spectrum. Although the DEPT spectrum is not strictly quantitative, some sense of the relative amounts of the various carbon types can be gleaned by comparing the various spectra. Clearly, methylenes are the dominant type, with methyls and methines at lower abundance. Since methines indicate a branch point in an aliphatic chain (i.e. an isoprenoid), it is evident that there are relatively few such branch points in this sample. The methyl resonances upfield from 14.5 ppm arise from the terminal methyl of chains where C3 is a methine. The spectrum representing quaternary carbons shows essentially no resonances; all the resonances seen in this particular linear combination of the raw data correspond to strong resonances of other types and have to be attributed to imperfect cancellation of these other types. Resonances from non-protonated carbons are diminished in intensity by about a factor of four relative to those of protonated carbons because non-protonated carbons receive no transfer of proton magnetization. Nevertheless, it is clear that there are very few aliphatic, non-protonated carbons in this sample.



**Figure 2-4. Expanded aliphatic region (with height cropped for the peak at 30.1 ppm) of the quantC spectrum of GR2 bitumen dissolved in deuterated dichloromethane ( $\text{CD}_2\text{Cl}_2$ ). Labels are suggested by Dalling et al.<sup>13</sup>**

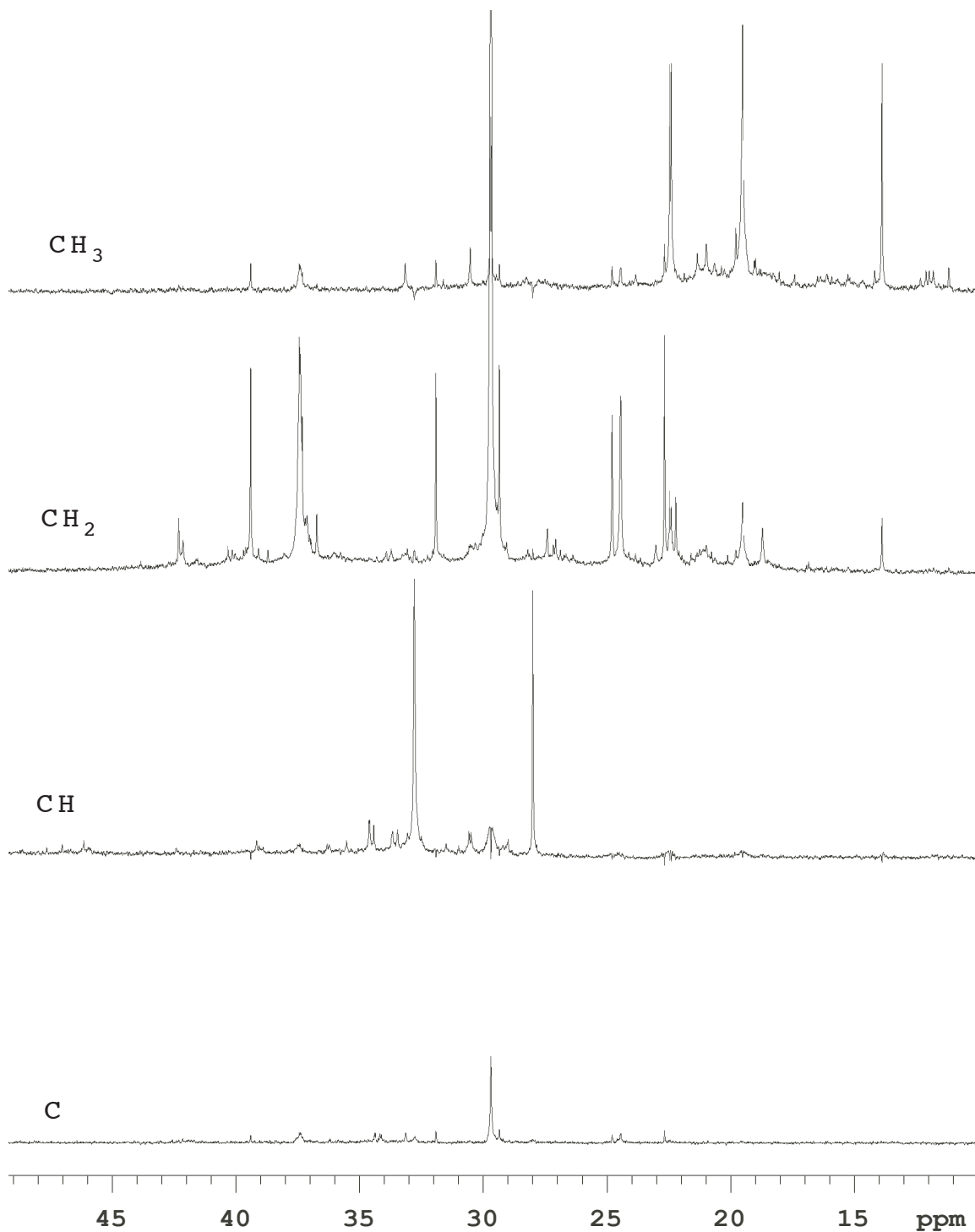


**Figure 2-5. Aliphatic region of the DEPT spectrum of GR2 bitumen dissolved in CD<sub>2</sub>C**  
Labels are the same as in Figure 2-4 (see Dalling et al.<sup>13</sup>).

Figure 2-6 shows the aromatic regions of the same DEPT spectrum as Figure 2-5. The spectra show resonances over a wide range of chemical shift for both substituted and non-substituted aromatics but with no dominant resonances. This indicates a wide variety of substituted aromatic molecules with differing substituents with no one molecular structure with relatively high abundance. Note that the CH<sub>2</sub> trace shows no resonances as would be the case if chains terminated by an alkene moiety were present. This has been observed previously<sup>9</sup> for solvent extraction of bitumens as opposed to pyrolysis extraction of organic matter from oil shale where considerable amounts of terminal alkenes were observed.<sup>36,37</sup>

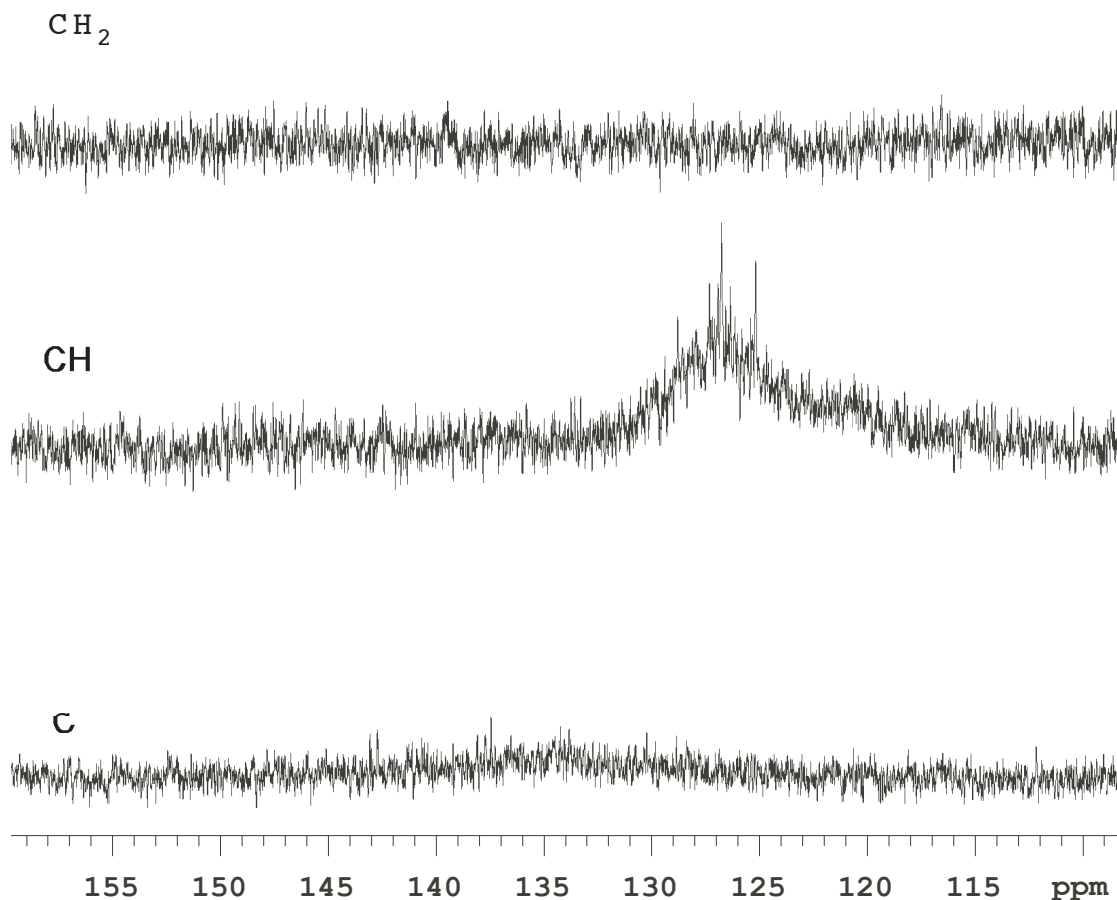


**Figure 2-6. Aromatic region of the DEPT spectrum of the GR2 bitumen dissolved CD<sub>2</sub>Cl<sub>2</sub>.**

## Solid-State NMR Techniques on Shale and Kerogen

### *<sup>13</sup>C Solid-state NMR Technique*

Solid-state <sup>13</sup>C NMR analysis was performed on each of the shales and the demineralized kerogen samples. All of these experiments were run on a Varian Direct Drive oversampled spectrometer operating at a carbon frequency of 25.1562 MHz and a proton frequency of 100.02 MHz. The spectrometer utilizes a 7.5 mm PENCIL rotor probe with a ceramic housing to remove carbon background. The experimental details consists of (1) a standard <sup>13</sup>C CP/MAS experiment with a 3 ms contact time ( $> 4.5x T_{df}$ )<sup>41</sup>, (2) a variable contact (vc) time experiment with 21 different contact times ranging from 5  $\mu$ s to 25 ms, (3) a dipolar dephasing (dd) experiment using a 3 ms contact time, and (4) a single pulse experiment. The details of these experimental protocols have been described by Solum and coworkers.<sup>22, 28, 29, 31</sup> Approximately 136 mg of kerogens and 428 mg of the shales were required for this analysis. The method of Solum et al.<sup>22, 31</sup> was used to take the measured fraction of bridgehead carbons and the elemental analysis to determine average structural parameters, including the number of attachments per aromatic cluster, the molecular weight per aromatic cluster, and the average molecular weight of a side chain. When applied to the unreacted kerogen samples, Solum's method for determining the fraction of attachments that are bridges (i.e.,  $P_0$ ) was subject to substantial errors due to the large number of CH<sub>2</sub> groups relative to methyl groups in the sample. The bleed through from this larger band may overestimate the aliphatic chain branching resulting in more methyl groups being counted than exist. Other methods based on three spin coherence may be able to give more information but were not possible with the current available equipment.<sup>42, 43</sup>

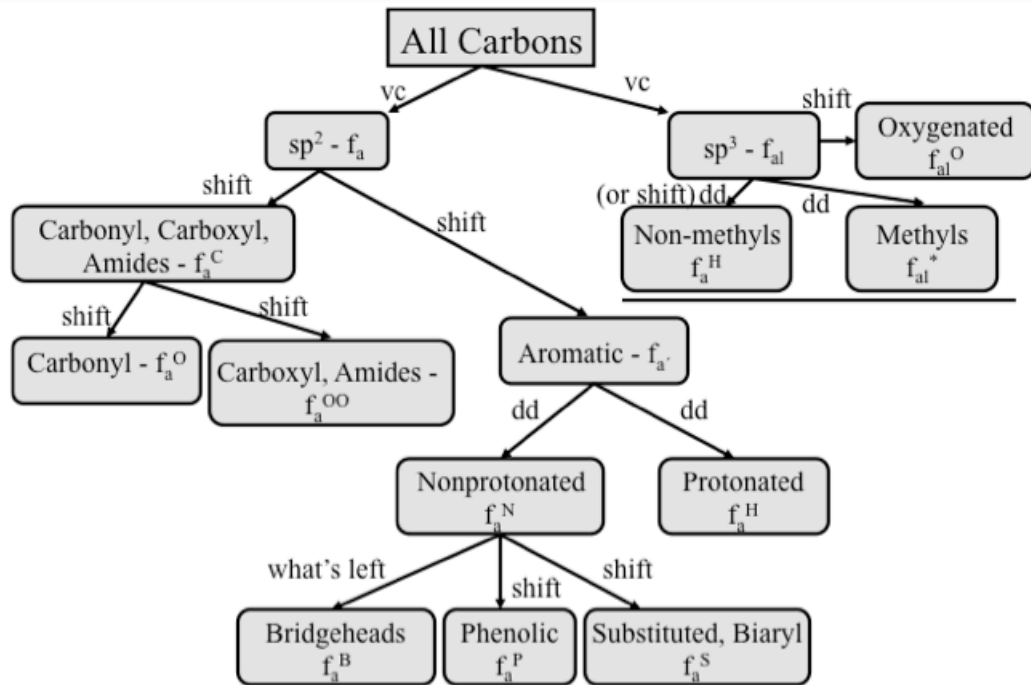
The process for obtaining the structural and lattice parameters from the various components of the solid-state spectra is reviewed in Figure 2-7 with definitions in Table 2-1. The values of these structural and lattice parameters are given in Table 2-5.

### *Solid-state NMR Spectra of Shales and Kerogen Samples*

Figure 2-8 contains the single pulse spectra (SP/MAS) and Figure 2-9 the CP/MAS spectra of the three oil shale samples (GR1, GR2, GR3)CP/MAS. The SP/MAS spectra contain both the inorganic (e.g. carbonates) and organic carbon while the CP/MAS data primarily contains the organic carbon structural elements. The structural and lattice parameters are given in Table 2-5 for the shales and their respective kerogen concentrates. SP/MAS spectra of the kerogen concentrates (GR1.9, GR2.9, GR3.9) produced from the shales are shown in Figure 2-10 and the CP/MAS spectra of the kerogen concentrates are shown in Figure 2-11.

In Figure 2-8 there is a large peak at about 170 ppm seen in each of the three SP/MAS spectra of the shale samples that is not seen in the corresponding CP/MAS spectra. This peak probably comes from inorganic carbonates such as dolomite, calcite, and siderite that are not close to any protons and do not cross-polarize. The bicarbonates and hydroxy-carbonates (dawsonite) most likely would be seen in the CP/MAS spectra if they were present in large quantities. Nahcolite might not be seen because of its long proton  $T_1$ . Because of this large peak, aromaticities were not calculated for SP/MAS spectra of the shales. The large amount of carbonates in Green River shale is well known and the SP/MAS spectra in Figure 2-8 are not surprising. However, in other types of carbonaceous materials where the amount of inorganic carbonates is much less, the difference in aromaticities between SP and CP experiments can be attributed to other causes.<sup>44</sup>

## FUNCTIONAL GROUP DIVISION



shift – fraction determined by integration of a selected chemical shift range.

vc – fraction determined by a variable contact time experiment and the magnetizations obtained by separately fitting the aromatic and aliphatic regions.

dd – fraction determined from a dipolar dephasing experiment; works well for the aromatic region where the two time constants for the two components are quite different (12 – 40  $\mu$ s and 300  $\mu$ s – 3 ms), but not for the aliphatic region with its molecular motion and similar time constants for each component ( all <  $\sim$ 130  $\mu$ s).

**Figure 2-7. Definition and source of information for determining 14 structural and 8 lattice parameters used to define critical structural components of carbonaceous materials including oil shale kerogens.**

**Table 2-5. Green River Shales and Their Kerogens from Three Cores.**

Structural Parameters														
Compound	$f_a$	$f_a^C$	$f_a^O$	$f_a^{OO}$	$f_{a'}$	$f_a^H$	$f_a^N$	$f_a^P$	$f_a^S$	$f_a^B$	$f_{al}$	$f_{al}^H$	$f_{al}^*$	$f_{al}^O$
<b>GR1 (CP) cr</b>	0.25	0.04	0.02	0.02	0.21	0.07	0.14	0.04	0.07	0.03	0.75	0.62	0.13	0.02
<b>GR1.9 (CP)</b> $C_{100}H_{150}N_3O_8S_1$	0.24	0.04	0.01	0.03	0.20	0.06	0.14	0.03	0.07	0.04	0.76	0.65	0.11	0.00
<b>GR1.9 (SP)</b>	0.25										0.75			
<b>GR2 (CP) nc</b>	0.22	0.04	0.02	0.02	0.18	0.06	0.12	0.03	0.06	0.03	0.78	0.65	0.13	0.00
<b>GR2.9 (CP)</b> $C_{100}H_{153}N_3O_8S_1$	0.23	0.05	0.02	0.03	0.18	0.06	0.12	0.03	0.06	0.03	0.77	0.66	0.11	0.01
<b>GR2.9 (SP)</b>	0.24										0.76			
<b>GR3 (CP) cr</b>	0.27	0.03	0.01	0.02	0.24	0.06	0.18	0.04	0.08	0.06	0.73	0.60	0.13	0.05
<b>GR3.9 (CP)</b> $C_{100}H_{148}N_3O_8S_2$	0.24	0.04	0.01	0.03	0.20	0.05	0.15	0.03	0.07	0.05	0.76	0.63	0.13	0.00
<b>GR3.9 (SP)</b>	0.25										0.75			
Lattice Parameters														
Compound	$\chi_b$	$C$	$\sigma+I$	$P_0$	$B.L.$	$S.C.$	$M.W.$	$M_\delta$						
<b>Gr1 (CP)</b>	0.143	8.4	4.4	-0.18	--	--	--	--						
<b>Gr1.9 (CP)</b>	0.200	10.0	5.0	-0.10	--	--	776	131						
<b>Gr2 (CP)</b>	0.167	9.0	4.5	-0.44	--	--	--	--						
<b>Gr2.9 (CP)</b>	0.167	9.0	4.5	-0.22	--	--	775	148						
<b>Gr3 (CP)</b>	0.250	12.0	6.0	-0.08	--	--	--	--						
<b>Gr3.9 (CP)</b>	0.250	12.0	5.9	-0.30	--	--	946	135						

1. cr - corrected for large aliphatic sidebands due to ferrimagnetic particles in raw shale.
2. nc – not corrected for very small aliphatic sidebands due to ferrimagnetic particles in raw shale

As can be seen in Figure 2-10 the inorganic carbon peak shown in Figure 2-8 for the shale has completely disappeared in the single pulse spectra of the kerogen concentrates. Therefore the CP/MAS spectra can be analyzed without interference from inorganic carbon. Within the small S/N difference, the CP/MAS spectra are identical to the SP/MAS spectra of the kerogen concentrates with the mineral matter removed. These results are typical of the many different kinds of carbonaceous materials run in this laboratory with varying aromaticities. The very large differences others have seen in other kerogens at higher magnetic fields<sup>42, 45</sup> are generally not seen here (we used 25 MHz for <sup>13</sup>C and 4.1 kHz spinning). Large differences between CP and SP experiments are usually seen in our laboratory only for very carbonized and conductive samples with very few protons or when a large amount of molecular motion is present. Highly carbonized material, even when setting the match condition and measuring pulse widths on the sample, not a standard, sometimes show those large differences.

Another unique feature of the spectra of the shales, especially GR3 and GR1, is a sideband at about -133 ppm seen more clearly in the much higher S/N CP/MAS spectra of Figure 2-9. This is the spinning speed away from the aliphatic resonance centered at about 31 ppm. Due to the small chemical shift anisotropy of aliphatic carbons compared to aromatic carbons, one usually does not see spinning sidebands at this spinning speed. There is also a corresponding sideband under the carbonyl/carboxyl region between 165 and 240 ppm. This effect occurs when ferromagnetic or ferrimagnetic material is present in the sample while spinning. In these samples, this effect could come from ferrimagnetic Fe<sub>3</sub>O<sub>4</sub> or other iron-containing minerals. It was difficult to accurately take this sideband effect into account, particularly for the GR3 shale, in the calculation of the structural parameters such as carbonyl/carboxyl,  $f_a^C$ , in Table 2-5. This aliphatic sideband is essentially gone in the high S/N CP/MAS spectra of the kerogen concentrates in Figure 2-11 showing that demineralization was effective in removing these minerals.

In comparing the structural parameters in Table 2-5 for the three kerogens, there does not appear to be any large difference among the three samples in the structure of the insoluble organic matter. There are only small differences in aromaticity among the three shales and between each of their respective kerogen concentrates. There appears to be much larger differences in the inorganic matter between the three cores as reflected in the SP/MAS spectra in Figure 2-8. The three kerogens have a total fraction of sp<sup>2</sup>-hybridized carbon of 0.23 or 0.24 with about 0.04 or 0.05 of that being carbonyl/carboxyl groups. The SP/MAS results are within 0.01 of the CP/MAS aromaticity for all samples, well within the experimental errors. One must subtract the carbonyl/carboxyl carbons (165 -240 ppm) from the total aromaticity,  $f_a$ , to get a corrected aromaticity,  $f_a'$ , consisting of only aromatic carbons (in preliminary experiments, no evidence of alkenes were seen either in 40,000 Hz spinning <sup>1</sup>H or 2D wide-line separation (WISE) experiments at 800 MHz on GR2.9). Therefore, it is assumed that there are no ethylenic carbons included in the data in Table 2-5. The high-resolution <sup>13</sup>C spectra does not appear to contain ethylene structures. However, the kerogen pyrolysis tars are known to contain alkane/alkene pairs.<sup>36, 37</sup>

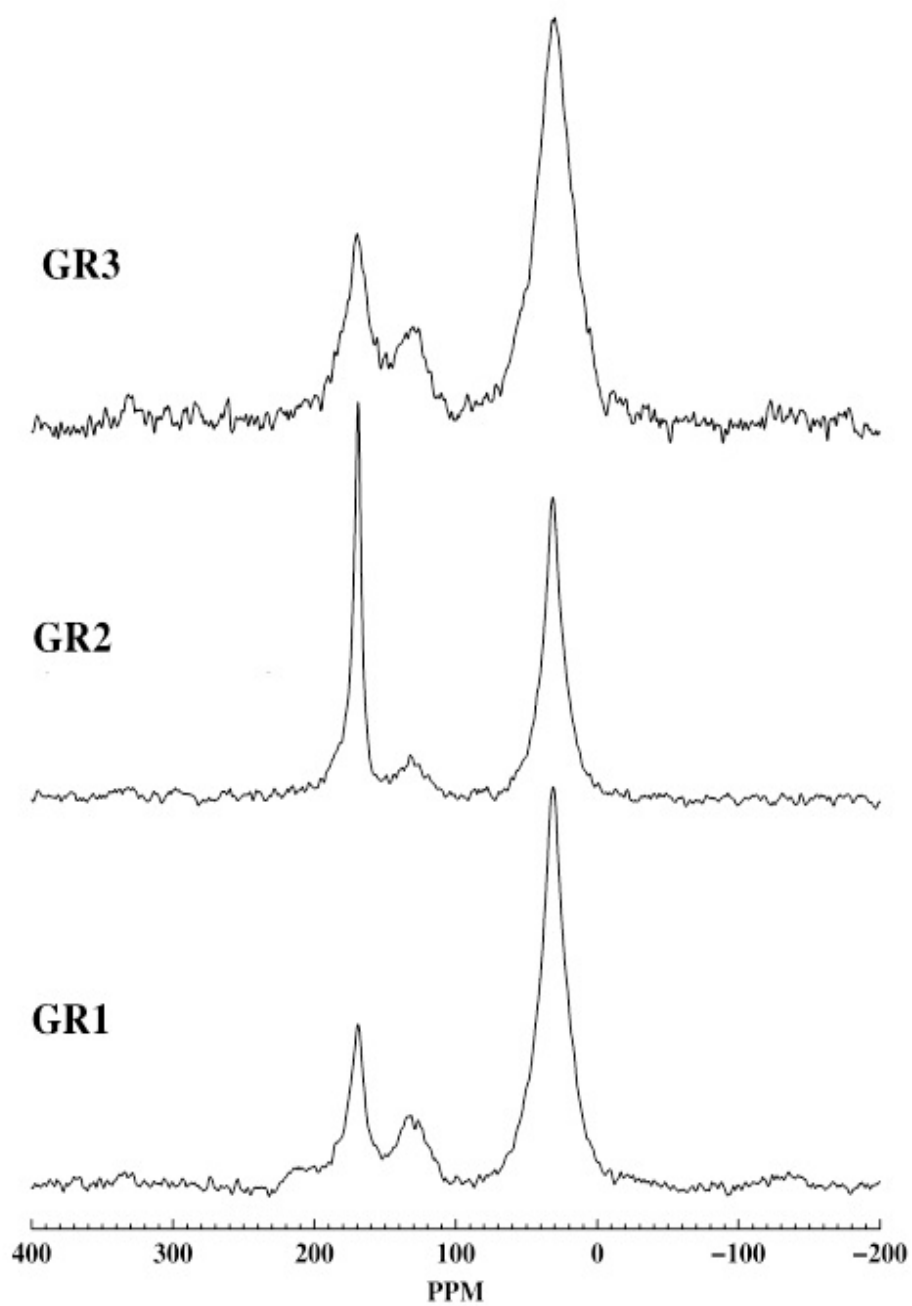


**Figure 2-8. SP/MAS spectra on the three shale samples. The pulse delay was 30 s.**

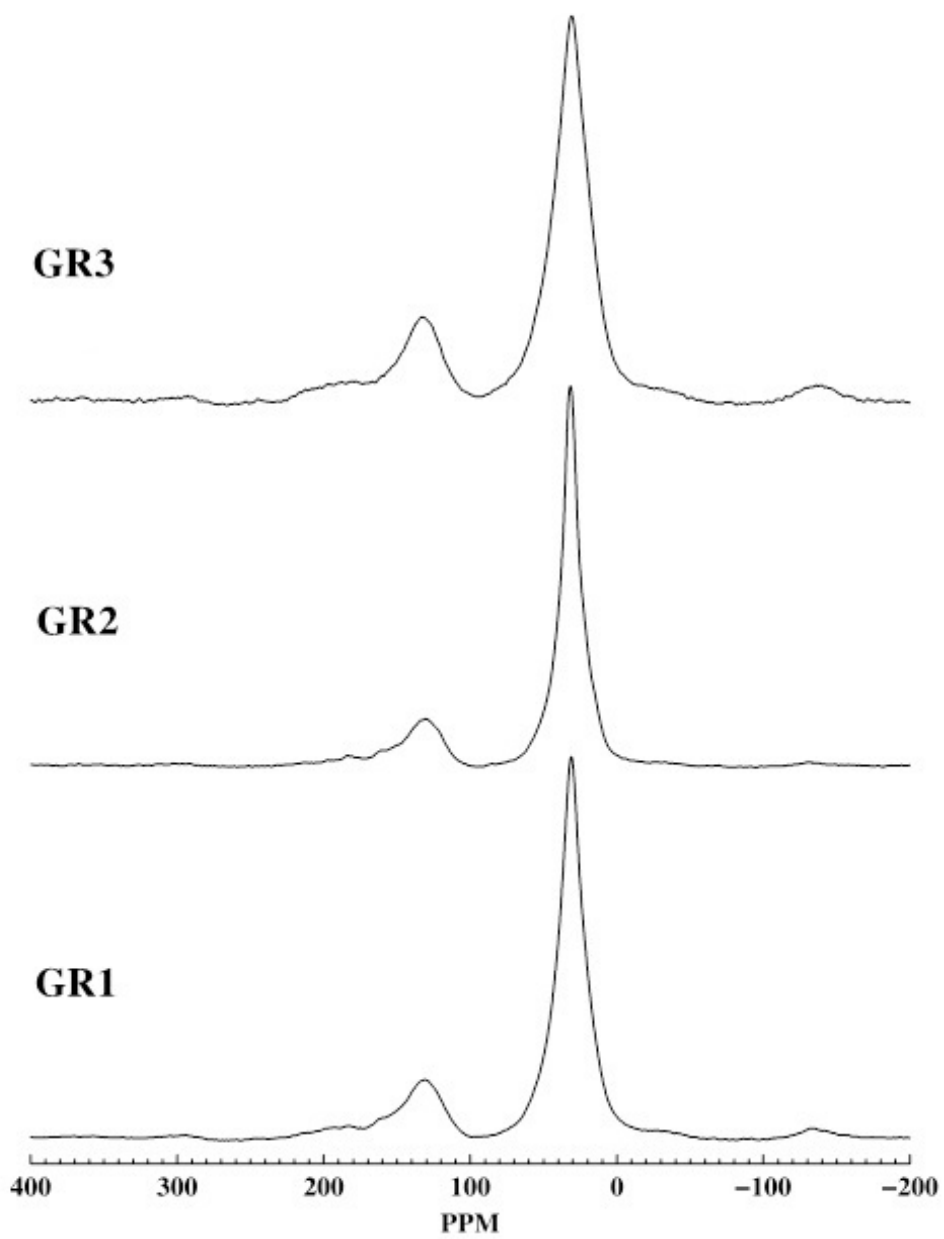


**Figure 2-9. CP/MAS spectra of the three shales. The contact time was 3 ms and the pulse delay was 1 s.**

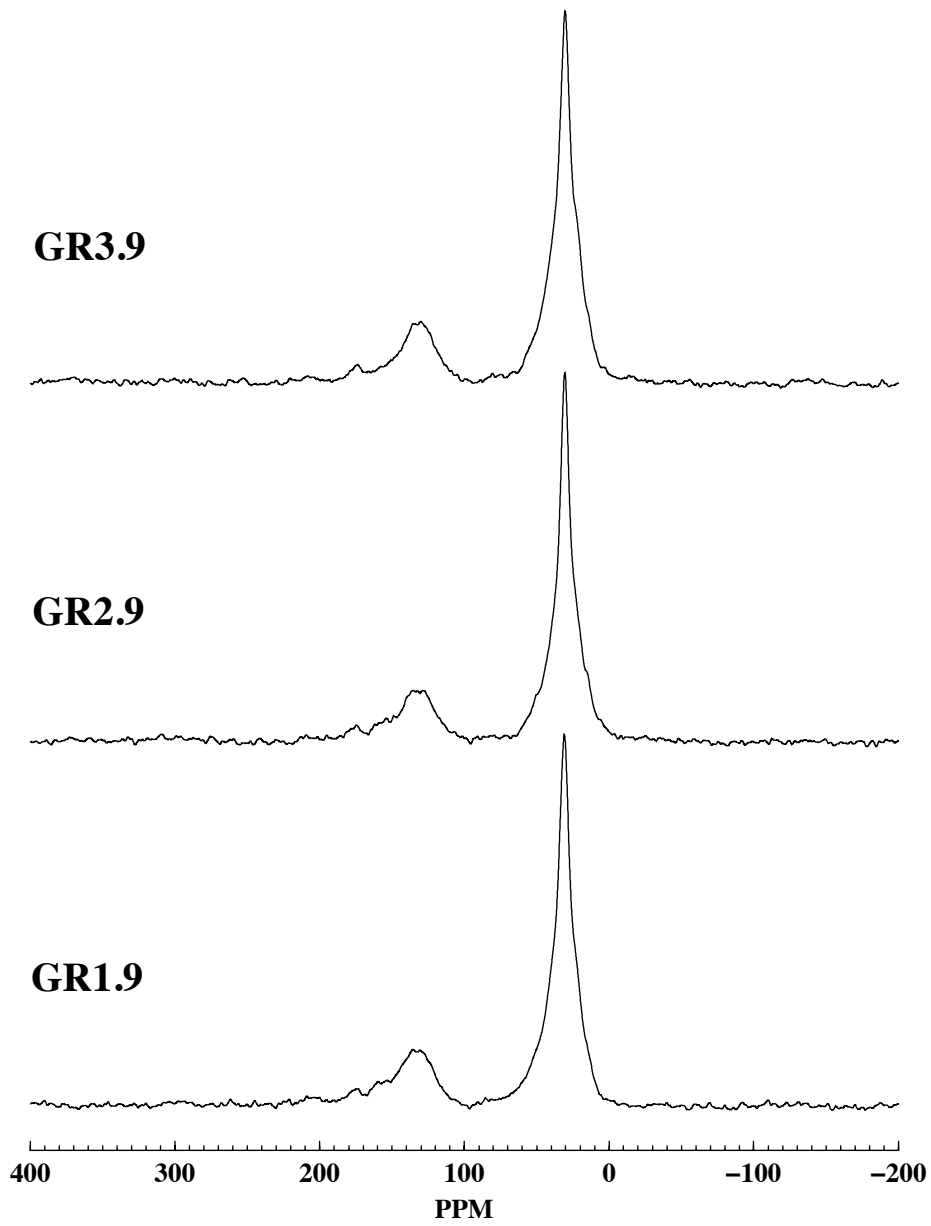


**Figure 2-10.** SP/MAS spectrum of the three kerogen concentrates. The pulse delay was 30 s.

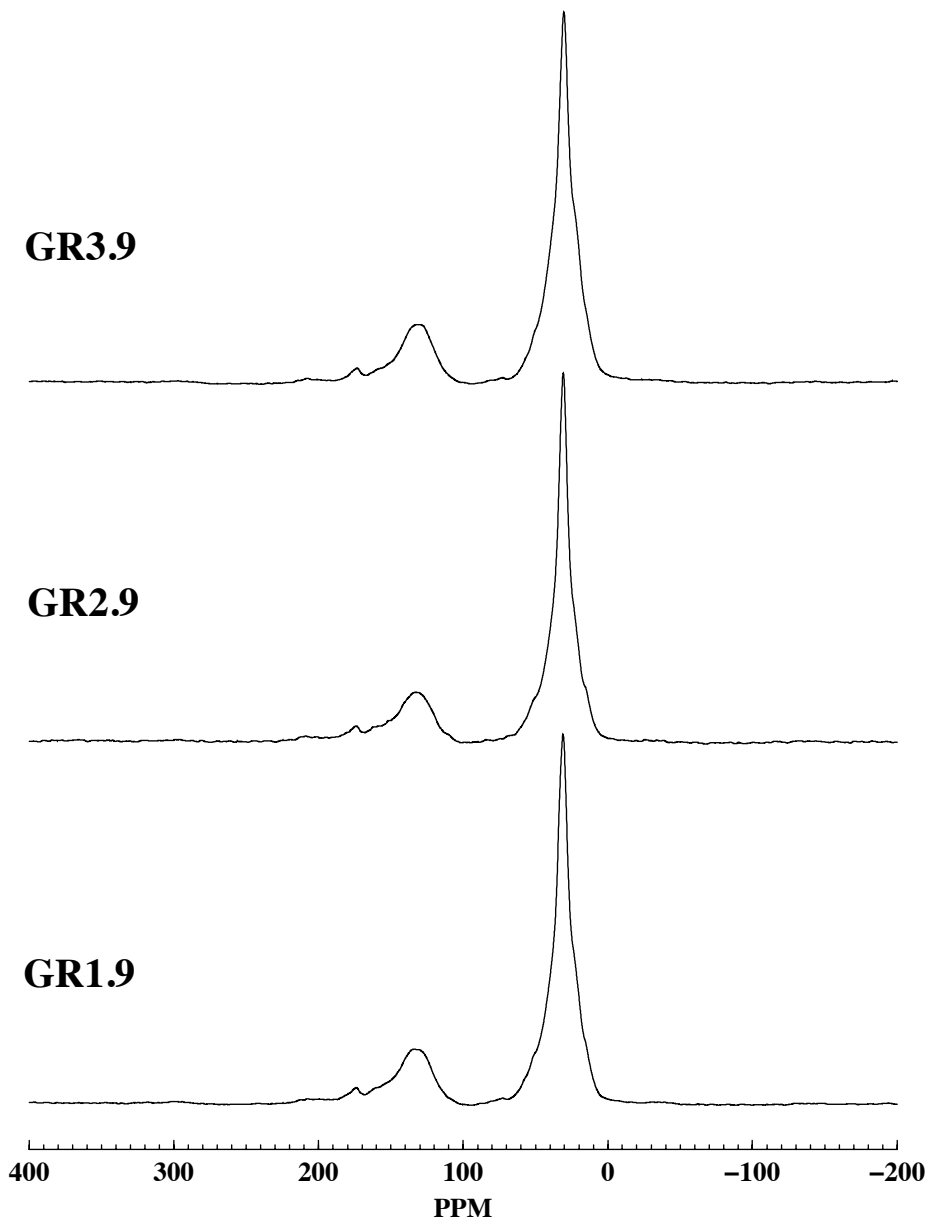


**Figure 2-11. CP/MAS spectra of the three kerogen concentrates. The contact time was 3 ms and the pulse delay was 1 s.**

Figure 2-9 is the corresponding CP/MAS spectra of the three shales. After subtracting the protonated,  $f_a^H$ , phenolic,  $f_a^P$ , and substituted,  $f_a^S$ , aromatic carbons from the corrected aromaticity, one has only the bridgehead aromatic carbons left which can then be used to estimate an “average” aromatic cluster size.<sup>22</sup> One should note that biaryl linkages (zero mass bridges) are considered substituted aromatic carbons as their shift tensor and isotropic shift shows.<sup>46</sup> In previous work,<sup>47</sup> seven pyrene molecules were hooked together having  $f_a^S = 12/112 = 0.11$  and no aliphatic material. There is only a loose correlation between the amount of substituted carbons and the amount of aliphatic material when biaryl linkages are present. There is some confusion on this issue.<sup>42</sup>

The data analysis indicates that the average aromatic cluster size (carbon atoms per cluster) is about 10 for the GR1.9 kerogen, 9.0 for the GR2.9 kerogen and about 12.0 for the slightly deeper GR3.9 kerogen. Hence, while the average cluster size is about the size of naphthalene, nothing can be said about the distribution of cluster sizes. The number of attachments per cluster (bridges plus side chains),  $\sigma + 1$ , is on the order of 5 for the three kerogens. This is consistent with the observation that the oil yield in shale correlates with the aliphatic carbon, not with the aromatic carbon atoms that remain in the spent shale.<sup>15-18</sup> If one estimates an average carbon chain length,  $f_{al}/f_a^S$ , one obtains a value of about 11–13 carbons for the three kerogen concentrates. This is half of a bridge between aromatic clusters or the size of an average side chain. This accounts for an average bridge mass of 131, 148 and 135 for GR1.9, GR2.9, and GR3.9 respectively. These values are consistent with mostly methylene carbons with an occasional biaryl linkage. The total cluster mass, including both aromatic centers and attachments, were 776, 775 and 946 for the three samples. These are much larger than the Argonne Coals<sup>22</sup> that ranged from 269–408 having much less bridge material and slightly larger aromatic clusters. The average carbon chain length is smaller than the size of extractable material analyzed by FTICR-MS where the chains group around 20–30 carbons.<sup>14</sup> In Table 2-5, all of the  $P_0$  values are negative. This parameter, the fraction of intact bridges, should be between 0 and 1.0 if all chains terminate in a single methyl group, a reasonable approximation for coals.<sup>22</sup> The negative values show significant branching in the aliphatic chains with multiple methyl groups on a single chain. When this parameter is negative, one cannot separate bridges and loops (bridge back on the same aromatic cluster) from side chains.

Dipolar dephased spectra of the kerogen concentrates using a dephasing time of 42  $\mu$ s are shown in Figure 2-12. The aliphatic region consists of three main peaks. The peak at 15 ppm is from the terminal methyl groups of aliphatic chains. The peak centered between 22 and 23 ppm is a composite peak from methyls on aromatic rings and the first methylene group in from the terminal methyl. The largest peak at about 30 ppm is from most of the methylene carbons in long chains. There must be a high degree of motion in some parts of these chains or this peak would be mostly suppressed at this dephasing time. A test molecule used in this laboratory, decylpyrene, has all of its nine methylene carbons suppressed at this dephasing time as is true for most static methylenes. Because of the dominance of the large methylene peak and the degree of motion in the sample, a better analysis using spectral editing techniques based on the dipolar interaction has not been possible on the available spectrometer.

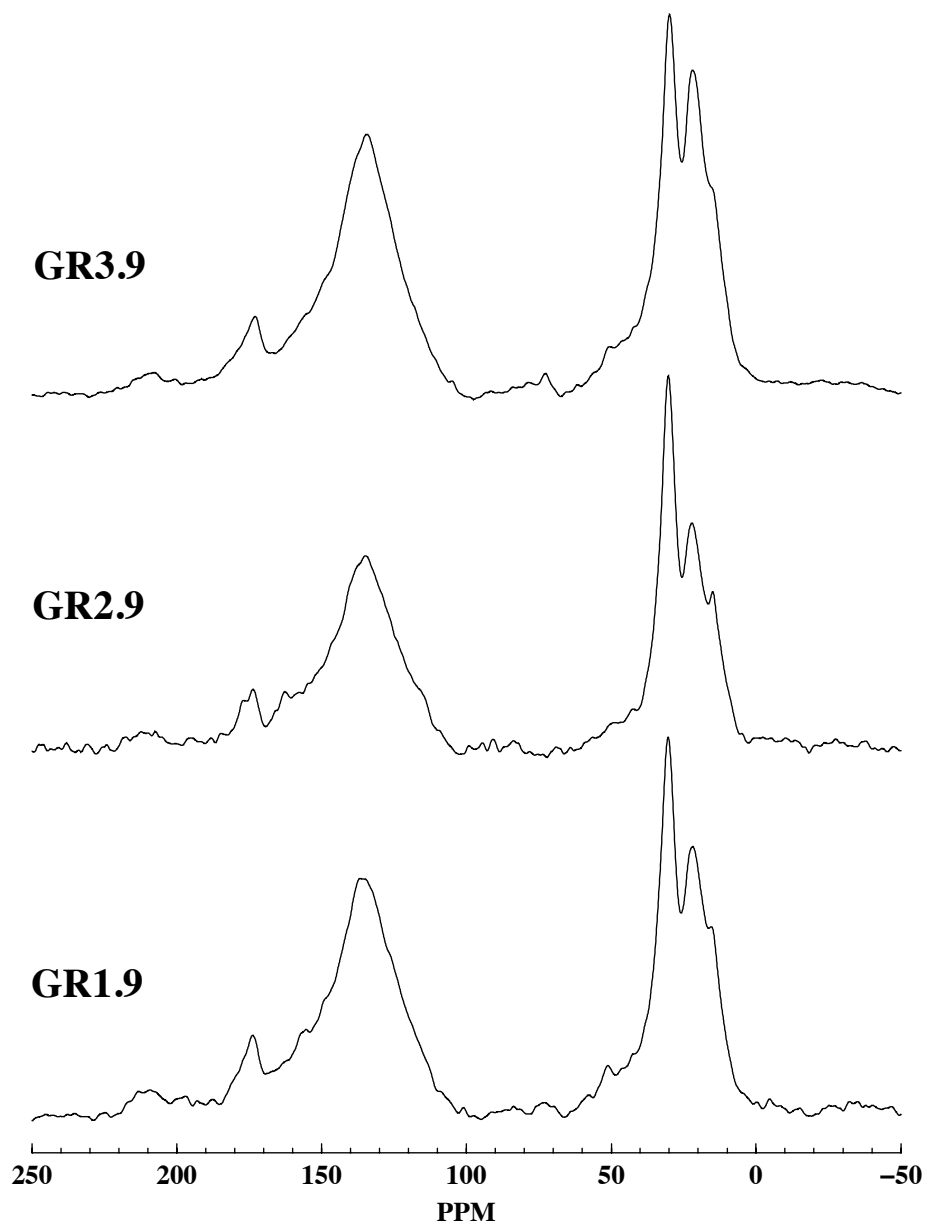


**Figure 2-12. Dipolar dephasing ( $\tau=42$  ms) spectra of the kerogen concentrates. Only non-protonated, methyl, and carbons with a high degree of motion remain.**

## Conclusions

The purpose of this study was to examine various sections of a carefully prepared shale core taken from the Mahogany zone in the eastern Utah Green River formation (Uinta Skyline 16 location). Three one-foot sections were taken from the central portion of the 4-inch diameter core. These one-foot sections were separately crushed, sieved, and then demineralized. The organic content varied with each section (15.8, 20.51, and 25.95 wt.%), but the organic structural components of the shale (the bitumen and kerogen isolates) are quite similar. The aromatic content of the kerogens from GR1, GR2, and GR3 were essentially identical (24%, 23%, and 24%) within experimental error. The fraction of aromatic carbons in the extracted bitumen was 11%, 9%, and 7% for the three shale samples. The S/N on the bitumen samples is very low and the aromatic content is within experimental error for all three bitumen samples. The bitumen aliphatic structure is dominated by long chains with an average length of about 24 carbons. However, there is evidence that the amount of branching is small but not insignificant, which relates to the isoprenoids that have been observed in pyrolysis experiments.

The single pulse C<sup>13</sup> NMR experiments on the demineralized kerogen showed the absence of inorganic carbon structures (i.e., carbonates). The C<sup>13</sup> CP/MAS NMR experiments allowed, for the first time, determination of lattice parameters for the kerogen, showing that the kerogen had approximately 10 aromatic carbons per cluster with an average side chain length of 11 to 13 carbons. The average molecular weight per cluster ranged from 775 to 946 for the three demineralized samples with an average molecular weight per side chain of 131 to 148. The number of attachments per side chain, or coordination number, ranged from 4.5 to 5.9 for the three demineralized kerogen samples. The value of these chemical structure data and lattice parameters are in interpreting pyrolysis data and in generation of chemical structure-based pyrolysis models.

Chapter 4 contains supporting data for these estimates based on the GCMS analysis of the pyrolysis tars (see Fletcher et al<sup>48</sup>). That chapter focuses on structural changes associated with pyrolysis and the subsequent product yields of tar and char residue from the kerogen concentrates at pyrolysis temperatures in ranges from 300–525°C. The evolution of the tar and gas components as well as the dynamics of the structural and lattice parameters during pyrolysis are followed. These data are then used to model the pyrolysis process of the kerogen.

## References

1. Miknis, F. P., Composition, chemistry and conversion of oil shales. In *NATO ASI Series; Series C: Mathematical and Physics Sciences*, Snape, C., Ed. 1994; Vol. 455, pp 69-91.
2. Maciel, G. E.; Dennis, L. W., Comparison of oil shales and kerogen concentrates by <sup>13</sup>C nuclear magnetic resonance. *Organic Geochemistry* **1981**, 3, (4), 105-109.
3. Oil Shale: Energy to Fuel Our Future, 2013 Update, National Oil Shale Association, pp. 1-24 (2013).
4. Dyni, J. R., *Geology and resources of some world oil-shale deposits*. Report No. 2005-5294; Scientific Investigations Report, U. S. Department of the Interior, U. S. Geological Survey: 2005; p 42.
5. Johnson, R. C.; Mercier, T. J.; Brownfield, M. E.; Pantea, M. P.; Self, J. G., An assessment of in-place oil shale resources in the Green River Formation, Piceance Basin, Colorado. *Oil-shale assessment of the Piceance Basin, Colorado: U.S. Geological Survey Digital*

- Data Series DDS-69-Y, Chap. 1*, U.S. Geological Survey Oil Shale Assessment Team, Eds., 2010; pp 1-197.
6. Vandenbroucke, M., Kerogen: from types to models of chemical structure. *Oil & Gas Science and Technology* **2003**, 58, (2), 243-269.
  7. Siskin, M.; Scouten, C. G.; Rose, K. D.; Aczel, D.; Colgrove, S. G.; Pabst, R. E., Detailed structural characterization of the organic material in Rundle Ramsay crossing and Green River oil shales. In *Composition, Geochemistry and Conversion of Oil Shales*, Snape, C., Ed. Kluwer Academic: Boston, 1995; p 143.
  8. Orendt, A. M.; Pimiienta, I. S. O.; S. R. Badu, S. R.; Solum, M. S.; Pugmire, R. J.; Locke, D. R.; Chapman, K. W.; Chupas, P. J.; Winans, R. E., Three-dimensional structure of the Siskin Green River oil shale kerogen model: A comparison between calculated and observed properties. *Energy and Fuels* **2013**, 27, 702-710.
  9. Netzel, D. A.; McKay, D. R.; Heppner, R. A.; Guffey, F. D.; Cooke, S. D.; Varie, D. L.; Linn, D. E., <sup>1</sup>H- and <sup>13</sup>C-n.m.r. studies on naphtha and light distillate saturate hydrocarbon fractions obtained from in-situ shale oil. *Fuel* **1981**, 60, (4), 307-320.
  10. Burnham, A. K., Oil evolution from a self-purging reactor: kinetics and composition at 2°C/min and 2°C/h. *Energy & Fuels* **1991**, 5, (1), 205-214.
  11. Burnham, A. K.; Gregg, H. R.; Ward, R. L.; Knauss, K. G.; Copenhaver, S. A.; Reynolds, J. G.; Sanborn, R., Decomposition kinetics and mechanism of n-hexadecane-1,2-<sup>13</sup>C<sub>2</sub> and dodec-1-ene-1,2-<sup>13</sup>C<sub>2</sub> doped in petroleum and n-hexadecane. *Geochimica et Cosmochimica Acta* **1997**, 61, (17), 3725-3737.
  12. Ward, R. L.; Burnham, A. K., Identification by <sup>13</sup>C N.M.R. of carbon types in shale oil and their relation to pyrolysis conditions. *Fuel* **1984**, 63, (7), 909-914.
  13. Dalling, D. K.; Pugmire, R. J.; Grant, D. M.; Hull, W. E., The use of high-field carbon-13 NMR spectroscopy to characterize chiral centers in isopranes. *Magnetic Resonance in Chemistry* **1986**, 24, (3), 191-198.
  14. Bartuska, V. J.; Maciel, G. E.; Schaefer, J.; Stejskal, E. O., Prospects for carbon-13 nuclear magnetic resonance analysis of solid fossil-fuel materials. *Fuel* **1977**, 56, (354-358).
  15. Resing, H. A.; Garroway, A. N.; Hazlett, R. N., Determination of aromatic hydrocarbon fraction in oil shale by <sup>13</sup>C N.M.R. with magic-angle spinning. *Fuel* **1978**, 57, (8), 450-454.
  16. Maciel, G. E.; Bartuska, V. J.; Miknis, F. P., Improvement in correlation between oil yields of oil shales and <sup>13</sup>C N.M.R. spectra. *Fuel* **1979**, 58, (2), 155-156.
  17. Miknis, F. P.; Maciel, G. E.; Bartuska, V. J., Cross polarization magic-angle spinning <sup>13</sup>C NMR spectra of oil shales. *Organic Geochemistry* **1979**, 1, (3), 169-176.
  18. Miknis, F. P.; Szeverenyi, N. M.; Maciel, G. E., Characterization of the residual carbon in retorted oil-shale by solid-state C-13 NMR. *Fuel* **1982**, 61, (4), 341-345.
  19. Hagaman, E. W.; Schell, F. M.; Cronauer, D. C., Oil-shale analysis by CP/MAS-<sup>13</sup>C NMR spectroscopy. *Fuel* **1984**, 63, (7), 915-919.
  20. Petsch, S. T.; Smernik, R. J.; Eglinton, T. I.; Oades, J. M., A solid-state <sup>13</sup>C-NMR study of kerogen degradation during black shale weathering. *Geochimica et Cosmochimica Acta* **2001**, 65, (12), 1867-1882.
  21. Salmon, E.; Behar, F.; Hatcher, P. G., Molecular characterization of Type I kerogen from the Green River Formation using advanced NMR techniques in combination with electrospray ionization/ultrahigh resolution mass spectrometry. *Organic Geochemistry* **2011**, 42, (4), 301-315.

22. Solum, M. S.; Pugmire, R. J.; Grant, D. M., Carbon-13 solid-state NMR of Argonne Premium Coals. *Energy & Fuels* **1989**, 3, (2), 187-193.
23. Van Niekerk, D.; Pugmire, R. J.; Solum, M. S.; Painter, P. C.; Mathews, J. P., Structural characterization of vitrinite-rich and inertinite-rich Permian-aged South African bituminous coals. *International Journal of Coal Geology* **2008**, 76, (4), 290-300.
24. Fletcher, T. H.; Kerstein, A. R.; Pugmire, R. J.; Grant, D. M., Chemical percolation model for devolatilization. 2. Temperature and heating rate effects on product yields. *Energy & Fuels* **1990**, 4, (1), 54-60.
25. Fletcher, T. H.; Kerstein, A. R.; Pugmire, R. J.; Solum, M. S.; Grant, D. M., Chemical percolation model for devolatilization. 3. Direct use of carbon-13 NMR data to predict effects of coal type. *Energy & Fuels* **1992**, 6, (4), 414-431.
26. Genetti, D.; Fletcher, T. H.; Pugmire, R. J., Development and application of a correlation of <sup>13</sup>C NMR chemical structural analyses of coal based on elemental composition and volatile matter content. *Energy & Fuels* **1998**, 13, (1), 60-68.
27. Grant, D. M.; Pugmire, R. J.; Fletcher, T. H.; Kerstein, A. R., Chemical model of coal devolatilization using percolation lattice statistics. *Energy & Fuels* **1989**, 3, (2), 175-186.
28. Fletcher, T. H.; Solum, M. S.; Grant, D. M.; Critchfield, S.; Pugmire, R. J., Solid-state <sup>13</sup>C and <sup>1</sup>H NMR studies of the evolution of the chemical structure of coal char and tar during devolatilization. *Twenty-Third Symposium (International) on Combustion* **1990**, 23, 1231-1237.
29. Fletcher, T. H.; Solum, M. S.; Grant, D. M.; Pugmire, R. J., Chemical structure of char in the transition from devolatilization to combustion. *Energy & Fuels* **1992**, 6, (5), 643-650.
30. Jiang, Y. J.; Solum, M. S.; Pugmire, R. J.; Grant, D. M.; Schobert, H. H.; Pappano, P. J., A new method for measuring the graphite content of anthracite coals and soots. *Energy & Fuels* **2002**, 16, (5), 1296-1300.
31. Solum, M. S.; Sarofim, A. F.; Pugmire, R. J.; Fletcher, T. H.; Zhang, H., <sup>13</sup>C NMR analysis of soot produced from model compounds and a coal. *Energy & Fuels* **2001**, 15, (4), 961-971.
32. Yan, S.; Jiang, Y.-J.; Marsh, N. D.; Eddings, E. G.; Sarofim, A. F.; Pugmire, R. J., Study of the evolution of soot from various fuels. *Energy & Fuels* **2005**, 19, (5), 1804-1811.
33. Zhang, H.; Fletcher, T. H.; Perry, S. T.; Solum, M. S.; Pugmire, R. J. *Soot formation during coal pyrolysis*, 11th International Conference on Coal Science, Sept. 30-Oct. 5, San Francisco, CA, 2001.
34. Kelemen, S. R.; Siskin, M.; Homan, H. S.; Pugmire, R. J.; Solum, M. S., "Fuel, lubricant and additive effects on combustion chamber deposits." Report No. 982715; Copyright 1998 Society of Automotive Engineers, Inc.
35. Siskin, M.; Kelemen, S. R.; Most, W. J.; Kwiatek, P. J.; Pugmire, R. J.; Solum, M. S., "Combustion chamber deposits from base fuel and commercial IVD detergent packages." Report No. 982716; Copyright 1998 Society of Automotive Engineers Inc.
36. Hillier, J. L. Pyrolysis kinetics and chemical structure considerations of a Green River oil shale and its derivatives. Ph.D. Dissertation, Chemical Engineering Department, Brigham Young University, Provo, UT, 2011.
37. Hillier, J. L.; Fletcher, T. H.; Solum, M. S.; Pugmire, R. J., Characterization of macromolecular structure of pyrolysis products from a Colorado Green River oil shale. *Industrial & Engineering Chemistry Research* **2013**, 52, (44), 15522-15532.

38. Vandegrift, G. F.; Winans, R. E.; Scott, R. G.; Horwitz, E. P., Quantitative study of the carboxylic acids in Green River oil shale bitumen. *Fuel* **1980**, 59, (9), 627-633.
39. Crouch, R., Acquiring quantitative small-molecule NMR data with QDEPT, Agilent Technologies Application Note. (see [www.agilent.com](http://www.agilent.com)): January 30, 2012.
40. Henderson, T. J., Sensitivity-enhanced quantitative  $^{13}\text{C}$  NMR spectroscopy via cancellation of  $^1J_{\text{CH}}$  dependence in DEPT polarization transfers. *Journal of the American Chemical Society* **2004**, 126, (12), 3682-3683.
41. Kolodziejcki, W.; Klinowski, J., Kinetics of cross-polarization in solid-state NMR: A guide for chemists. *Chemical Reviews* **2002**, 102, (3), 613-628.
42. Mao, J.; Fang, X.; Lan, Y.; Schimmelmann, A.; Mastalerz, M.; Xu, L.; Schmidt-Rohr, K., Chemical and nanometer-scale structure of kerogen and its change during thermal maturation investigated by advanced solid-state  $^{13}\text{C}$  NMR spectroscopy. *Geochimica et Cosmochimica Acta* **2010**, 74, (7), 2110-2127.
43. Mao, J. D.; Schmidt-Rohr, K., Methylene spectral editing in solid-state  $^{13}\text{C}$  NMR by three-spin coherence selection. *Journal of Magnetic Resonance* **2005**, 176, (1), 1-6.
44. Snape, C. E.; Axelson, D. E.; Botto, R. E.; Delpuech, J. J.; Tekely, P.; Gerstein, B. C.; Pruski, M.; Maciel, G. E.; Wilson, M. A., Quantitative reliability of aromaticity and related measurements on coals by  $^{13}\text{C}$  n.m.r. A debate. *Fuel* **1989**, 68, (5), 547-548.
45. Werner-Zwanziger, U.; Lis, G.; Mastalerz, M.; Schimmelmann, A., Thermal maturity of type II kerogen from the New Albany Shale assessed by  $^{13}\text{C}$  CP/MAS NMR. *Solid State Nuclear Magnetic Resonance* **2005**, 27, (1-2), 140-148.
46. Barich, D. H.; Pugmire, R. J.; Grant, D. M.; Iuliucci, R. J., Investigation of the structural conformation of biphenyl by solid-state  $^{13}\text{C}$  NMR and quantum chemical NMR shift calculations. *The Journal of Physical Chemistry A* **2001**, 105, (28), 6780-6784.
47. Winans, R. E.; Tomczyk, N. A.; Hunt, J. E.; Solum, M. S.; Pugmire, R. J.; Jiang, Y. J.; Fletcher, T. H., Model compound study of the pathways for aromatic hydrocarbon formation in soot. *Energy & Fuels* **2007**, 21, (5), 2584-2593.
48. Fletcher, T. H.; Gillis, R.; Adams, J.; Hall, T.; Mayne, C. L.; Solum, M. S.; Pugmire, R. J., Characterization of macromolecular structure elements from a Green River oil shale, II. Characterization of pyrolysis products by  $^{13}\text{C}$  NMR, GC/MS, and FTIR. *Energy and Fuels* **2014**, 28, 2959-2970.

## CHAPTER 3. THERMOGRAVIMETRIC ANALYSIS

Thermogravimetric analyses (TGA) data were obtained for 3 samples of oil shale from the Green River Basin. Approximately 10 mg of each sample was heated to 850°C at one of three heating rates (1, 5, and 10 K/min) and one of two pressures (atmospheric pressure and 40 bar). Samples had a dwell time at 850°C of 5 minutes. This resulted in a total of 6 possible conditions for each sample and a total of 18 unique experiments when three samples were examined, as shown in Table 3-1.

**Table 3-1. Experimental Conditions for Each of the 3 Samples.**

	1 K/min	5 K/min	10 K/min
Atmospheric	X	X	X
40 bar	X	X	X

Characteristic TGA data are shown in Figure 3-1. The actual data are shown superimposed on the smoothed data. Flow rates of the helium (He) were kept constant for all runs in order to minimize randomizing factors. As expected, two separate reactions are observed in Figure 3-1. At atmospheric pressure, the kerogen pyrolyzes at approximately 450°C and the calcium carbonate at 650°C. We have shown previously that the temperature where pyrolysis occurs increases slightly with elevated heating rate. Separate kinetic coefficients were determined for each sample at each pressure.

Figure 3-2 shows an example of how buoyancy curves were used to analyze data. Curves are extrapolated from regions where the sample is not reacting in order to subtract buoyancy effects. The sample is removed from the TGA and weighed at the end of the experiment. The final corrected mass is checked against the final measured mass for consistency.

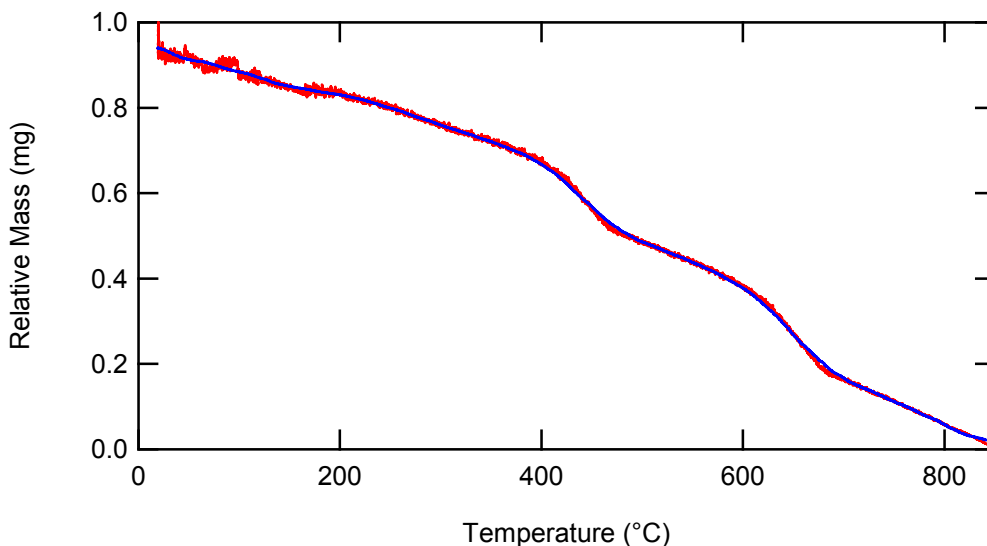


**Figure 3-1. GR1 raw sample at 10 K/min and 1 atmosphere (atm).**

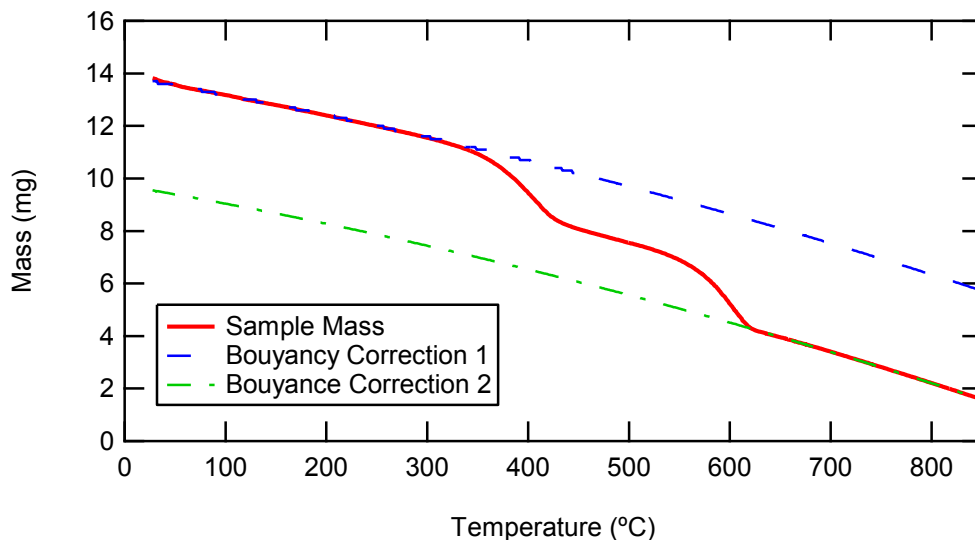


**Figure 3-2. Method to correct for buoyancy (adapted from Hillier<sup>1</sup>).**

### Modeling of Data

Once the data are reduced to eliminate noise and the effects of buoyancy, the data were fit with a first-order reaction rate expression (Eq. 3-1) or a Distributed Activation Energy Model (DAEM) (Eq. 3-2), following the method of Hillier et al.<sup>2,3</sup>

$$\frac{dm}{dt} = -A e^{-E/RT} m \quad (3-1)$$

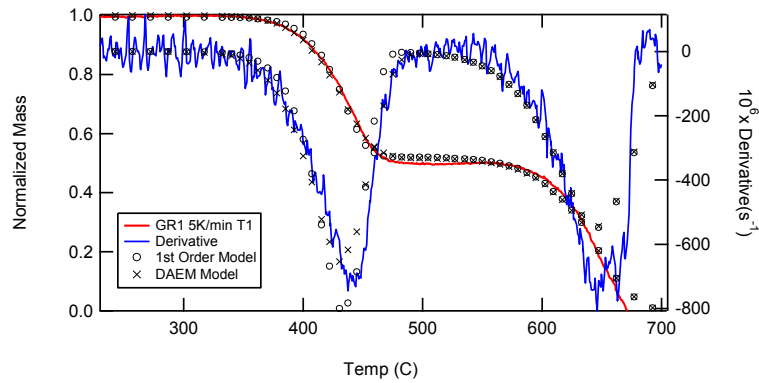
$$\frac{dm}{dt} = -A e^{-(E \pm \sigma)/RT} m \quad (3-2)$$

Here,  $m$  is the sample mass,  $A$  and  $E$  are kinetic coefficients,  $R$  is the gas constant, and  $T$  is the temperature. The standard deviation ( $\sigma$ ) of the activation energy ( $E$ ) is a fitting parameter in the first-order DAEM. An optimization program was used to determine the coefficients  $A$  and  $E$  (and  $\sigma$ ). A sequential form of the DAEM is used where the activation energy becomes a function of the extent of conversion, and only one activation energy is used at each time step.

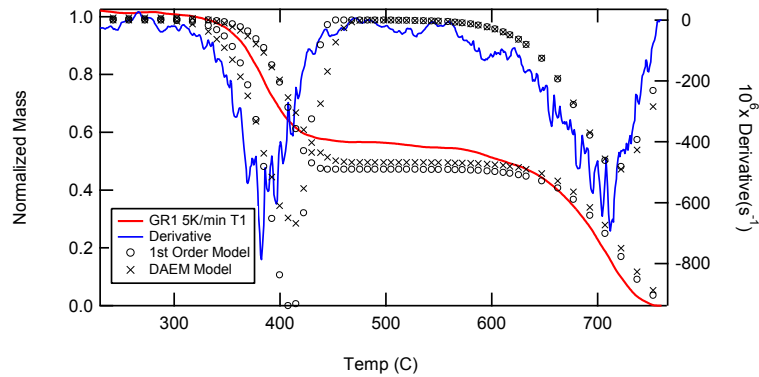
All pressurized and atmospheric TGA experiments on the three Green River pulverized oil shale samples were completed, despite several delays with the higher pressure runs due to malfunctions of the electronic balance. These samples had a mass mean diameter of 60  $\mu\text{m}$ . The kinetic coefficients from all TGA experiments were determined for both the first-order model and the distributed activation energy model. Figure 3-3 shows sample TGA data along with the corresponding curve fits for a sample at 5 K/min at both atmospheric pressure and 40 bar. The kinetic coefficients were determined by fitting data from three heating rates (1, 5, and 10 K/min). Table 3-2 shows the resulting kinetic coefficients from this study for all three GR samples.

**Table 3-2. Kinetic Coefficients Determined from TGA Pyrolysis of GR Oil Shale Samples.**

Sample		First-Order		DAEM	
		1 atm	40 bar	1atm	40 bar
GR1	A (1/s)	8.90E+13	2.80E+14	9.20E+13	1.00E+14
	E (kJ/mol)	221	219	223	215
	$\sigma$ (kJ)	--	--	4	2.6
GR2	A (1/s)	4.50E+13	8.00E+13	2.60E+14	3.00E+14
	E (kJ/mol)	216.9	210	228.1	219.4
	$\sigma$ (kJ)	--	--	2.6	6.7
GR3	A (1/s)	9.50E+13	1.50E+14	9.40E+13	3.50E+14
	E (kJ/mol)	220	217	222	225
	$\sigma$ (kJ)	--	--	4.6	5.3



(a) Atmospheric pressure



(b) 40 bar

**Figure 3-3. TGA pyrolysis data and best-fit model calculations for GR1 oil shale crushed and sieved to 60  $\mu\text{m}$  mass mean diameter, heated at 5 K/min.**

## Comparison of Oil Shale Pyrolysis Models

A comparison of the rates of pyrolysis at different heating rates reported by Dr. Fletcher's group at BYU and Dr. Deo's group at the University of Utah has been performed by Drew Gillespie at BYU. Only atmospheric pyrolysis data were compared. BYU data were averaged from several runs and fit with a sigmoid curve. This comparison included the following steps:

1. Reproducing the first-order model with variable activation energy reported by Tiwari and Deo.<sup>4</sup>
2. Digitizing the data from that paper.
3. Comparing the first-order and distributed activation energy models from BYU vs. the Tiwari and Deo data at 1, 5 and 10 K/min.
4. Comparing the first-order and distributed activation energy models from BYU vs. the BYU data at 0.5, 1, 5 and 10 K/min.
5. Comparing the Tiwari and Deo first-order model with variable activation energy vs. the BYU data at 0.5, 1, 5 and 10 K/min.
6. Plotting the data from BYU and the University of Utah on the same plot.

This comparison has been completed (see Figure 3-4). Of particular note, the 1 K/min data do not compare very well. There is about a 25 K difference between the two data sets in the temperatures at which the pyrolysis occurs. This has important implications when extrapolating models to lower heating rates. The BYU data were calibrated using Curie point metals and a magnet, as suggested by Dr. Alan Burnham. Dr. Burnham also noted agreement between his published rates and the BYU-published rates. We therefore have more confidence in the BYU TGA data and rates. The 0.5 K/min data are much closer, suggesting that perhaps only the 1 K/min data are not in agreement.

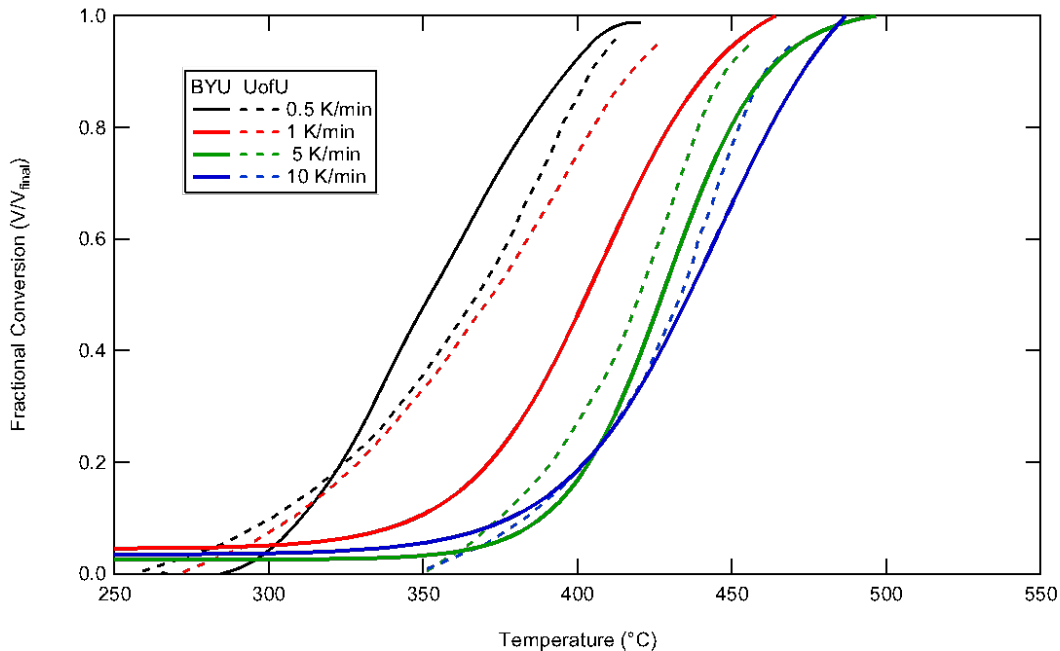


**Figure 3-4. Comparison of BYU vs. University of Utah pyrolysis data from the GR2 sample at atmospheric pressure and heating rates of 0.5, 1.0, 5.0 and 10 K/min.**

## References

1. Hillier, J. L. Pyrolysis kinetics and chemical structure considerations of a Green River oil shale and its derivatives. Ph.D. Dissertation, Chemical Engineering Department, Brigham Young University, Provo, UT, 2011.
2. Hillier, J.; Bezzant, T.; Fletcher, T. H., Improved method for determination of kinetic parameters from non-isothermal TGA data. *Energy & Fuels* **2010**, *24*, 2841-2847.
3. Hillier, J. L.; Fletcher, T. H., Pyrolysis kinetics of a green river oil shale using a pressurized TGA. *Energy & Fuels* **2011**, *25*, 232-239.
4. Tiwari, P.; Deo, M., Detailed kinetic analysis of oil shale pyrolysis TGA data. *AIChE Journal* **2012**, *58*, (2), 505-515.

## CHAPTER 4. PRODUCTS OF KEROGEN PYROLYSIS

---

### Background

The Green River oil shale formation spans parts of eastern Utah, southern Wyoming, and western Colorado, and contains approximately 60% of the known world reserves of oil shale, with estimates of as high as 2.8 trillion barrels of oil equivalent.<sup>1-3</sup> Oil shale was studied extensively in the 1970s and early 80s when oil prices were high, but research slowed due to low oil prices in the late 80s. High oil prices have increased interest in recovery of unconventional sources of oil such as oil shale.

Reviews of pyrolysis rates and chemical analyses of volatile products from oil shale were recently published by Hillier<sup>4-6</sup> and Tiwari.<sup>7-9</sup> Light gases have been studied by several research groups (e.g., Campbell et al.<sup>10</sup>, Burnham, et. al.<sup>11-13</sup> and Meuzelaar<sup>14</sup>). Huizinga and coworkers<sup>15</sup> used pyrolysis mass spectrometry (py-ms) to view the nature and distribution of products of kerogen pyrolysis of an immature Green River sample from the Red Point mine in Piceance, Colorado. The experiment included pressures of 100 psi (6.8 atm) of He over a mixture of the sample and water. The sample was collected and analyzed in a mass spectrometer. Huizinga found that the pyrolysis products included n-alkane/alkene pairs with a preference for odd carbon numbers. Reynolds et al.<sup>16</sup> performed on-line mass spectrometry to analyze the gas evolution and species during oil shale pyrolysis. Tiwari and Deo<sup>7-9</sup> used TGA coupled with mass spectrometry (i.e., TG/MS) to study the evolution of species in the 300 amu range during pyrolysis of a Utah oil shale at heating rates of 0.5 to 10 K/min. Lighter species evolved slightly earlier on the temperature scale and significant amounts of alkenes were reported.

Hagaman et al.<sup>17</sup> used <sup>13</sup>C NMR spectroscopy to estimate potential oil yields from shales by utilizing the aliphatic content ( $f_{al}$ ). They also found that throughout the Mahogany zone (the zone of highest oil yield per ton of rock) of a Green River oil shale, the aliphatic carbon fraction was nearly constant. Boucher et al.<sup>18</sup> utilized NMR and a complimentary ruthenium oxide (RuO<sub>2</sub>) mild oxidation technique on a type II kerogen, reporting a carbon aromaticity of 25.8% with predominantly CH<sub>2</sub> groups in rings or chains or attached to oxygen.

Miknis et al.<sup>19-21</sup> performed NMR on several oil samples and residual carbons from oil shale retorts, showing differences between shales of different geological formations. Maciel et al.<sup>22</sup> reported that oil yields from oil shale correlated with aliphatic carbon content as measured by <sup>13</sup>C NMR spectroscopy, and a more general correlation was developed by Miknis and Conn.<sup>23</sup> Solomon and Miknis<sup>24</sup> developed a similar correlation of oil yield using aliphatic carbon content as measured by FTIR spectroscopy on crushed oil shale pressed into potassium bromide (KBr) pellets.

Solum et al.,<sup>25,26</sup> using solid-state <sup>13</sup>C NMR to characterize the Argonne Premium Coals, developed a protocol for determining 14 structural parameters as well as 8 other derived lattice parameters for each coal. These NMR parameters can be used in conjunction with the elemental composition to obtain other chemical structure parameters such as the number of aromatic carbons per cluster and the molecular weight of clusters and side chains. The procedure followed in obtaining the functional group components as well as the lattice parameters found wide application not only in coal structures but also in modeling devolatilization of coal structures, char structure, soot formation, and combustion deposits. The details for definition of these functional group and lattice parameters can be found in the appendices of Grant et al.<sup>27</sup> and Solum et al.<sup>26</sup> This NMR technique was previously applied to a demineralized Green River oil

shale from Colorado as well as to the solid pyrolysis residue from that demineralized kerogen by Hillier et al.<sup>4,6</sup> The papers by Hillier et. al.<sup>4,6</sup> presented the first data set that incorporated detailed chemical structural features as well as the lattice parameters for pyrolysis of oil shale-derived kerogen. However, since Hillier's work was sponsored by an industrial firm, the exact locations and sampling techniques to obtain the shales used in that study were not published. The samples used by Hillier were from rock samples on the ground at the mine mouth or from surface outcrops. Therefore, it is not clear that the samples were free from oxidation effects. The sample depths are also unknown.

In order to provide a more carefully designed set of samples for this study, ISCE and UGS obtained an appropriate sample core from the Utah Green River formation and then selected sections from that core. The data obtained in this study came from a carefully selected procedure to obtain multiple samples from different sections of the core with known depths and identification of the oil-bearing zone. From a chemistry standpoint, knowledge of the precise location and history of the sample is extremely important, which is justification for performing the experiments described in the current paper. This chapter presents data on the composition and yields of pyrolysis products from three demineralized samples of the Utah Green River oil shale core using a combination of <sup>13</sup>C NMR, GC/MS, and FTIR techniques. In addition to the solid-state <sup>13</sup>C NMR analysis of the pyrolyzed kerogen char samples obtained at different temperatures (in a manner similar to Hillier et al.<sup>4,6</sup>), liquid-state <sup>13</sup>C NMR analysis was performed on the associated tars collected during pyrolysis. This chapter is related to Chapter 2, which describes the solid-state NMR characteristics of the unreacted Green River oil shale from this core together with the corresponding demineralized oil shale kerogen and bitumen. The detailed NMR data presented here at different stages of pyrolysis for a well-characterized oil shale sample are unique and add to the understanding of the thermal decomposition of oil shale. Sample characterization of the demineralized kerogen was reported in Chapter 2.

## **Experiment Descriptions**

### ***Kerogen Retort***

A pyrolysis reactor was built to pyrolyze the demineralized oil shale and collect char and tar samples in sufficient quantity for further analysis (see Figure 4-1). This reactor is referred to as a kerogen retort and is described in detail by Hillier.<sup>4,5</sup> The kerogen retort was designed to mimic conditions (10 K/min) found in previous TGA experiments.<sup>6</sup>

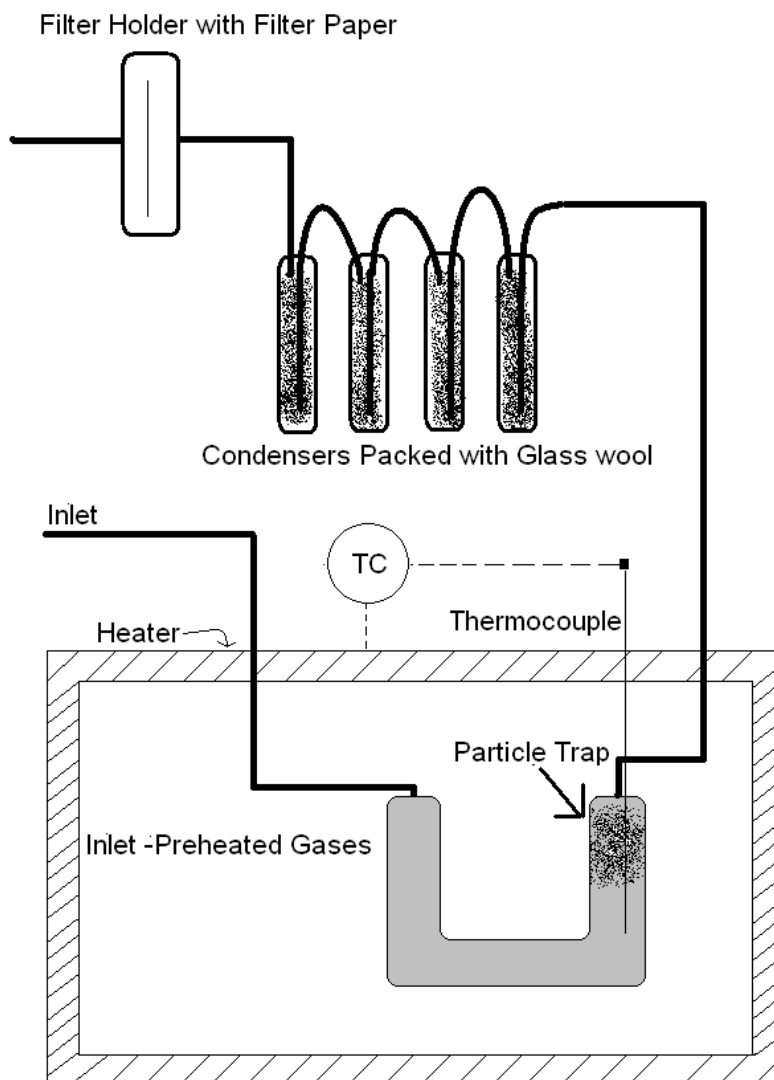


**Figure 4-1. Schematic of the kerogen retort used for generating chars and tars.**

The retort was made from  $\frac{3}{4}$ -in stainless steel tubing bent into a U-like shape as seen in Figure 4-1. The inlet was 3 ft of  $\frac{1}{4}$ -in copper tubing wrapped in a coil inside the heater, with additional tubing outside of the heater connected to a gas source. The inlet tubing inside the heater served to preheat the gases. The outlet of the heater was designed to allow for thermocouple access and was made of  $\frac{1}{4}$ -in stainless steel tubing. The kerogen particles were very light and easily entrained in the gas, so a glass wool plug was included in the outlet region of the reactor to prevent particles from becoming entrained and traveling into the condensers while allowing the vaporized tars and other gases to freely exit the furnace. The condensers were constructed by packing a fine glass wool into a test tube (2.5 cm diameter, 14 cm effective length) and using a rubber cork to close the top. Two holes were drilled into the cork through which  $\frac{1}{4}$ -in stainless steel tubing was tightly fitted. The inlet to each condenser was long enough to reach the bottom while the outlet was short. The gases entered and passed through the glass wool before exiting. The four condensers were immersed in a cooling bath (isopropanol and dry ice) to aid condensation. By cooling the condensers in a bath, the tars were collected on the glass

wool and were easily extracted via a dichloromethane wash. A filter holder with filter paper was included downstream of the condensers to verify that tars did not travel downstream. The filter turned brown in experiments where the combination of glass wool packing and temperature were insufficient to condense all the tars. Generally the exhaust gases were vented into a fume hood ventilation system, though in some experiments the outlet gases were directed into a collection bag for gas analysis.

Approximately 1 gram of sample, spread out inside the reactor tube, was used for each experiment. The gas used in this experiment was N<sub>2</sub>, which flowed at approximately 1 L/min. An additional experiment was conducted with He and the results did not differ from the N<sub>2</sub> experiments. The heating rate used in these experiments was 10 K/min. The retort was physically removed from the furnace once the final temperature was achieved, which cooled the retort and samples at approximately 100 K/min. The final temperature was kept below 525°C to prevent CO<sub>2</sub> release from the carbonates in the shale.

### ***Elemental Analysis***

The elemental analysis of the chars from the kerogen retort were performed at Huffman Laboratories in Golden, Colorado, and are reported in Table 4-1.

**Table 4-1. Elemental Analysis of the Chars from the Kerogen Retort.**

		Wt% Dry, ash-free				
	T(°C)	C	H	N	O by diff	S
<b>GR1.9</b>	300	78.85%	9.58%	2.90%	6.56%	2.11%
	375	81.25%	9.96%	3.09%	3.73%	1.98%
	410	80.38%	9.67%	3.13%	4.91%	1.93%
	445	81.57%	9.65%	3.42%	3.51%	1.85%
	495	85.16%	6.14%	5.42%	-1.28%	4.56%
<b>GR2.9</b>	425	80.44%	9.60%	3.05%	4.38%	2.52%
	445	82.65%	9.30%	3.42%	2.58%	2.04%
	475	83.40%	8.40%	4.04%	1.21%	2.95%
	525	86.80%	3.98%	5.89%	-3.76%	7.09%
<b>GR3.9</b>	400	79.77%	9.45%	2.91%	5.19%	2.68%
	434	80.84%	9.22%	3.12%	2.93%	3.89%
	450	81.22%	8.61%	3.46%	3.44%	3.27%
	460	82.64%	8.32%	3.78%	1.78%	3.48%
	470	82.31%	7.89%	3.96%	1.84%	3.99%
	490	82.50%	4.93%	5.22%	0.86%	6.49%
	525	82.64%	3.77%	5.52%	1.25%	6.81%

### ***<sup>13</sup>C NMR Analysis***

Solid-state <sup>13</sup>C NMR analysis was performed on the demineralized kerogen samples and the char remaining after kerogen pyrolysis in the kerogen retort. The liquid <sup>13</sup>C NMR data for the extracted bitumen is reported in Chapter 2 and by Solum et al.<sup>27</sup> The solid-state NMR analysis included careful integration of the characteristic chemical shift ranges in both the normal cross-polarization, magic angle spinning (CP/MAS) and the dipolar dephased data, as described by Solum and coworkers.<sup>25</sup> Approximately 120–250 mg of sample was required for this analysis. The method of Solum et al.<sup>25, 26</sup> was used to derive 14 structural elements plus 8 lattice

parameters derived from the structural elements. Lattice parameters derived for the pyrolyzed char samples include the number of attachments per aromatic cluster ( $\sigma+I$ ), the number of aromatic carbons per aromatic cluster ( $C$ ), and the number of aliphatic carbons in a side chain. Solum's method to determine the fraction of attachments that are bridges (i.e.,  $p_0$ ) for the unreacted kerogen samples was subject to large errors due to the large number of  $\text{CH}_3$  and  $\text{CH}_2$  groups in the sample. This may have been due to aliphatic chain branching resulting in more methyl terminating groups than could be accounted for without chain branching.

The tar samples from pyrolysis of the GR1, GR2, and GR3 kerogen concentrates at various temperatures were collected on glass wool and then extracted into methylene chloride- $d_2$  at BYU. Samples as received at the University of Utah had varying total volumes of solvent plus tar. Each sample was transferred to a 5 mm NMR tube with a screw cap and PTFE-lined septum to prevent solvent loss during data acquisition. The total volume was then adjusted to 0.7 mL either by adding methylene chloride- $d_2$  or by evaporating some of the solvent using a stream of dry  $\text{N}_2$ . All solution-state  $^{13}\text{C}$  NMR data were acquired using an Agilent Technologies Direct Drive 500 MHz spectrometer with a 5 mm switchable broadband probe equipped with z-axis pulsed field gradient coil and sample temperature control. The sample temperature was controlled at  $26^\circ\text{C}$  using a stream of dry  $\text{N}_2$  at 10 L/min. Two methods were used to acquire quantitative  $^{13}\text{C}$  spectra. The first method (called quantC in the following discussion) used the classical gated decoupling method to obtain decoupled spectra with NOE suppressed.<sup>29</sup> Typical acquisition parameters were: relaxation delay of 20 s, acquisition time of 2 s, 45 degree tip angle, 67,500 complex samples of the FID, and 22 hours total acquisition time. This method retains both protonated and non-protonated carbon resonances but sacrifices considerable sensitivity due to suppression of the NOE.

The second method (called quantD in the following discussion) used the Agilent-supplied QDEPT pulse sequence and quantdept macro,<sup>30</sup> as discussed in Chapter 2 for the analysis of bitumen. Typical acquisition parameters were: relaxation delay of 10 s, acquisition time of 4 s., 125,000 complex samples of the FID, 22 hours total acquisition time. These spectra were integrated using the standard Agilent VNMRJ software integration tools.

DEPT spectra were obtained using the standard Agilent QDEPT pulse sequence to differentiate among non-protonated  $\text{CH}$ ,  $\text{CH}_2$ , and  $\text{CH}_3$  carbons. The QDEPT sequence incorporates shaped broadband inversion pulses to obtain more uniform inversion of the carbon magnetization across the entire carbon chemical shift range. This sequence also retains resonances from non-protonated carbons, in contrast to the classical DEPT technique that suppresses non-protonated carbon resonances.

### ***GC/MS Analysis***

The mass spectrometer used was a TSQ 7000 triple quadrupole instrument manufactured by Finnigan. The inlet for most experiments was a Varian 3400 CX gas chromatograph (GC). The GC was operated in Splitless Injection mode utilizing a DB-1 microbore column manufactured by J&W Scientific. The column was a DB-1, 20 meter, 0.1 mm I.D. microbore, and had a 0.4 micron film. The temperature program for the GC method started at  $50^\circ\text{C}$  and 1 minute. Next the column was heated at 8 K/min to  $300^\circ\text{C}$  and held at that temperature for 15 minutes. The solvent used to bring the pyrolyzate into solution was dichloromethane. Additional details of the GC/MS system and technique are found in Hillier.<sup>4</sup>

### ***FTIR Analysis***

The FTIR instrument was a Bomem® MB-155 FTIR equipped with a 10 m multi-pass gas cell (Infrared Analysis, Inc). The IR beam source was a Globar IR source. All the spectra were acquired with a resolution of  $1\text{ cm}^{-1}$  and a spectral range of  $400\text{--}4000\text{ cm}^{-1}$  though they are presented with narrower ranges. The detector was liquid  $\text{N}_2$ -cooled and the detection limit of the FTIR was as low as 50 parts per billion (ppb) for certain types of gases (including ammonia, ethane, and ethylene). The detection limits for other gases are generally about 100 ppb.

FTIR experiments were performed to determine the nature of the species in the gas phase. The species of interest were the light hydrocarbons, carbon monoxide (CO), and methanol. The experiments were carried out by collecting all the effluent gas from the kerogen retort at three specific temperature ranges. These ranges were  $200\text{--}295^\circ\text{C}$ ,  $300\text{--}395^\circ\text{C}$ , and  $400\text{--}495^\circ\text{C}$ . These ranges were designed to span the early, middle, and late gas generation phases as seen on a TGA trace. The gases were collected by using a 100L Tedlar® gas sampling bag. The FTIR was prepared by purging the sample cell with  $\text{N}_2$  and the contents were pumped through the gas cell for a period of time to ensure a representative sample was present.

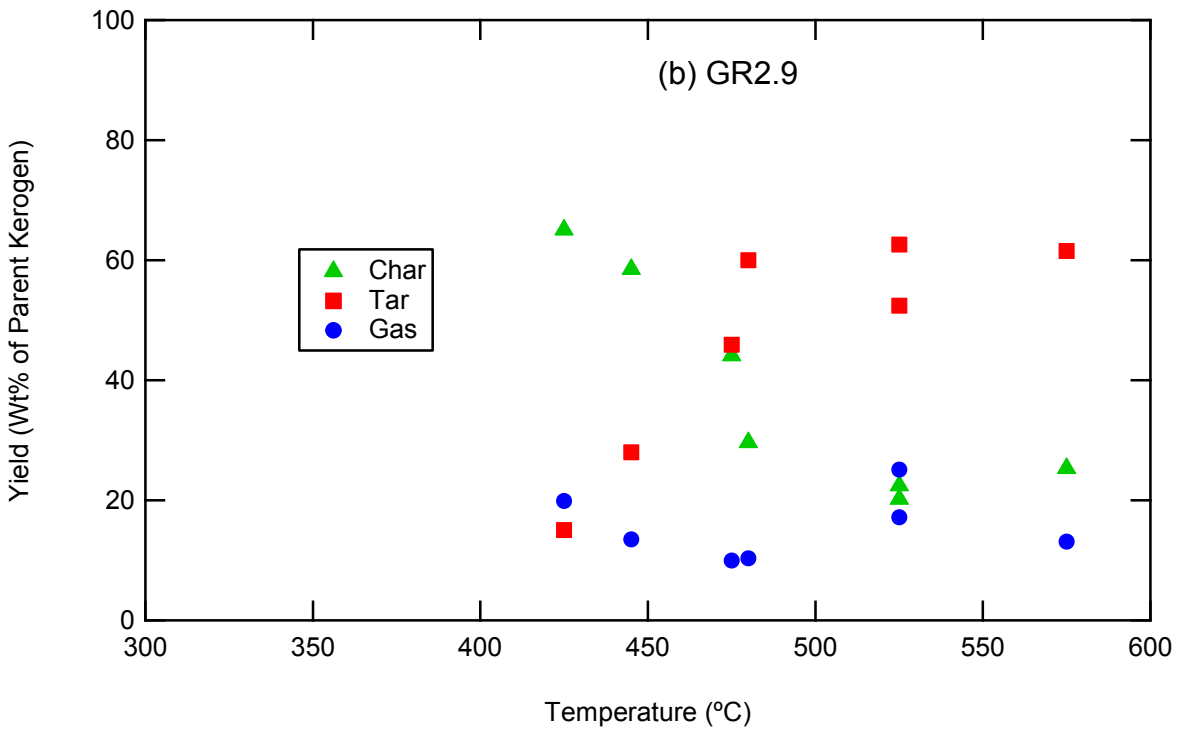
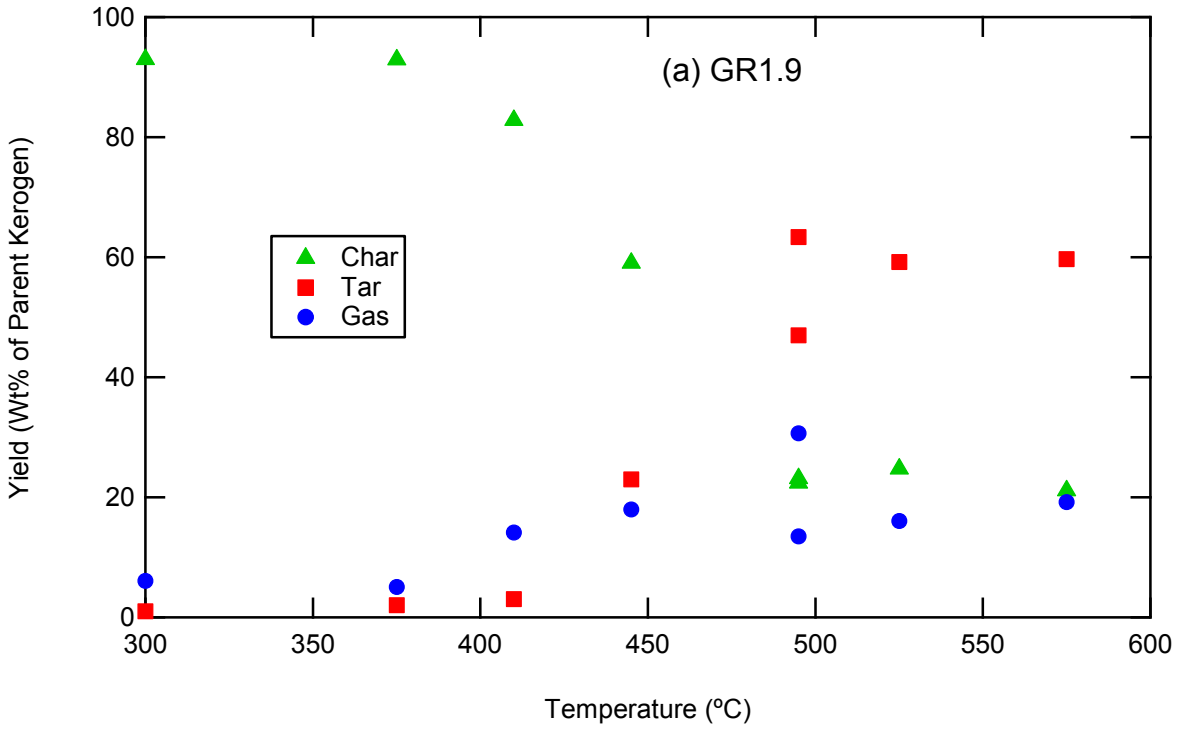
## **Results**

### ***Kerogen Retort Data***

Yields of tar, char, and light gas from the pyrolysis of the demineralized kerogen samples in the kerogen retort are shown in Figure 4-2 with tabulated values in Table 4-2. All of these data were obtained at a heating rate of 10 K/min. The experiments at  $575^\circ\text{C}$  likely were influenced by the decomposition of the carbonates in the shale minerals. Based on the data at  $525^\circ\text{C}$ , the total volatiles yields on a daf basis were 75.2, 78.7, and 83.8% for the GR1.9, 2.9, and 3.9 samples (see Tables 4-3 thru 4-5). Tar yields for the same samples were 59.2, 57.5, and 69%, respectively. The average uncertainty based on the difference from the mean for duplicate samples was 4 wt% for the tar yield and 1 wt% for the total volatiles yield. It is interesting that the daf yields of both tar and total volatiles were highest for the GR3.9 demineralized kerogen, since that kerogen was derived from the shale with the lowest Fischer oil assay and not the highest total organic content (see Table 2-2). However, the yields of bitumen and kerogen from the extraction process were not well known, so it is difficult to compare the yields in the kerogen retort to the Fischer assays.

**Table 4-2. Yields of Char, Tar, and Light Gas from the Kerogen Retort  
(wt% of parent kerogen)**

<b>GR1.9</b>			
<b>Temperature (°C)</b>	<b>Char</b>	<b>Tar</b>	<b>Light Gas</b>
300	92.9	1.0	6.1
375	92.9	2.0	5.1
410	82.8	3.0	14.1
445	59.0	23.0	18.0
495	22.4	47.0	30.6
495	23.2	63.3	13.5
525	24.8	59.2	16.1
575	21.1	59.7	19.2
<b>GR2.9</b>			
<b>Temperature (°C)</b>	<b>Char</b>	<b>Tar</b>	<b>Light Gas</b>
425	65.1	15.0	19.9
445	58.5	28.0	13.5
475	44.1	45.9	10.0
480	29.7	60.0	10.3
525	20.2	62.6	17.2
525	22.5	52.4	25.1
575	25.3	61.6	13.1
<b>GR3.9</b>			
<b>Temperature (°C)</b>	<b>Char</b>	<b>Tar</b>	<b>Light Gas</b>
400	75.7	8.1	16.2
434	68.5	8.7	22.8
450	57.2	19.2	23.6
460	46.8	44.1	9.1
460	46.9	40.0	13.1
470	43.7	43.3	13.0
470	45.6	50.5	3.8
490	18.4	63.5	18.1
525	16.7	69.5	13.9
525	15.7	68.6	15.7



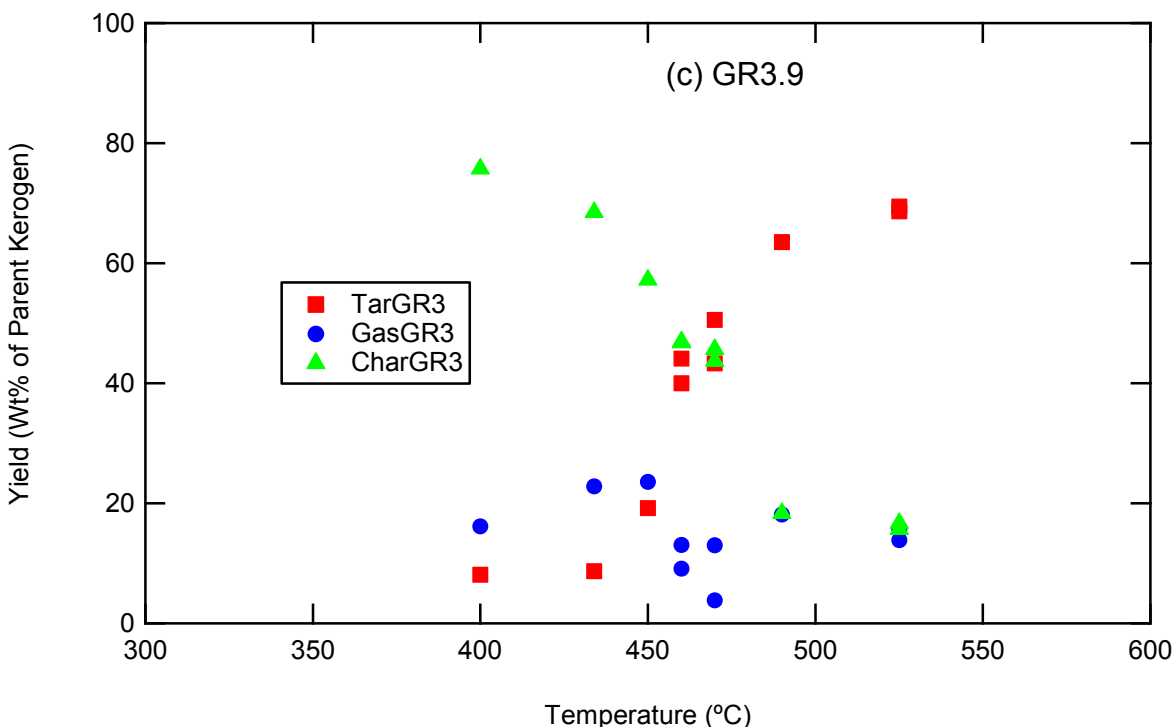


**Figure 4-2.** Yields of char, tar, and light gas from pyrolysis of (a) GR1, (b) GR2, and (c) GR3 in the kerogen retort in  $N_2$  at a heating rate of 10 K/min. Multiple data points at a given temperature represent repeat experiments.

### ***NMR Analysis of Char from Kerogen Retort***

The solid-state  $^{13}C$  NMR chemical structure data and derived lattice parameters for the kerogen concentrates and resulting chars produced in the kerogen retort are presented in Tables 4-3 thru 4-5. The  $^{13}C$  CP/MAS spectra for the chars from the GR3.9 sample are shown in Figure 4-3 and the 42  $\mu s$  dipolar dephased spectra are shown in Figure 4-4. The raw kerogen concentrate had a carbon aromaticity ( $f_a'$ ) of about 20% in all three kerogens, with 9–12 aromatic carbons per cluster ( $C$ ), and 11–12 aliphatic carbons per side chain (estimated by dividing the molecular weight by the appropriate number of carbons and hydrogens typical of aliphatic chains). This value is a little lower than that expected from the mass spectrometer analysis but is within a reasonable error. The fraction of aliphatic carbon ( $f_{al}$ ) in the three kerogen chars decreased from approximately 76% to as low as 8% during pyrolysis, as shown in Figures 4-4 and 4-5 (as well as Tables 4-3 thru 4-5), with a corresponding increase in the carbon aromaticity. The decrease in aliphatic carbon was very similar to the decrease in mass due to devolatilization, as shown by the  $m/m_0$  curve in Figure 4-5. All three kerogen chars (GR1, GR2, and GR3) showed very similar trends in the changes in aromaticity and aliphatic carbon with temperature; the bulk of the changes occurring in a narrow temperature window, beginning to change at 425°C, changing rapidly by 475°C, and finishing by about 525°C. The high aromaticity in kerogen chars above 500°C is similar to the high aromaticity observed in spent oil shales observed by Miknis et al.<sup>20</sup>

The increase in aromaticity seen in Figure 4-5 is not merely due to the effect of losing aliphatic carbon. The average number of aromatic carbons per cluster ( $C$ ) increases from roughly 10 to about 20, as illustrated in Figure 4-6. This corresponds to an average growth in the number of aromatic rings per cluster from 2 to 5. The number of attachments per cluster also increases

from about 5 to 8, meaning that some crosslinking has occurred. The approximate average length of the aliphatic side chains for these three samples,  $f_{al}/f_a^S$  (half of a bridge or a side chain)<sup>31</sup> decreases from about 11 at room temperature to less than 1 at the highest temperatures. The parameter  $f_a^S$  also includes biaryl zero mass bridges which become more important at the higher temperatures or for higher rank materials; the quantity of biaryl bridges is not well understood. The molecular weight per cluster of the chars were determined in conjunction with the elemental analysis of the chars.

**Table 4-3. Carbon Structural Parameters Determined from <sup>13</sup>C NMR Spectroscopy for Demineralized Kerogen (GR1.9) and Resulting Chars Collected at Different Temperatures (at a Heating Rate of 10 K/min).**

<i>Structural Parameter</i>	<b>GR1.9</b>	<b>300°C</b>	<b>375°C</b>	<b>410°C</b>	<b>445°C</b>	<b>495°C</b>
aromatic carbon, $f_a = f_a^A + f_a^C$	0.24	0.23	0.28	0.28	0.35	0.73
carbonyl, $f_a^C$	0.04	0.04	0.03	0.01	0.03	0.04
aldehydes and ketones, $f_a^O$	0.01	0.02	0.015	0.005	0.01	0.01
acids and esters, $f_a^{OO}$	0.03	0.02	0.015	0.005	0.02	0.03
aromatic carbon, carbonyl subtracted, $f_a^A$	0.2	0.19	0.25	0.27	0.32	0.69
protonated aromatic carbon, $f_a^H$	0.06	0.05	0.08	0.09	0.12	0.11
nonprotonated aromatic carbon, $f_a^N = f_a^P + f_a^S + f_a^B$	0.14	0.14	0.17	0.18	0.2	0.58
aromatic carbon with oxygen attachment (phenolic), $f_a^P$	0.03	0.03	0.04	0.03	0.04	0.08
aromatic carbon with alkyl attachment, $f_a^S$	0.07	0.06	0.08	0.07	0.1	0.19
aromatic bridgehead and inner carbon $f_a^B$	0.04	0.05	0.05	0.08	0.06	0.31
aliphatic carbon, $f_{al}$	0.76	0.77	0.72	0.72	0.65	0.27
aliphatic CH and CH <sub>2</sub> , $f_{al}^H$	0.65	0.66	0.63	0.61	0.54	0.19
aliphatic CH <sub>3</sub> and nonprotonated carbon, $f_{al}^*$	0.11	0.11	0.09	0.11	0.11	0.08
aliphatic with oxygen attachment, $f_{al}^O$	0.0	0.01	0.01	0.01	0.01	0.01
aromatic bridgehead carbons, $\chi_b$	0.200	0.263	0.2	0.296	0.188	0.449
average number of carbons per cluster, $C$	10	12.6	10	14.4	9.6	21.9
total attachments per cluster, $\sigma + l$	5	6	4.8	5.3	4.2	8.4
fraction of intact bridges per cluster, $p_0$	-0.1	-0.22	0.25	-0.01	0.21	0.7
bridges and loops per cluster, $B.C.$	--	--	1.2	--	0.9	5.9
side chains per cluster, $S.C.$	--	--	3.6	--	3.3	2.5
molecular weight per cluster, $MW_{cl}$	776	1010	591	797	442	448
molecular weight per side chain, $m_s$	131	143	98	117	77	22
Ratio $f_{al}/f_a^S$	10.86	12.83	9.00	10.29	6.50	1.42
Mass Release (wt% of parent kerogen)	0.0%	7.1%	7.1%	17.2%	41.0%	77.6%

\* $p_0$  for the kerogen has a large error due to high quantities of CH<sub>2</sub>.

Note: Italicized symbols are the same as used by Solum et al.<sup>25, 26</sup>

**Table 4-4. Carbon Structural Parameters Determined from  $^{13}\text{C}$  NMR Spectroscopy for Demineralized Kerogen (GR2.9) and Resulting Chars Collected at Different Temperatures (at a heating rate of 10 K/min).**

<i>Structural Parameter</i>	<b>GR2.9</b>	<b>375°C</b>	<b>425°C</b>	<b>445°C</b>	<b>475°C</b>	<b>525°C</b>
aromatic carbon, $f_a = f_a^O + f_a^C$	0.23	0.23	0.37	0.4	0.53	0.92
carbonyl, $f_a^C$	0.05	0.02	0.02	0.03	0.09	0.11
aldehydes and ketones, $f_a^O$	0.02	0.01	0.01	0.01	0.05	0.04
acids and esters, $f_a^{OO}$	0.03	0.01	0.01	0.02	0.04	0.07
aromatic carbon, carbonyl subtracted, $f_a^I$ ,	0.18	0.21	0.35	0.37	0.44	0.81
protonated aromatic carbon, $f_a^H$	0.06	0.06	0.11	0.12	0.1	0.17
nonprotonated aromatic carbon, $f_a^N = f_a^P + f_a^S + f_a^B$	0.12	0.15	0.24	0.25	0.34	0.64
aromatic carbon with oxygen attachment (phenolic), $f_a^P$	0.03	0.03	0.05	0.05	0.08	0.14
aromatic carbon with alkyl attachment, $f_a^S$	0.06	0.06	0.1	0.11	0.15	0.21
aromatic bridgehead and inner carbon $f_a^B$	0.03	0.06	0.09	0.09	0.11	0.29
aliphatic carbon, $f_{al}$	0.77	0.77	0.63	0.6	0.47	0.08
aliphatic CH and CH <sub>2</sub> , $f_{al}^H$	0.66	0.67	0.52	0.5	0.37	0.04
aliphatic CH <sub>3</sub> and nonprotonated carbon, $f_{al}^*$	0.11	0.1	0.11	0.1	0.1	0.04
aliphatic with oxygen attachment, $f_{al}^O$	0.01	0.01	0.02	0.01	0.02	0.01
aromatic bridgehead carbons, $\chi_b$	0.167	0.286	0.257	0.243	0.25	0.358
average number of carbons per cluster, $C$	9	13.8	12.3	11.7	12	17.8
total attachments per cluster, $\sigma + l$	4.5	6	5.4	5	6.2	7.6
fraction of intact bridges per cluster, $p_0$	-0.22	-0.1	0.27	0.38	0.57	0.89
bridges and loops per cluster, $B.C.$	--	--	1.5	1.9	3.5	6.8
side chains per cluster, $S.C.$	--	--	3.9	3.1	2.7	0.8
molecular weight per cluster, $MW_{cl}$	775	--	525-	460	393	304
molecular weight per side chain, $m_\delta$	148	--	69	63	40	11
Ratio $f_{al}/f_a^S$	12.83	12.83	6.30	5.45	3.13	0.38
Mass Release (wt% of parent kerogen)	0.0%	n.a.	34.9%	41.5%	55.9%	78.7%

\* $p_0$  for the kerogen has a large error due to high quantities of CH<sub>2</sub>.

Note: Italicized symbols are the same as used by Solum et al.<sup>25, 26</sup>

**Table 4-5. Carbon Structural Parameters Determined from  $^{13}\text{C}$  NMR Spectroscopy for Demineralized Kerogen (GR3.9) and Resulting Chars Collected at Different Temperatures (at a heating rate of 10 K/min).**

<i>Structural Parameter</i>	GR3.9	400°C	430°C	434°C	450°C	460°C	470°C	490°C	525°C
aromatic carbon, $f_a = f_a^H + f_a^C$	0.24	0.32	0.38	0.39	0.42	0.47	0.51	0.8	0.87
carbonyl, $f_a^C$	0.04	0.03	0.04	0.03	0.04	0.04	0.03	0.07	0.06
aldehydes and ketones, $f_a^O$	0.01	0.01	0.02	0.01	0.02	0.02	0.01	0.03	0.02
acids and esters, $f_a^{OO}$	0.03	0.02	0.02	0.02	0.02	0.02	0.02	0.04	0.04
aromatic carbon, carbonyl subtracted, $f_a^I$	0.2	0.29	0.34	0.36	0.38	0.43	0.48	0.73	0.81
protonated aromatic carbon, $f_a^H$	0.05	0.09	0.13	0.14	0.11	0.13	0.12	0.15	0.16
nonprotonated aromatic carbon, $f_a^N = f_a^P + f_a^S + f_a^B$	0.15	0.2	0.21	0.22	0.27	0.3	0.36	0.58	0.65
aromatic carbon with oxygen attachment (phenolic), $f_a^P$	0.03	0.04	0.04	0.04	0.04	0.04	0.05	0.08	0.09
aromatic carbon with alkyl attachment, $f_a^S$	0.07	0.09	0.11	0.1	0.11	0.12	0.14	0.18	0.22
aromatic bridgehead and inner carbon, $f_a^B$	0.05	0.07	0.06	0.08	0.12	0.14	0.17	0.32	0.34
aliphatic carbon, $f_{al}$	0.76	0.68	0.62	0.61	0.58	0.53	0.49	0.2	0.13
aliphatic CH and $\text{CH}_2$ , $f_{al}^H$	0.63	0.57	0.53	0.51	0.46	0.41	0.37	0.12	0.08
aliphatic $\text{CH}_3$ and nonprotonated carbon, $f_{al}^*$	0.13	0.11	0.09	0.1	0.12	0.12	0.12	0.08	0.05
aliphatic with oxygen attachment, $f_{al}^O$	0	0.01	0	0.01	0.01	0.01	0.01	0.02	0.03
aromatic bridgehead carbons, $\chi_b$	0.25	0.241	0.176	0.222	0.316	0.326	0.354	0.438	0.42
average number of carbons per cluster, $C$	12	11.6	9.3	10.8	15.6	16.1	17.6	21.4	20.6
total attachments per cluster, $\sigma + 1$	5.9	5.2	4.1	4.2	6.3	5.9	7	7.6	7.9
fraction of intact bridges per cluster, $p_0$	-0.3	0.15	0.4	0.29	0.2	0.25	0.37	0.69	0.84
bridges and loops per cluster, $B.C.$	--	0.8	1.6	1.2	1.3	1.5	2.6	5.2	6.6
side chains per cluster, $S.C.$	--	4.4	2.5	3	5	4.4	4.4	2.4	1.3
molecular weight per cluster, $MW_{cl}$	946	602-		446	607	544	535	427	370
molecular weight per side chain, $m_\delta$	135	88		74	66	59	46	22	15
Ratio $f_{al}/f_a^S$	10.86	7.56	5.64	6.10	5.27	4.42	3.50	1.11	0.59
Mass Release (wt% of parent kerogen)		24.3%	n.a.	31.5%	42.8%	53.2%	55.3%	81.6%	83.8%

\* $p_0$  for the kerogen has a large error due to high quantities of  $\text{CH}_2$ .

Note: Italicized symbols are the same as used by Solum et al.<sup>25, 26</sup>

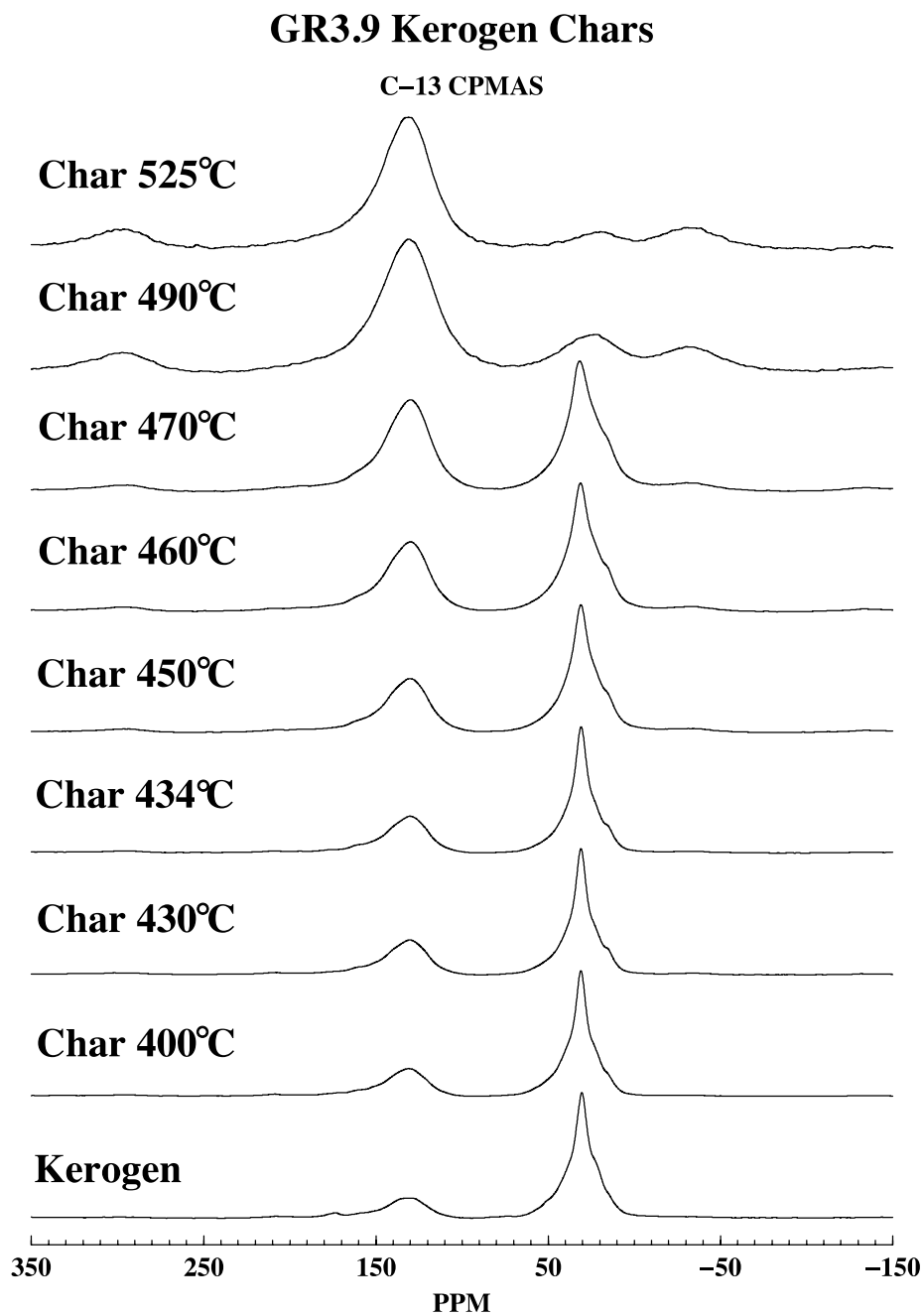


Figure 4-3. CP/MAS spectra of the GR3.9 kerogen concentrate and chars made from the concentrate. The spectra were taken with a 3 ms contact time and 1 s pulse delay.

## GR3.9 Kerogen Chars

C-13 CP/MASDD tau=42 us

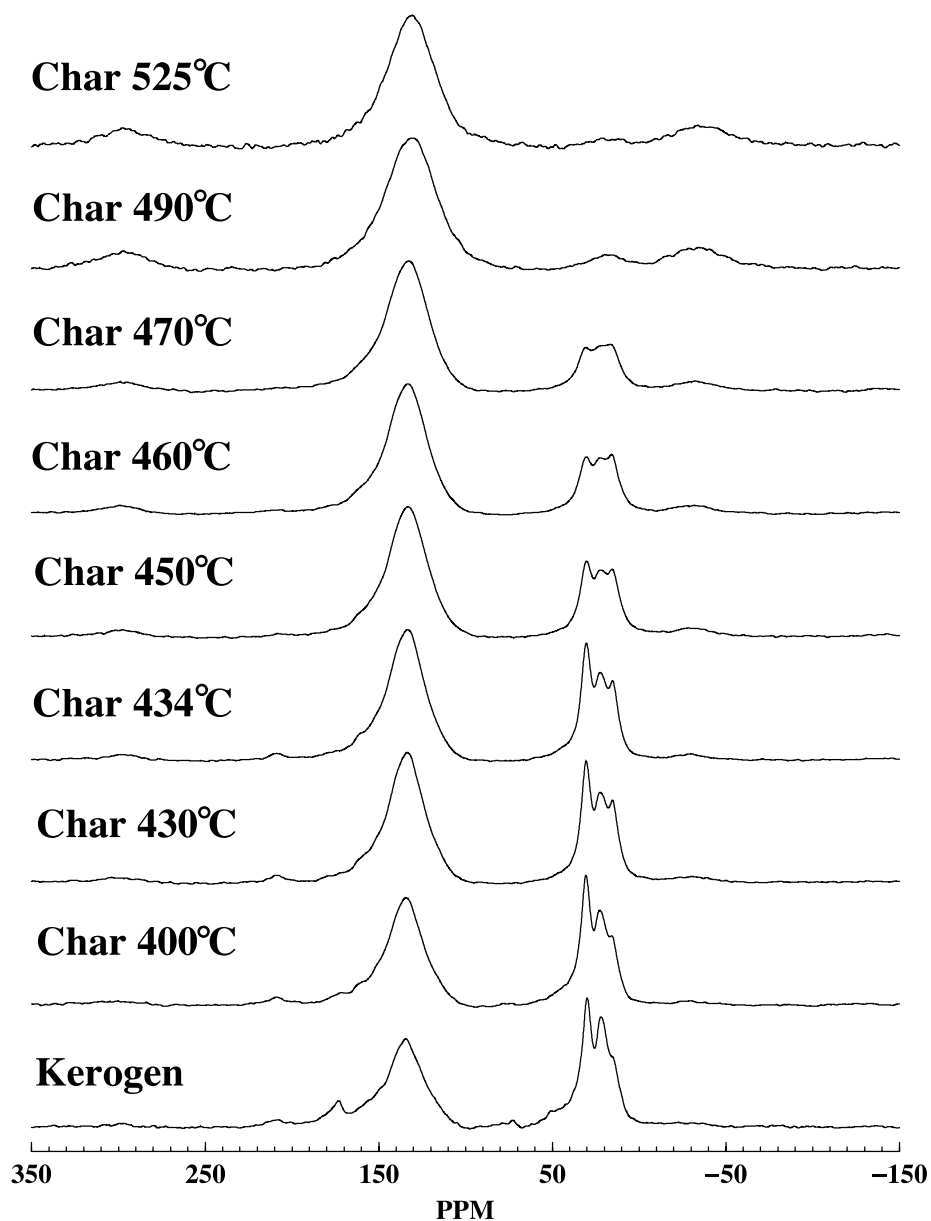


Figure 4-4. CP/MAS dipolar dephased spectra of the GR3.9 kerogen concentrate and chars made from the concentrate. The spectra were taken with a dephasing time of 42  $\mu$ s, a 1 s pulse delay and a 3 ms contact time. Only nonprotonated, methyl, and highly motional carbons remain.

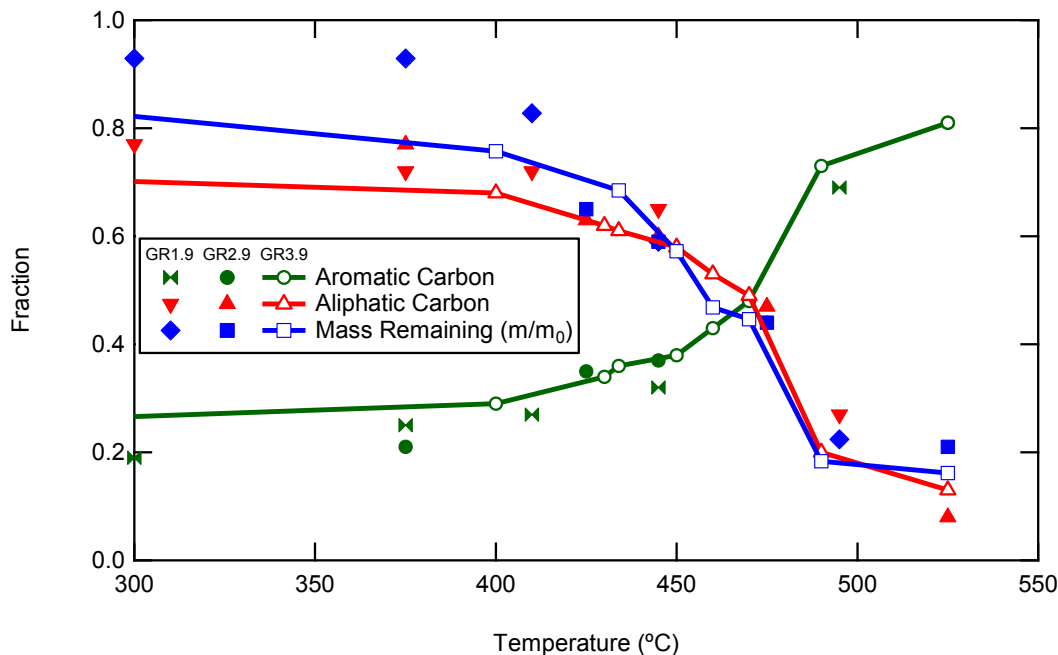


Figure 4-5. Aromatic and aliphatic carbon fractions for the kerogen chars formed at 10 K/min in the kerogen retort. Solid lines are drawn through the GR3.9 data with open symbols. Data below 300°C are given in Tables 4-3 thru 4-5.

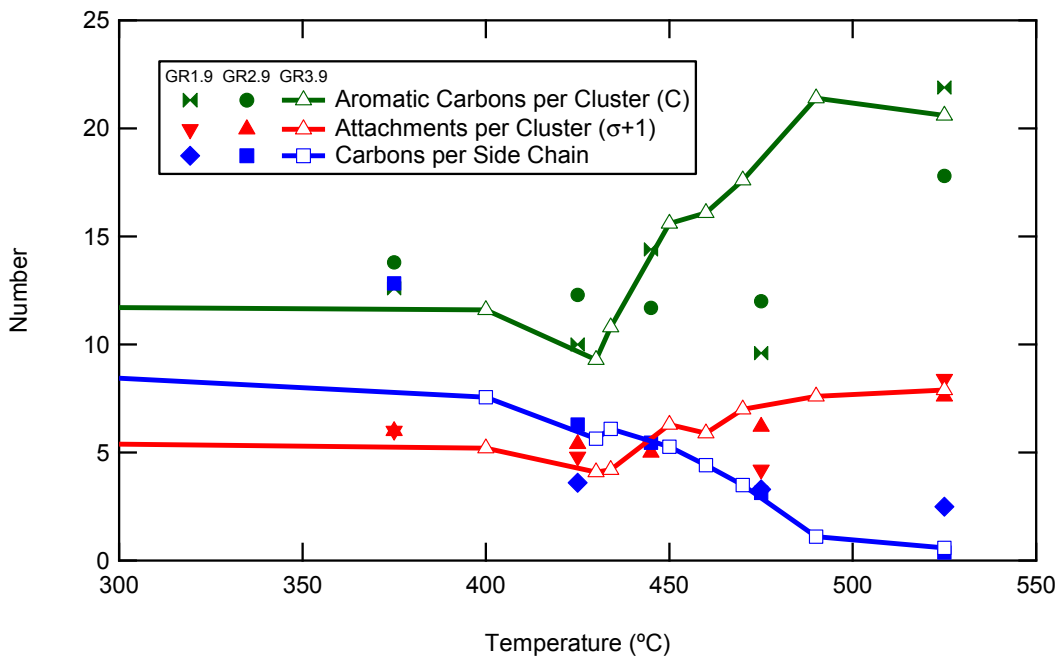


Figure 4-6. Aromatic carbons per cluster (C), attachments per cluster ( $\sigma+1$ ), and estimated carbons per side chain in kerogen chars. Solid lines are drawn through the GR3.9 data with open symbols. Data below 300°C are given in Tables 4-3 thru 4-5.

### ***Solution-state $^{13}\text{C}$ NMR Analysis of Tars from the Kerogen Retort***

The quantC and quantD carbon spectra of the various tar samples condensed from the effluent of the kerogen pyrolysis experiments are qualitatively very similar but differ somewhat in the relative amounts of the various major components. An example of the GR2 pyrolysis tar data dissolved in DCM is shown in Figure 4-7 for the GR2.9 kerogen pyrolyzed at 445°C. Spectra A and B were obtained using quantC and quantD experimental protocols, respectively. At 19%, the aromatic carbon content of this tar is similar to that of the unreacted kerogen concentrate. Within experimental error all of the tars have approximately the same aromatic carbon content. In addition, the two carbon resonances observed at 114 and 140 ppm clearly delineate the terminal alkene structures that are present in the pyrolysis tar. These peaks were never observed in the bitumen spectra.<sup>27</sup> However, these two peaks in the aromatic region are consistent with the presence of terminal alkene functional groups. These two functional groups are also consistent with the alkane/alkene pairs that are found in the GC/MS data.

Figure 4-8 presents the aliphatic region of a set of DEPT spectra of the tar from GR2.9 containing resonances of various carbons according to the number of attached protons. Note that the scale has been adjusted so that the intense methylene resonance at 30.1 ppm is off-scale to permit closer examination of the other resonances. The letters and sub-numbers in Figure 4-8 are explained in Table 4-6. For instance, A<sub>n</sub> represents the n<sup>th</sup> carbon in a straight chain normal paraffin. The letters B, C, D, E, and P represent different types of carbon branching found in isoprenes, etc. The sub-term C<sub>m</sub> is representative of branching points of various lengths.

Due to various instrumental limitations, cancellation of one carbon type from the spectrum of another carbon type is not perfect. Note, for example, that the methyl resonance at 14.5 ppm appears at diminished intensity in the methylene spectrum. Although the DEPT spectra

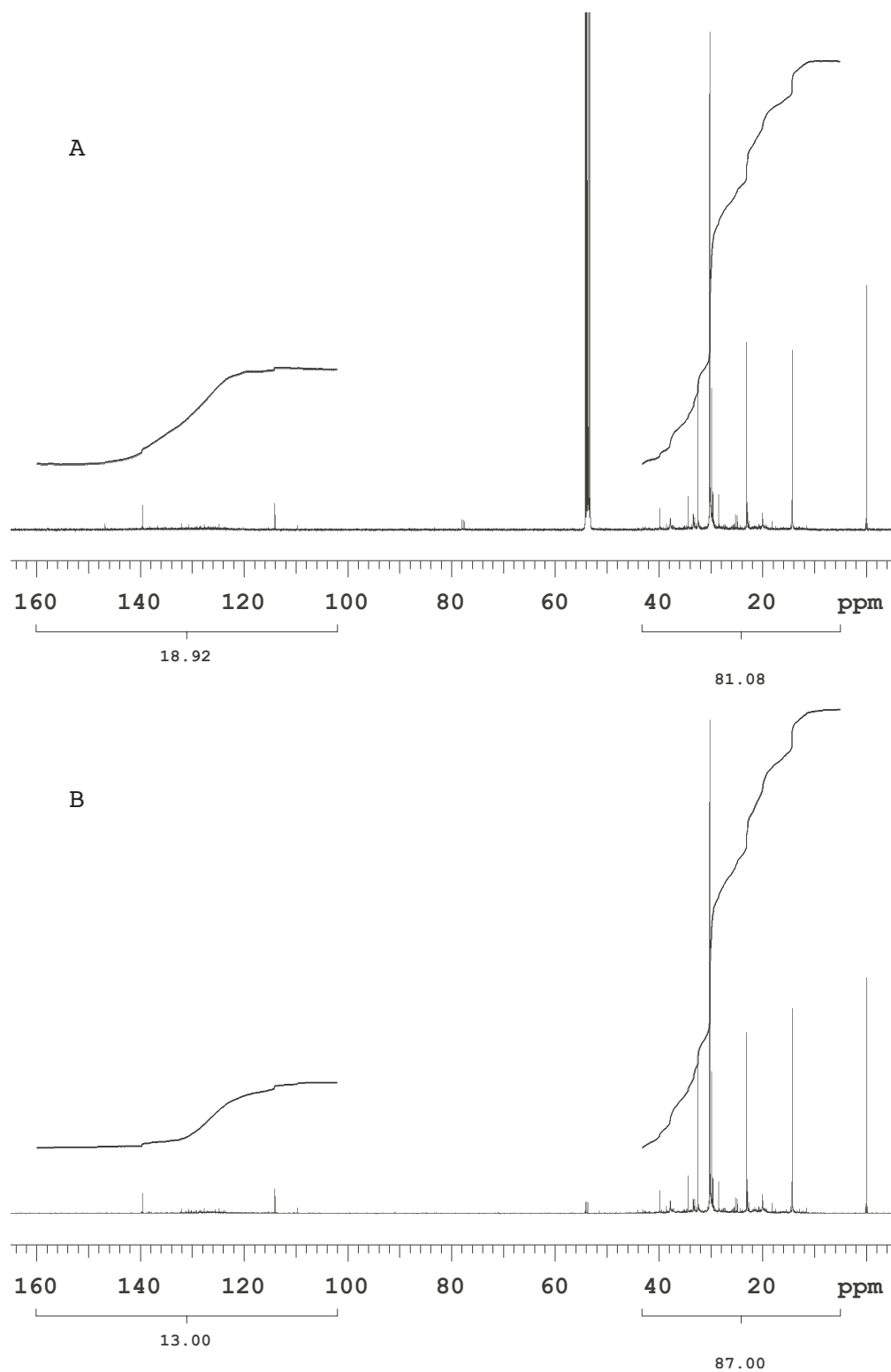
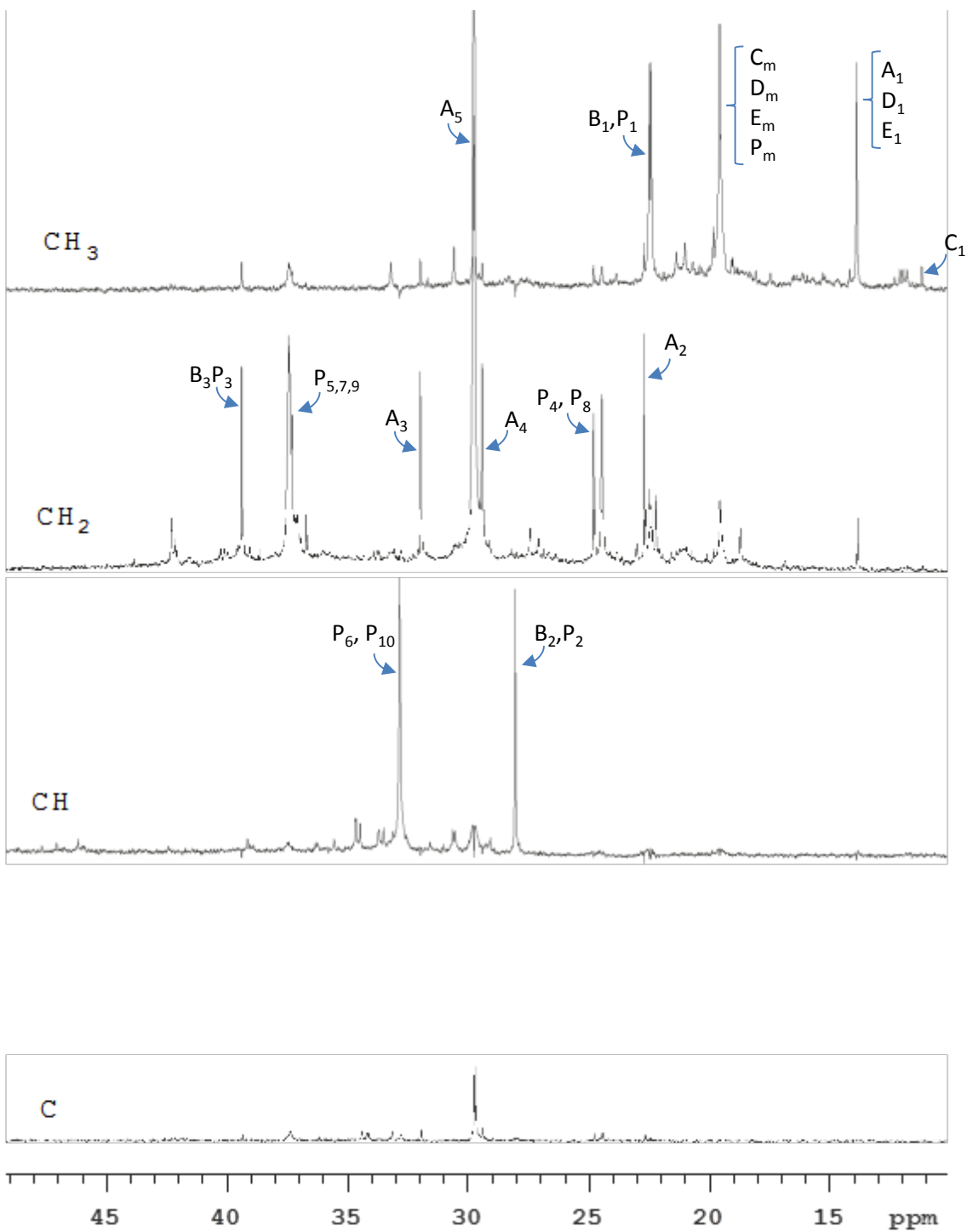


Figure 4-7.  $^{13}\text{C}$  spectra of tar from GR2 kerogen pyrolyzed at 445°C dissolved in DCM. (A) quantC and (B) quantD experiments.

are not strictly quantitative, some sense of the relative amounts of the various carbon types can be gleaned by comparing the various spectra. Clearly, methylenes are the dominant type, with methyls and methines at lower abundance. Since methines indicate a branch point in an aliphatic chain, it is evident that there are relatively few such branch points in these tars. The weak methyl resonances upfield from 14.5 ppm arise from the terminal methyl of chains where C3 is a methine. As confirmed by the integrals in Figure 4-7, these terminal methyls are much less abundant than those of the long chain n-alkyl moieties. The spectrum representing quaternary carbons shows essentially no resonances. All of the resonances seen in this particular linear combination of the raw data correspond to strong resonances of other types and have been attributed to imperfect cancelation of these other types. Resonances from non-protonated carbons are diminished in intensity by a factor of about four relative to those of protonated carbons because non-protonated carbons receive no transfer of proton magnetization. Nevertheless, it is clear that there are very few aliphatic non-protonated carbons in this sample. Since this is the case, one can compare the quantC (all aromatic carbons) and quantD (only protonated carbons) integrals of Figure 4-7. Assuming that the integrals of the aliphatic region represent the same number of carbons in both cases, one can normalize the integrals of the aromatic region as below to find that 64% of the aromatic carbons are protonated.

$$\frac{13.00 \times 81.08}{18.92 \times 87.00} \times 100 = 64.03\% \quad (1)$$

The S/N in the aromatic region is low making the experimental error rather high, but one can confidently say that a little over half of the aromatic carbons are protonated.



**Figure 4-8. Aliphatic region of the DEPT spectrum of GR2.9 tar dissolved in DCM. Peak labels are explained in Table 4-6.**

**Table 4-6. Explanation of Peak Labels in Figures 4-8 and 4-9  
(as suggested by Dalling et al.<sup>32</sup>)**

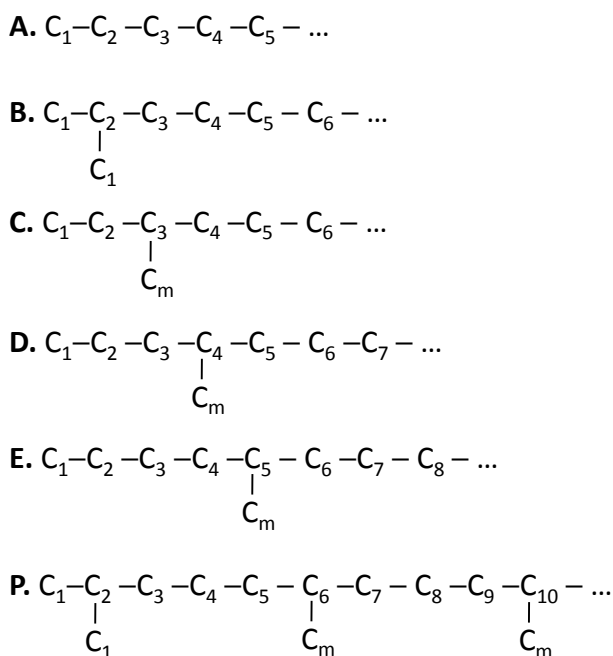
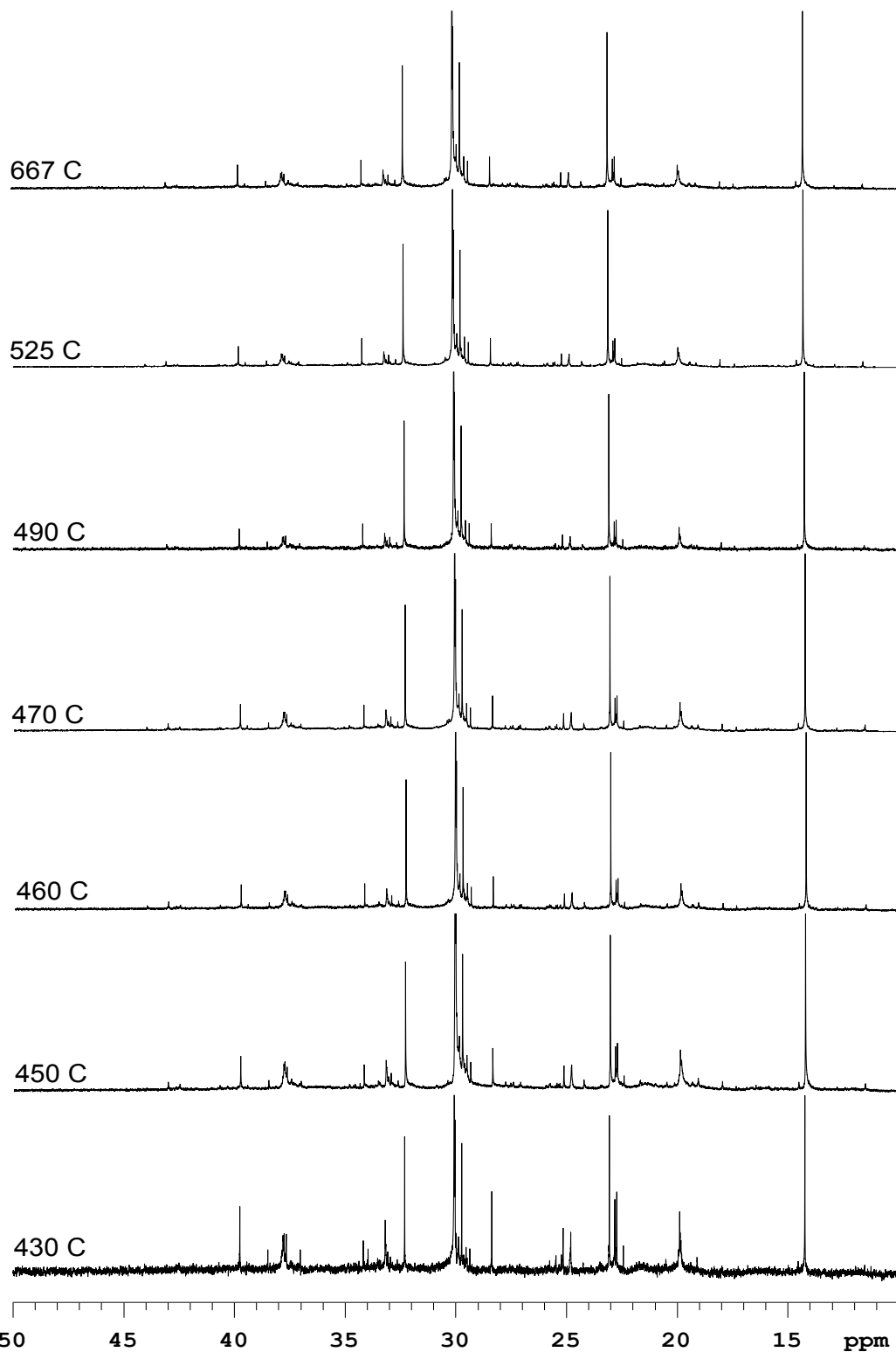


Figure 4-9 shows the aliphatic region of the QuantD spectra of the GR3 kerogen tars. All of the spectra are dominated by n-alkyl chains. The intense resonances near 30.1 ppm arise from all the carbons located at five or more carbons from the methyl end of each n-alkyl chain. The high intensity of this resonance compared to all others (e.g. Figure 4-7) shows that all of these tars contain a significant amount of long chain normal hydrocarbons. The corresponding methyl is located at 14.3 ppm with carbons 2,3, and 4 located at 23.1, 32.3, and 29.8 ppm respectively. Note that the peaks for carbons 1–4 have similar intensities and, in a long n-alkyl chain, each would represent two carbons (one from each end of the molecule). Since the ratio of the intensity of the peak at 30.1 ppm to the average intensity of the first four peaks in the chain is about four (i.e., 8 carbons), one can assert that the average length of these normal chains is about 16 carbons. This result is consistent with the GC/MS results (see below). Of course, these n-alkyl chains can be attached to aromatic centers or have alkyl side-chains, but as long as the n-alkyl part of the molecule is 10 carbons or longer, the resonances from carbons at least five carbons removed from the aromatic ring or branch point will contribute to the resonances discussed above. This possibility constitutes a source of systematic error in the determination of the chain length. Although the same resonances appear in both the bitumen (see Reference 1) and the kerogen pyrolysis spectra (see Figure 4-9), intensities for the condensate resonances corresponding to carbons other than the n-alkyl carbons are much lower than for corresponding resonances in the bitumens. This is true for all the pyrolysis temperatures studied, but there is a definite trend toward a higher proportion of n-alkyl carbons with increasing maximum pyrolysis temperature as shown in Figure 4-9.



**Figure 4-9. QuantD spectra of GR3 kerogen pyrolysis tars pyrolyzed at various maximum temperatures. Each spectrum is scaled so that the CH<sub>3</sub> resonance at 14.3 ppm is near full-scale. The intense CH<sub>2</sub> resonance at 30.1 ppm is off-scale.**

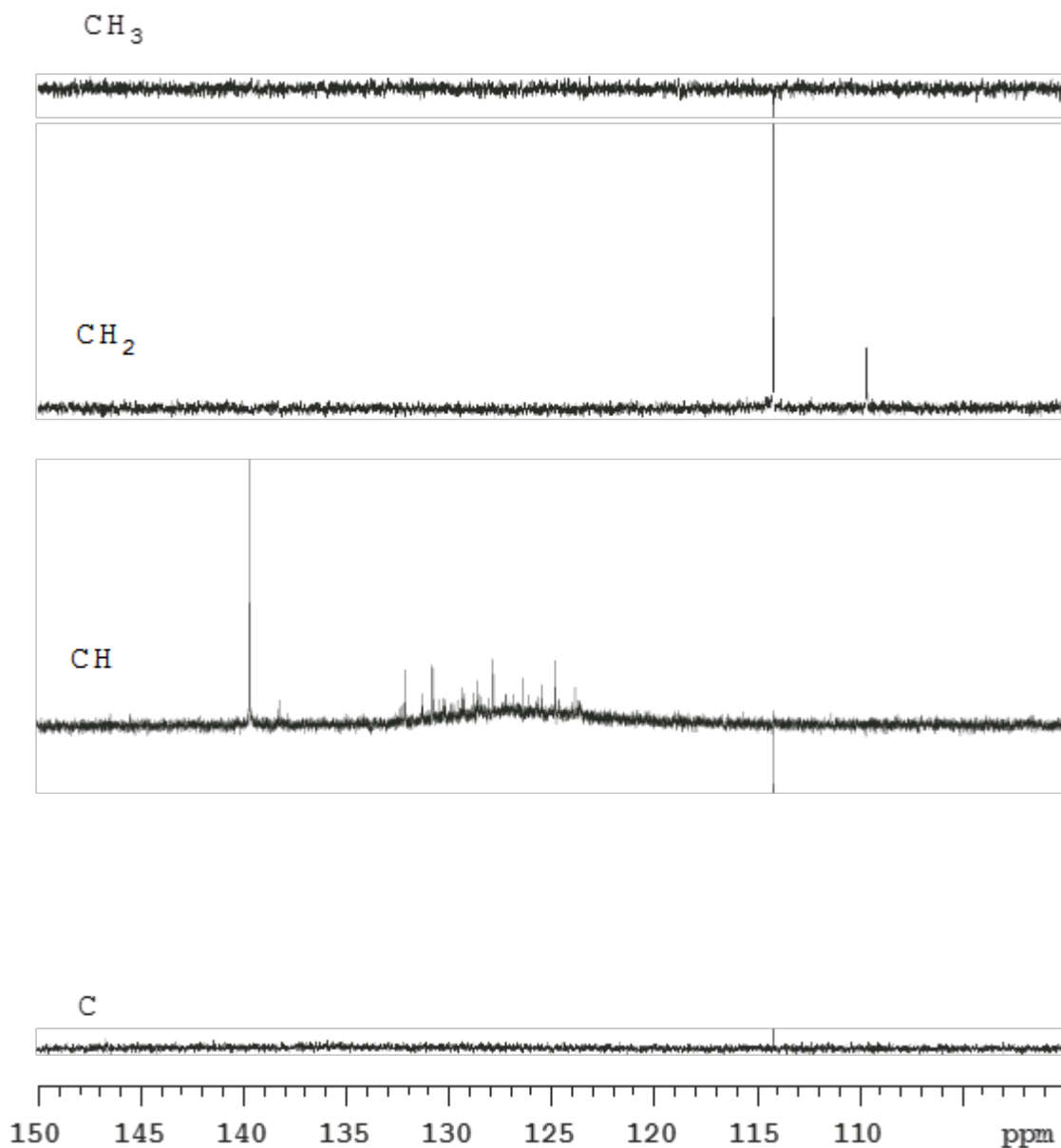


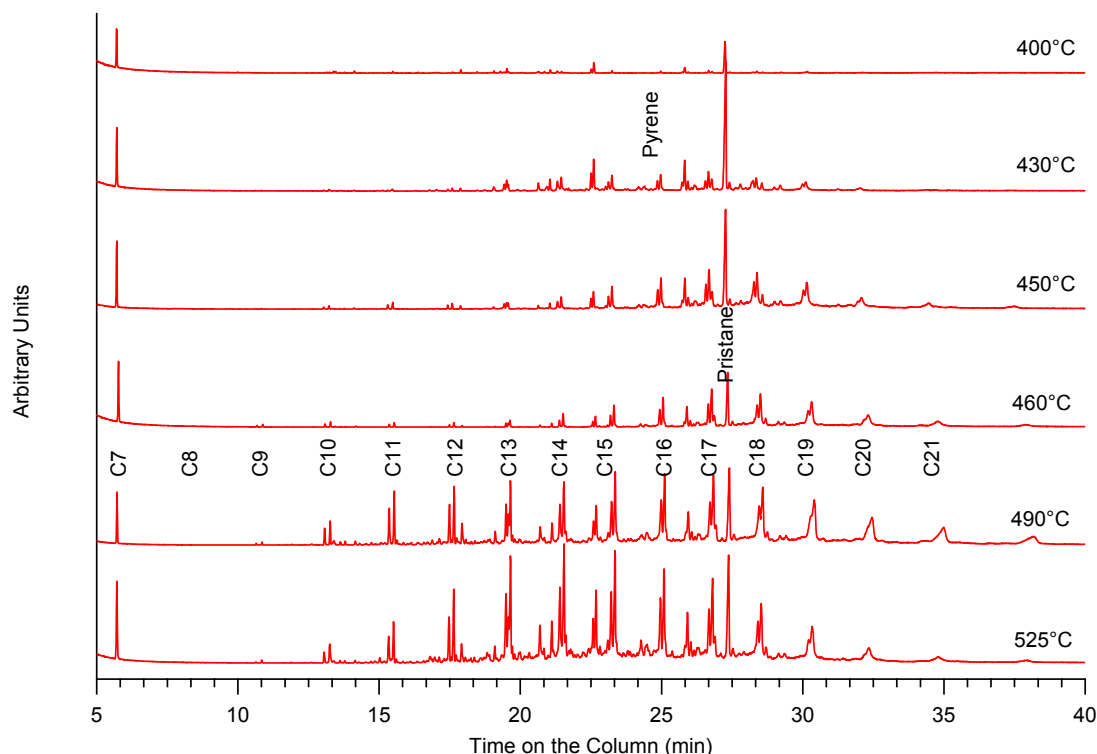
Figure 4-10. Aromatic region of the DEPT spectrum of tar from GR2 kerogen pyrolyzed at 445°C.

Figure 4-10 shows the aromatic region of the DEPT spectrum of the GR2 kerogen pyrolyzed at 445°C. The CH<sub>2</sub> at 114 ppm and the CH at 140 ppm were seen in all of the pyrolysis tars but were not seen in the corresponding bitumen spectra (see Solum et al.<sup>27</sup>). These two resonances arise from C1 and C2, respectively, of n-alkenes with chain length of at least 7. These functional groups are consistent with alkane/alkene pairs that are found in the GC/MS data (see below). It is presumed that they arise from thermal cleavage of n-alkyl groups from aromatic rings during pyrolysis. These two resonances are present in every pyrolysis experiment and seem to have little dependence on maximum pyrolysis temperature. Long chain di-alkenes (e.g. 1,7-octadiene) would also give rise to these two characteristic resonances, but molecules of this type were not detected by GC/MS.

### GC/MS Analysis

Gas chromatograms of the tars generated in the kerogen retort from the GR3.9 kerogen sample collected at various temperatures are presented in Figure 4-11; chromatograms of the other samples show similar results. Prominent peaks from the gas chromatograms were identified with the mass spectrometer using fragmentation patterns and are listed in Table 4-7. The lightest identified molecule was 1-heptene, which was eluted from the GC column only shortly after the solvent. The heaviest molecule identified was tetracosane ( $C_{24}H_{50}$ ), which was detected nearly 50 minutes after injection. The remaining molecules were primarily alkane/1-alkene pairs between 7 and 24 carbons in length, with the largest peaks observed for chains with 15 to 17 carbons. A notable exception to the alkane/alkene pairs was aromatic pyrene which was emitted about halfway through the process. Pyrene is a common species found in residues from incomplete combustion processes.

These tars were collected as a cumulative sample, so any compounds generated at lower temperatures would also be present at higher temperature in addition to the compounds generated at higher temperatures. Therefore, any compounds present in the 375°C sample should also be present in the 525°C sample, but some compounds present in the 525°C may not be present in the 375°C sample. The main features of tars collected at all temperatures were similar although more small, irresolvable peaks were present at higher temperatures. No significant differences in the composition of the tars from the three demineralized kerogen samples were observed in the GC/MS data.



**Figure 4-11. Gas chromatogram of components of GR 3.9 tar collected at various temperatures during pyrolysis (10 K/min).**

**Table 4-7. Selected Identified Peaks from Gas Chromatography Data in Figure 4-11.**

Time (min)	Compound	Time (min)	Compound
5.78	1-Heptene	21.7	Tetradecane
5.96	Heptane	22.84	2-Pentadecanone
8.21	1-Octene	23.4	1-Pentadecene
8.41	Octane	23.53	Pentadecane
10.7	1-Nonene	24.61	Pyrene
10.92	Nonane	25.19	1-Hexadecene
13.15	1-Decene	25.3	Hexadecane
13.35	Decane	26.12	2-Heptadecanone
15.47	1-Undecene	26.93	1-Heptadecene
15.63	Undecane	27.04	Heptadecane
17.6	1-Dodecene	27.58	Pristane
17.77	Dodecane	28.67	1-Octadecene
18.05	2-Tridecanol	28.79	Octadecane
19.22	Dodecanone	30.62	Nonadecane
19.65	1-Tridencene	32.64	Eicosane
19.72	2-Tridecanone	35.25	Heneicosane
19.79	Tridecane	38.39	Docosane
21.3	2-Tetradecanone	42.68	Tricosane
21.57	1-Tetradecene	48.4	Tetracosane

### ***FTIR Analysis of Light Gases***

Figure 4-12 shows FTIR spectra of light gases collected from the kerogen retort during pyrolysis of GR1.9 kerogen. Spectra for the GR2.9 and GR3.9 tars showed very similar results. The temperatures over which the gases were collected are listed in Figure 4-13. The peaks for CO<sub>2</sub>, alkanes, and H<sub>2</sub>O were observed at all temperature ranges for both samples. The methane (CH<sub>4</sub>) and C<sub>2</sub>+ peaks increased dramatically at the higher temperatures. The CO peak was small but increased at higher temperatures.

Quantitative analysis of the FTIR spectra was performed by using calibrated gas standards, allowing the determination of the concentration of each of these three species in the sample gas at each of the three temperatures. A concentration coupled with a known factor of dilution allowed the amount of the component to be determined as a percentage of the original sample or of the amount of light gas evolved. Results of the quantitative analysis of light gas composition of CH<sub>4</sub>, CO, and CO<sub>2</sub> are shown in Figure 4-13. No significant differences are seen between the gases from the two kerogen samples. The fraction of light gases that are CH<sub>4</sub>, CO, and CO<sub>2</sub> increases to about 65 wt% for the gas samples collected at 525°C. The “other” category in this figure is comprised of H<sub>2</sub>O and light hydrocarbons (presumably alkanes).

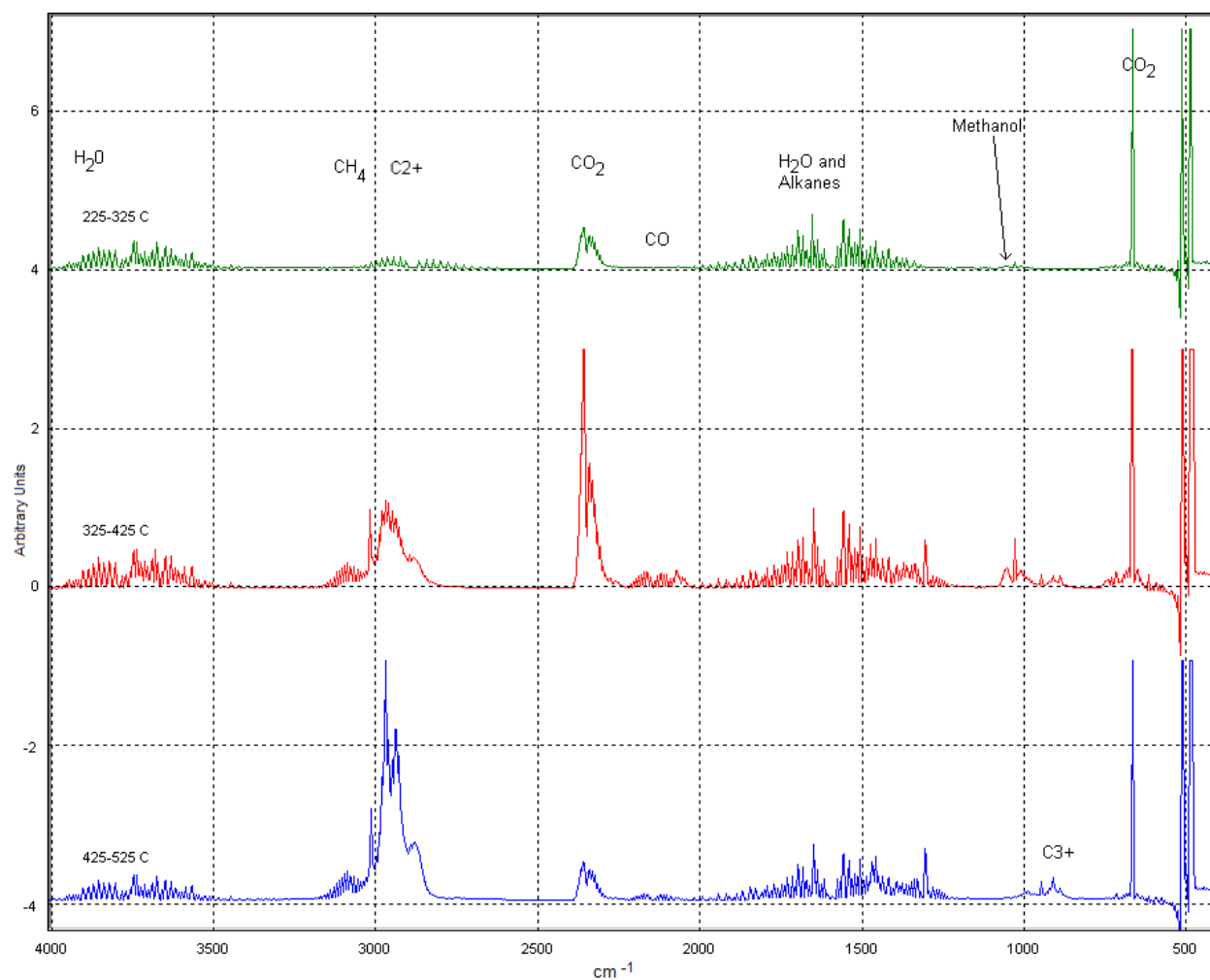
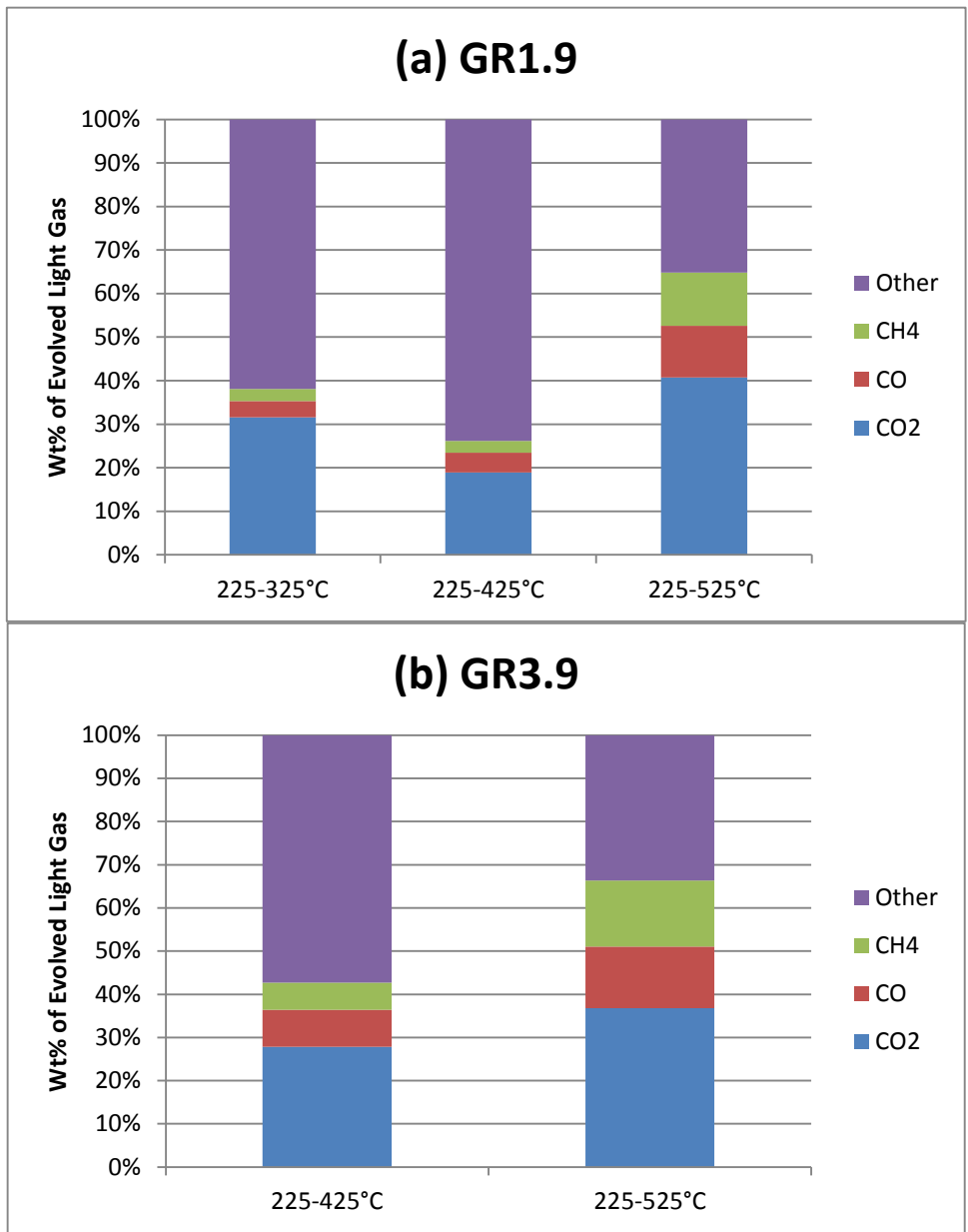


Figure 4-12. FTIR spectra of light gas collected from pyrolysis of the GR1.9 kerogen sample in the kerogen retort at the listed temperatures.



**Figure 4-13. Composition of light gases evolved over different temperatures ranges from (a) GR1.9 kerogen and (b) GR3.9 kerogen determined by quantitative FTIR analysis. Corresponding light gas yields are given in Figure 4-2.**

## Discussion

The product analyses presented here were for three demineralized oil shale kerogens that were acquired at various depths from a 4-inch diameter, 1,000-foot long Utah Green River oil shale core. The shales and extracts were carefully characterized, as reported by Solum et al.<sup>27</sup> The results of the pyrolysis experiments and analyses are very similar to data for an oxidized Colorado Green River oil shale of unknown origin reported by Hillier et al.<sup>5,6</sup> In the present study the tar yield in the 10 K/min pyrolysis experiments ranged from 60 to 69% of the parent kerogen at the highest temperature in the kerogen retort (525°C) with total volatile yields ranging from 75 to 84 wt% of the demineralized kerogen. The slight differences in the volatile and tar yields from the demineralized kerogen did not correlate with depth or the amount of organic material in the parent shale.

The solid-state NMR data for the char residue from pyrolysis of the demineralized kerogen showed 80% carbon aromaticity at the highest temperatures (525°C), with increases in the number of aromatic carbons per cluster and the number of attachments per cluster. These data indicate the manner in which the char residue is crosslinking in addition to losing aliphatic material. Therefore, a generalized oil shale pyrolysis model must treat both the crosslinking and the cleavage of aliphatic bonds. The measured time-dependent changes in the kerogen structural and lattice parameters reported in this paper provide both insight and quantitative comparisons to validate generalized oil shale pyrolysis models. Only by modeling the correct chemical mechanisms can one be confident in predictions of yield and quality at a range of possible heating rate and pressure conditions in future planned kerogen recovery processes.

The chemical structural data for the pyrolysis products from these pristine Utah oil shale cores matched the data reported by Hillier et al.,<sup>6</sup> implying that the NMR technique is consistent and that the degree of oxidation in the sample used by Hillier was low. Therefore the data reported by Hillier et al. can also be used to develop better generalized oil shale pyrolysis models without questioning the effects of oxidation on the data obtained.

The condensable pyrolysis gases (termed tar in this paper) consist mainly of alkane/1-alkene pairs, with average chain lengths of 15 to 17 carbons. The liquid-state NMR data agree with the GC/MS data for these tars. Relatively few changes are seen in the tar composition as a function of the maximum temperature achieved in the kerogen retort or the depth of the parent oil shale. The average chain lengths are similar to those obtained from demineralized kerogen by Boucher et al.<sup>18</sup> using mild oxidation by RuO<sub>2</sub>. Boucher reported that the most common straight chain hydrocarbon was C<sub>11</sub>, with C<sub>10</sub> through C<sub>13</sub> being the dominant species.

Two possible reactions for formation of alkane/1-alkene pairs are discussed by Hillier et al.<sup>4,6</sup> Breakage of the bond between the aromatic ring and an  $\alpha$ -carbon would form an alkene, and subsequent hydrogenation would form an n-alkane. Breakage of the bond between the  $\alpha$ -carbon and the  $\beta$ -carbon with hydrogen abstraction would produce the alkanes as well. Very little evidence was seen for di-alkenes.

The light gas analyses presented here are quite similar to those for the Colorado oil shale reported by Hillier.<sup>4,6</sup> At the highest temperatures, 40% of the light gases were not fully characterized by FTIR but seemed to be a combination of H<sub>2</sub>O and light hydrocarbons (likely alkane/alkene pairs that did not condense).

## Summary and Conclusion

The combination of analytical techniques used in this research is unique and adds important information to the existing body of knowledge regarding the chemistry of oil shale. The source for all samples was a well-characterized core from Green River oil shale from Utah, which is a Type I kerogen. Demineralized samples were obtained from three different depths in the core. Pyrolysis experiments on the kerogen at 10 K/min were performed to generate light gas, tar, and char for further analysis. Total volatiles content and tar yields from the kerogen pyrolysis showed only slight variations with sample origin. The volatiles yield from the pyrolysis experiments on the demineralized kerogen were about 80% on a daf basis, with a 60 wt% daf tar yield. Tar yield did not correlate with depth or organic content of the original sample, but the total volatiles yield increased slightly with depth of the parent shale.

NMR analysis of the demineralized kerogen showed a carbon aromaticity of only 20% with an average number of aromatic carbons per cluster of 10.3 but an average cluster molecular weight of 830. The aromaticity of the chars from pyrolysis of the demineralized kerogen increased to 80% in the char obtained at 525°C. The average length of a side chain in the char decreased from about 11 carbons to less than one carbon. These chemical structural data are consistent with the idea that the aromatic portion of the kerogen largely remains in the char, and the aliphatic chains break off and vaporize.

The liquid-phase NMR analysis of the tars from the pyrolysis of the demineralized kerogen showed more detail than previously reported in the literature with peaks for carbons in *n*-alkanes as well as branched alkanes. The NMR spectra was basically the same for all tars collected, regardless of the temperature achieved during pyrolysis or the depth of the parent shale. The carbon aromaticity of the tar was 19% with terminal alkene groups that were not observed in previous analyses of the bitumen from these shales. It was estimated that more than half of the aromatic carbons in the tar were protonated.

The pyrolysis products were analyzed by the mass spectrometer and show large amounts of alkane/1-alkene pairs with an average chain length of 15 to 17 carbons. The analysis of tars collected cumulatively at different maximum temperatures showed similar chemical structures dominated by the *n*-alkane/1-alkene pairs. The FTIR analysis showed that 60% of the light gases at the highest temperature (525°C) consisted of CH<sub>4</sub>, CO, and CO<sub>2</sub> with the balance likely a combination of H<sub>2</sub>O and alkane/alkene pairs less than C<sub>7</sub>.

The detailed chemical structure analysis of the demineralized kerogen from well-characterized oil shale samples, along with analysis of the pyrolysis products performed here are important data for development of improved pyrolysis models based on chemical structure rather than mere empiricism. The quantitative time-dependent changes in chemical structure reported here serve as a good source for validating generalized models of oil shale pyrolysis that would be applicable to wide ranges of heating rate and pressures.

## References

1. Andrews, A., *Oil shale: History, incentives, and policy*. Report No.; CRS Report for Congress: April 13, 2006, 2006.
2. Dyni, J. R., Geology and resources of some world oil-shale deposits: U.S. Geological Survey Scientific Investigations Report 2005–5294. Survey, U. S. G., Ed. 2006; p 42.
3. Johnson, R. C.; Mercier, T. J.; Brownfield, M. E.; Pantea, M. P.; Self, J. G., *An assessment of in-place oil shale resources in the Green River Formation, Piceance Basin, Colorado. In Oil Shale Assessment of the Piceance Basin, Colorado, Chapter 1*. Report No.; U.S. Geological Survey Digital Data Series DDS-69-Y; U.S. Geological Survey Oil Shale Assessment Team: Washington, D. C., 2010; pp 1-197.
4. Hillier, J. L. Pyrolysis kinetics and chemical structure considerations of a Green River oil shale and its derivatives. Ph.D. Dissertation, Chemical Engineering Department, Brigham Young University, Provo, UT, 2011.
5. Hillier, J. L.; Fletcher, T. H., Pyrolysis kinetics of a Green River oil shale using a pressurized TGA. *Energy & Fuels* **2011**, 25, 232-239.
6. Hillier, J. L.; Fletcher, T. H.; Solum, M. S.; Pugmire, R. J., Characterization of pyrolysis products from a Colorado Green River oil shale by <sup>13</sup>C NMR, XPS, GC/MS, and FTIR. *Industrial and Engineering Chemistry Research* **2013**, 52, (44), 15522-15532
7. Tiwari, P. Oil Shale Pyrolysis: Benchscale experimental studies and modeling. PhD Thesis, Chemical Engineering, University of Utah, Salt Lake City, UT, 2012.
8. Tiwari, P.; Deo, M., Detailed kinetic analysis of oil shale pyrolysis TGA data. *AIChE Journal* **2012**, 58, (2), 505-515.
9. Tiwari, P.; Deo, M., Compositional and kinetic analysis of oil shale pyrolysis using TGA–MS. *Fuel* **2012**, 94, (0), 333-341.
10. Campbell, J. H.; Koskinas, G. H.; Stout, N. D., Kinetics of oil generation from Colorado oil shale. *Fuel* **1978**, 57, (6), 372-376.
11. Braun, R. L.; Burnham, A. K.; Reynolds, J. G., Oil and gas evolution kinetics for oil shale and petroleum source rocks determined from pyrolysis-TQMS data at two heating rates. *Energy & Fuels* **1992**, 6, (4), 468-474.
12. Burnham Alan, K., Chemistry and kinetics of oil shale retorting. In *Oil shale: A Solution to the liquid fuel dilemma*, American Chemical Society: Washington, DC, 2010; pp 115-134.
13. Huss, E. B.; Burnham, A. K., Gas evolution during pyrolysis of various Colorado oil shales. *Fuel* **1982**, 61, (12), 1188-1196.
14. Meuzelaar HLC; Windig W; Futrell JH; Harper AM; SR, L., Pyrolysis mass spectrometry and multivariable analysis of several key world oil shale kerogens and some recent alginites. In *Mass spectrometric characterization of shale oils. ASTM STP 902*, T, A., Ed. American Society for Testing and Materials: Philadelphia, 1986; pp 81–105.
15. Huizinga, B. J.; Aizenshtat, Z. A.; Peters, K. E., Programmed pyrolysis-gas chromatography of artificially matured Green River kerogen. *Energy & Fuels* **1988**, 2, (1), 74-81.
16. Reynolds, J. G.; Crawford, R. W.; Burnham, A. K., Analysis of oil shale and petroleum source rock pyrolysis by triple quadrupole mass spectrometry: Comparisons of gas evolution at the heating rate of 10 degree C/min. *Energy & Fuels* **1991**, 5, (3), 507-523.
17. Hagaman, E. W.; Schell, F. M.; Cronauer, D. C., Oil-shale analysis by CP/MAS-<sup>13</sup>C NMR spectroscopy. *Fuel* **1984**, 63, (7), 915-919.

18. Boucher, R. J.; Standen, G.; Eglinton, G., Molecular characterization of kerogens by mild selective chemical degradation -- Ruthenium tetroxide oxidation. *Fuel* **1991**, 70, (6), 695-702.
19. Miknis, F. P.; Szeverenyi, N. M.; Maciel, G. E., Characterization of the residual carbon in retorted oil shale by solid-state <sup>13</sup>C NMR. *Fuel* **1982**, 61, (4), 341-345.
20. Miknis, F. P.; Turner, T. F.; Berdan, G. L.; Conn, P. J., Formation of soluble products from thermal decomposition of Colorado and Kentucky oil shales. *Energy & Fuels* **1987**, 1, (6), 477-483.
21. Netzel, D. A.; Miknis, F. P., NMR Study of US eastern and western shale oils produced by pyrolysis and hydrolysis. *Fuel* **1982**, 61, (11), 1101-1109.
22. Maciel, G. E.; Bartuska, V. J.; Miknis, F. P., Correlation between oil yields of oil shales and <sup>13</sup>C nuclear magnetic resonance spectra. *Fuel* **1978**, 57, (8), 505-506.
23. Miknis, F. P.; Conn, P. J., A common relation for correlating pyrolysis yields of coals and oil shales. *Fuel* **1986**, 65, (2), 248-250.
24. Solomon, P. R.; Miknis, F. P., Use of Fourier transform infrared spectroscopy for determining oil shale properties. *Fuel* **1980**, 59, (12), 893-896.
25. Solum, M. S.; Pugmire, R. J.; Grant, D. M., Carbon-13 Solid-state NMR of Argonne Premium Coals. *Energy & Fuels* **1989**, 3, (2), 187-193.
26. Solum, M. S.; Sarofim, A. F.; Pugmire, R. J.; Fletcher, T. H.; Zhang, H., C-13 NMR analysis of soot produced from model compounds and a coal. *Energy & Fuels* **2001**, 15, 961-971.
27. Solum, M. S.; Mayne, C. L.; Orendt, A. M.; Pugmire, R. J.; Hall, T.; Fletcher, T. H., Characterization of macromolecular structure elements from a Green River oil shale, I. Extracts. *Energy and Fuels* **2014**, 28, 453-465.
28. Vandegrift, G. F.; Winans, R. E.; Scott, R. G.; Horwitz, E. P., Quantitative study of the carboxylic acids in Green River oil shale bitumen. *Fuel* **1980**, 59, (9), 627-633.
29. Crouch, R. Acquiring quantitative small-molecule NMR data with QDEPT. [www.agilent.com](http://www.agilent.com) (January 30, 2012).
30. Henderson, T. J., Sensitivity-enhanced quantitative <sup>13</sup>C NMR spectroscopy via cancellation of 1JCH dependence in DEPT polarization transfers. *Journal of the American Chemical Society* **2004**, 126, (12), 3682-3683.
31. Kelemen, S. R.; Siskin, M.; Homan, H. S.; Pugmire, R. J.; Solum, M. S., *Fuel, lubricant and additive effects on combustion chamber deposits, SP-1396*. Report No. 982715; Copyright 1998 Society of Automotive Engineers, Inc., 1998.
32. Dalling, D. K.; Pugmire, R. J.; Grant, D. M.; Hull, W. E., The use of high-field carbon-13 NMR spectroscopy to characterize chiral centers in isopranes. *Magnetic Resonance in Chemistry* **1986**, 24, (3), 191-198.

## CHAPTER 5. MODELING KEROGEN PYROLYSIS WITH THE CPD MODEL

As our knowledge of the characterization of shale oil increases due to modern solid-state NMR, mass spectrometry, and gas chromatography, we are trying to improve the mechanistic description of oil shale pyrolysis. Current models empirically fit the mass released and may model individual species or tar. Mechanistic models may be able to describe oil shale pyrolysis over a broader range of heating conditions (heating rate, temperature, and pressure). The Chemical Percolation Devolatilization (CPD) model is a mechanistic pyrolysis model originally developed by Fletcher et al.<sup>1,2</sup> to describe coal pyrolysis. Coal is modeled as a system of aromatic clusters connected by aliphatic bridges. During pyrolysis, aliphatic bridges are either (a) cleaved, leaving two side chains, or (b) transformed into a stable char bridge by releasing their aliphatic portion. A Bethe lattice is used to describe the parent chemical structure with features such as cluster molecular weight, side chain molecular weight, and the number of attachments per cluster determined by solid-state <sup>13</sup>C NMR measurements. Percolation lattice statistics are used to relate the temperature-dependent rate of aliphatic bridge breaking to the number of clusters that are detached from the original infinite lattice. Detached clusters form a liquid pool that can evaporate as tar, depending on the vapor pressure of each cluster. Tar is defined as any volatile matter that will later condense at room temperature. Detached clusters that remain too long with the solid will crosslink to the char. The CPD model has been used successfully to describe pyrolysis of a variety of fuels including coal and biomass.<sup>2-4</sup>

Since the chemical structure of oil shale was recently measured in detail using solid-state <sup>13</sup>C NMR, the CPD model seemed like a logical choice for a mechanistic pyrolysis model. The kerogen structure parameters used in the CPD model are shown in Table 5-1 for the GR1.9, GR2.9, and GR3.9 samples, as reported by Solum et al.<sup>5</sup>

**Table 5-1. Chemical Structure Parameters Measured for the GR1.9, GR2.9, and GR3.9 Kerogen Samples.<sup>5</sup>**

	GR1.9	GR2.9	GR3.9
MW <sub>cluster</sub>	776	775	946
MW <sub>side chain</sub>	131	148	135
Attachments per cluster ( $\sigma+1$ )	5.0	4.5	5.9
Fraction of attachments that are bridges ( $p_0$ )*	0.5	0.5	0.5

\* $p_0$  could not be measured by the NMR technique for oil shale, but was assumed to be 0.5.

The bridge-breaking scheme in the CPD model is shown in Figure 5-1. An aliphatic “labile” bridge ( $\mathcal{E}$ ) is activated ( $\mathcal{E}^*$ ) and is either cleaved to form two side chains ( $\delta$ ) with rate  $k_\delta$ , or is transformed into a stable bridge ( $c$ ) (such as a bi-aryl bridge) while releasing the aliphatic material (with rate  $k_c$ ). The side chains will eventually degrade to form gases as well (with rate  $k_g$ ). Experience has shown that the ratio of  $k_\delta/k_c$  is relatively constant. The gas that is produced by the side chains that break off is referred to as  $g_1$  whereas the gas that is produced by the bridge transformation to a char bridge is referred to as  $g_2$ .

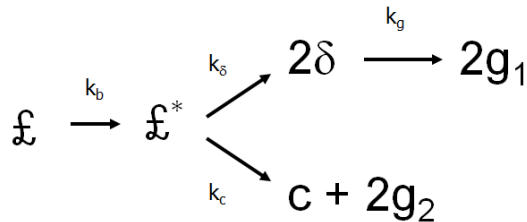
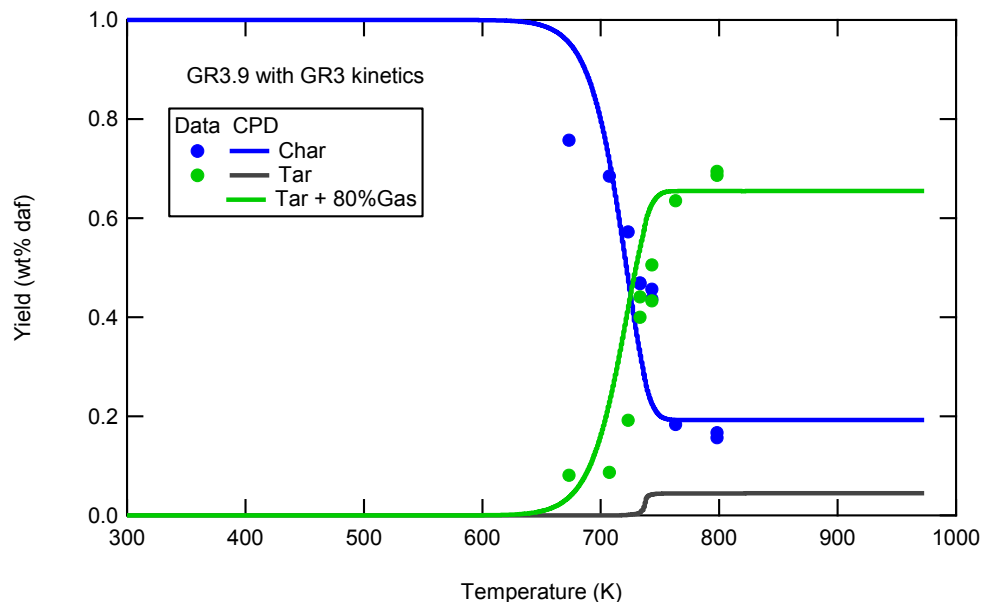


**Figure 5-1. Bridge-breaking scheme used in the CPD model.**

Predictions were made with the CPD model using the chemical structure parameters in Table 5-1 and the rate parameters for bridge breaking originally assigned for coal pyrolysis. These predictions did not compare well with the data obtained in the kerogen retort by Hillier et al.<sup>6</sup> and by Fletcher et al.<sup>7</sup> The next step was to use the rate coefficients determined for a first-order DAEM using TGA pyrolysis data reported in the October 2012 Quarterly Report. These rate coefficients (see Table 5-2) were used in the CPD model for both  $k_\delta$  and  $k_c$ . In this table, each  $k$  is an Arrhenius rate constant, with pre-exponential factor  $A$ , mean activation energy  $E$ , and  $\sigma$  is the standard deviation in the activation energy. Activation energies are normalized by the universal gas constant  $R$ . Predicted and measured yields of char and tar using the rate coefficients from Table 5-2 are shown in Figure 5-2. It can be seen that the predicted tar yield (black line) is quite low, assuming that the tar consists only of material containing an aromatic cluster (which is a good assumption for coal).

**Table 5-2. Rate Coefficients Determined for a First-Order DAEM for the GR1, GR2, and GR3 Oil Shale Samples from TGA Data at Three Heating Rates.**

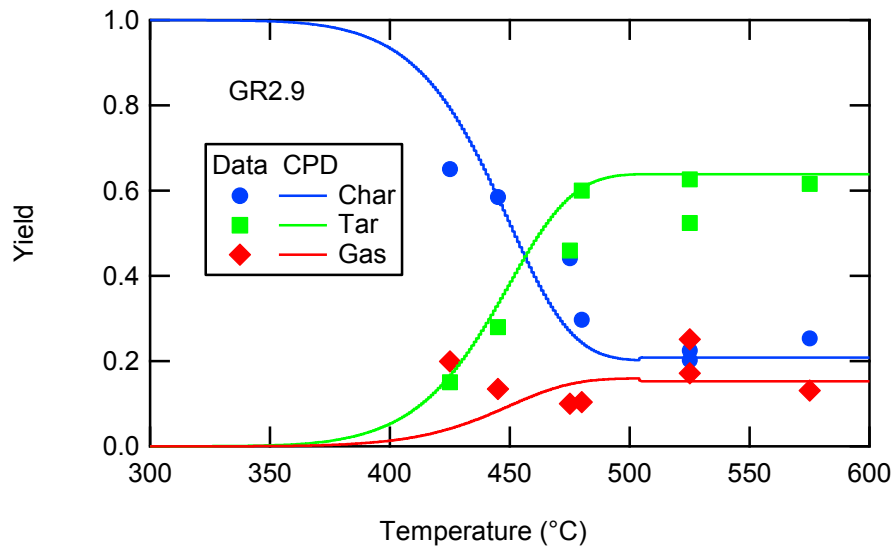
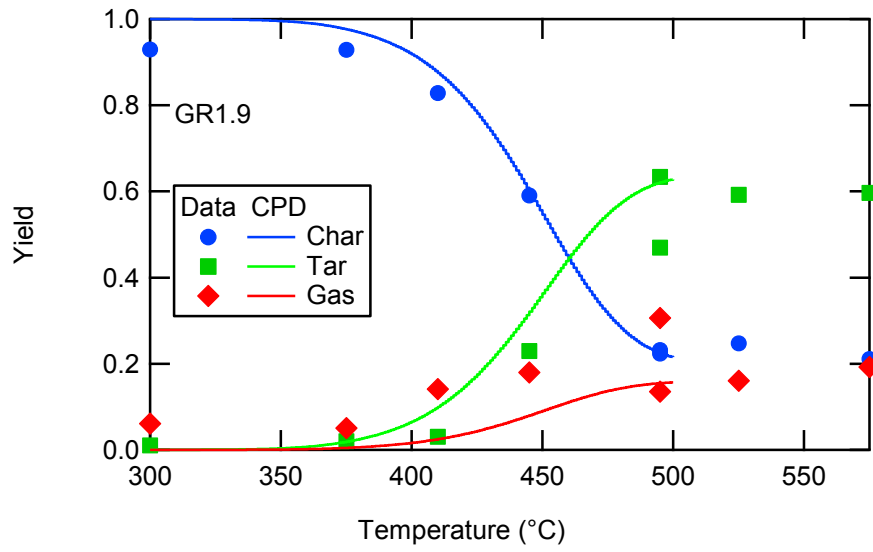
	$A$ ( $s^{-1}$ )	$E/R$ (K)	$\sigma/R$ (K)
GR1	$9.21 \times 10^{13}$	26,800	481
GR2	$2.63 \times 10^{14}$	27,400	313
GR3	$9.35 \times 10^{13}$	26,600	553



**Figure 5-2. Initial CPD predictions of tar and char yields for GR3.9 kerogen pyrolysis at 10 K/min. Data are from Fletcher et al.<sup>7</sup>**

At first, the prediction of a low tar yield was quite puzzling. However, kerogen in oil shale has a carbon aromaticity of only 20% compared to 70–80% in coal.<sup>5, 7-9</sup> The average molecular weight of a side chain in an unreacted coal ranges from 12 to 60 amu, whereas the side chain molecular weights in oil shale are 130–150 amu. The side chains in the oil shale kerogen are therefore 11 to 13 carbons in length, and the gases formed during pyrolysis of these side chains have a sufficiently large molecular weight to condense at room temperature and pressure. Therefore, if tar is defined as the volatile matter that condenses, a significant component of the tar will be the long chain aliphatic material that is not necessarily connected to an aromatic cluster. The carbon aromaticity of the tar from these samples was measured to be 19%.<sup>5</sup>

A rough guess was made that 80% of the mass of released side chain material would be condensable and therefore counted as tar. The green line in Figure 5-2 shows a CPD model prediction with 80% of the “light” gas counted as tar in a post-processing step. This prediction shows reasonable agreement with the measured tar yield. The char yield was unaffected by the assignment of “light gas” as tar. The CPD model was changed to incorporate this 80% factor into the flash calculation, and the resulting predictions using the TGA rates for each kerogen sample are shown in Figure 5-3. The agreement is generally good, but the data indicate earlier release of light gas than predicted by the model.



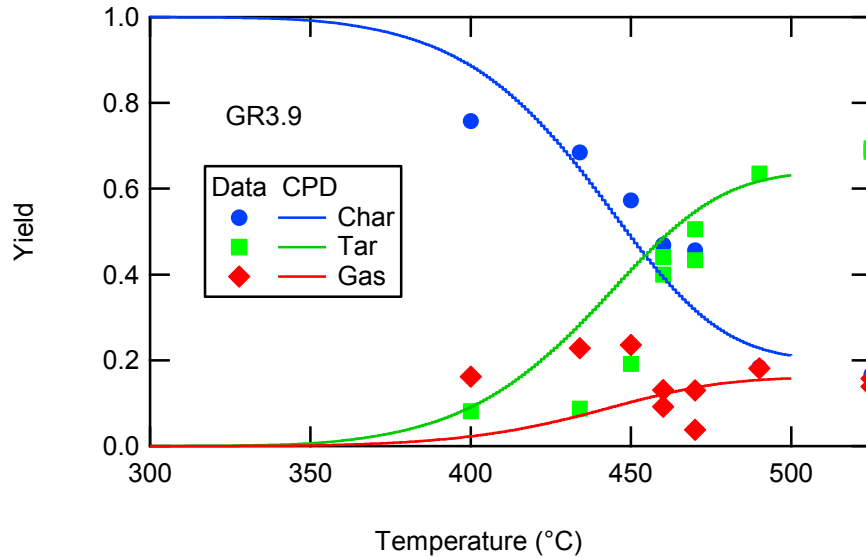


**Figure 5-3. CPD model calculations of tar and char yields for kerogen pyrolysis at 10 K/min using rate coefficients from Table 5-2 and counting 80% of the “light gas” as tar. Data are from Fletcher et al.<sup>7</sup>**

We performed a literature search to see if there were any data to show that 80% of side chains in oil shale kerogen were of high enough molecular weight to condense at room temperature. The only data available are after pyrolysis. Therefore, the tar yields obtained from the kerogen retort data of Fletcher et al.<sup>7</sup> are as good as any data available for determining this split. We then wondered if there might be a difference in the two pathways for “light gas” formation shown earlier in Figure 5-1. We arbitrarily assigned  $g_2$  as light gas and  $g_1$  as heavy gas in an attempt to remove the empiricism of assigning 80% of the light gas to be tar. The molecular weight of the light gas ( $MW_{lg}$ ) was set to 20 amu and the molecular weight of the heavy gas ( $MW_{hg}$ ) was then calculated from the combined gas molecular weight (calculated from the NMR parameters by the CPD model), as follows:

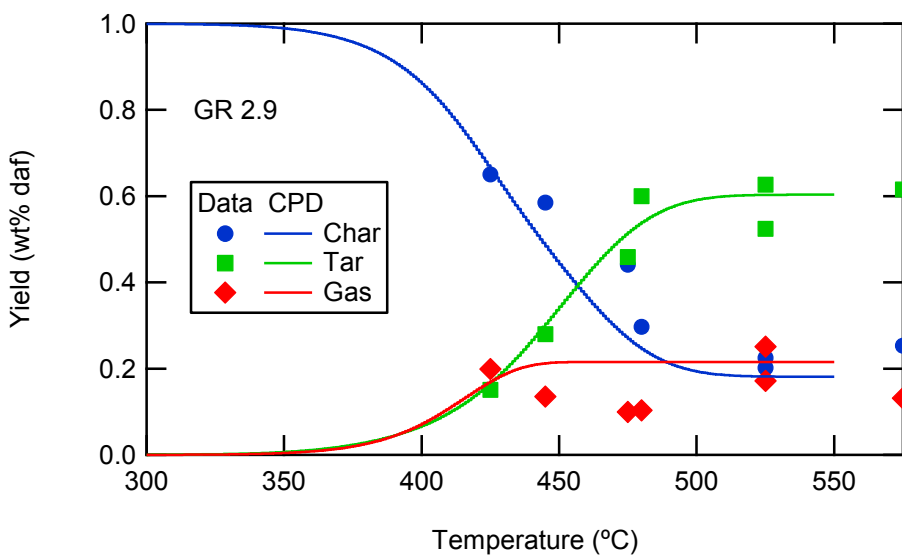
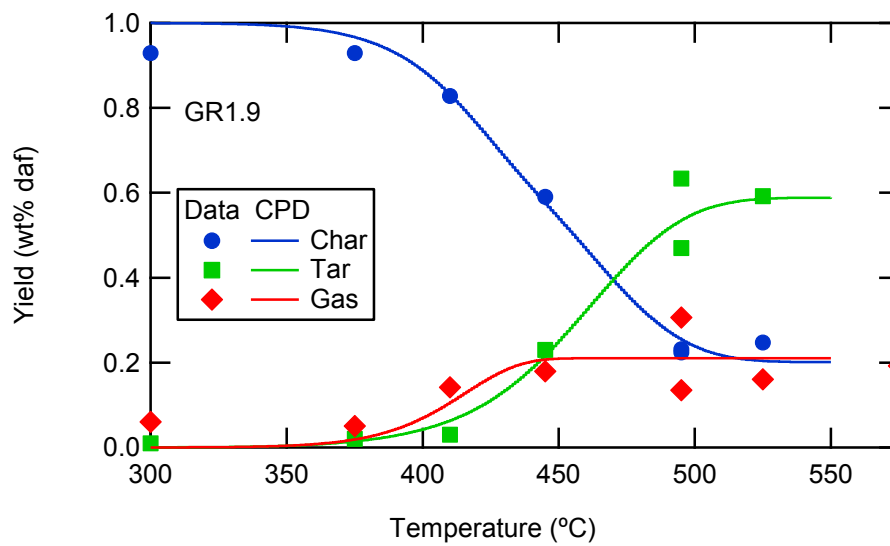
$$y_{lg}MW_{lg} + y_{hg}MW_{hg} = MW_{all\ gases} \quad (1)$$

where  $y_{lg} = g_2/(g_1 + g_2)$  and  $y_{hg} = g_1/(g_1 + g_2)$ , and  $y_{lg}$  and  $y_{hg}$  were set to 0.2 and 0.8, respectively.

The reaction rate coefficients were then adjusted slightly to obtain best fit with the kerogen retort data of Fletcher et al.<sup>7</sup> The new rate coefficients are shown in Table 5-3. Results of this prediction are shown in Figure 5-4. No empirical factor was used to count part of the light gas as tar, other than assigning  $g_1$  as tar. This distinction between light gas and heavy gas allowed the model to predict the early light gases that came off before the tar. The fact that much of the light gas has already left the kerogen is apparent in the graph and show that it is necessary to have two different reaction constants. The overall agreement with this modeling approach with the CPD model is very good.

**Table 5-3. Rate Coefficients Determined for Bridge Breaking in the CPD Model for the GR1.9, GR2.9, and GR3.9 Kerogen Samples to Fit the Kerogen Retort Data of Fletcher et al.<sup>7</sup>**

	GR1.9	GR2.9	GR3.9
$A_{\delta}$ ( $s^{-1}$ )	$9.8 \times 10^{12}$	$9.8 \times 10^{12}$	$1.8 \times 10^{15}$
$E_{\delta}/R$ ( $T^{-1}$ )	23,900	23,900	25,918
$\sigma_{E_{\delta}}/R$ ( $T^{-1}$ )	0	0	0
$A_g$ ( $s^{-1}$ )	$1.58 \times 10^{10}$	$2.58 \times 10^{10}$	$1.58 \times 10^{14}$
$E_g/R$ ( $T^{-1}$ )	21,000	21,000	27,600
$\sigma_{E_g}/R$ ( $T^{-1}$ )	300	300	300
$k_{\delta}/k_c$	0.9	0.9	1.8



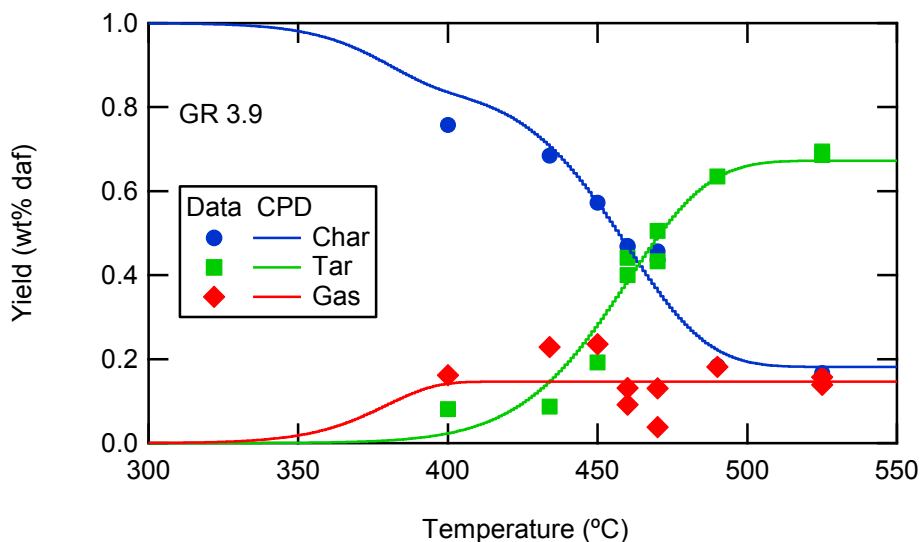


**Figure 5-4. CPD model calculations of tar and char yields for kerogen pyrolysis at 10 K/min using rate coefficients from Table 5-3 and assigning  $g_2$  as the “light gas” and  $g_1$  as the condensable “heavy gas.” Data are from Fletcher et al.<sup>7</sup>**

## Conclusion

We have been working on a mechanistic model of oil shale kerogen pyrolysis based on the CPD model. It is apparent that much of what is classified as tar (i.e., condensables at room temperature) comes from aliphatic side chain material that is 11–13 carbons in length. The condensable aliphatic material seems to constitute about 80% of the total aliphatic material. Rate coefficients were modified in the CPD model to fit tar and char yields from kerogen retort experiments at 10 K/min. Model agreement was good if 80% of the aliphatic side chains were assigned as tar. However, this approach did not yield good agreement with the light gas release rate. In an effort to be more mechanistic, light gases were assumed to come only from char bridge formation and heavy gases were assumed to come only from aliphatic bridge cleavage. This assignment of light and heavy gases resulted in very good agreement with the kerogen retort data for the three kerogen samples studied.

## References

1. Grant, D. M.; Pugmire, R. J.; Fletcher, T. H.; Kerstein, A. R., Chemical model of coal devolatilization using percolation lattice statistics. *Energy & Fuels* **1989**, 3, (2), 175-186.
2. Fletcher, T. H.; Kerstein, A. R.; Pugmire, R. J.; Solum, M. S.; Grant, D. M., Chemical percolation model for devolatilization. 3. Direct use of  $^{13}\text{C}$  NMR data to predict effects of coal type. *Energy & Fuels* **1992**, 6, (4), 414-431.
3. Fletcher, T. H.; Pond, H. R.; Webster, J.; Baxter, L. L., Prediction of tar and light gas during pyrolysis of black liquor and biomass. *Energy and Fuels* **2012**, 26, 3381-3387.
4. Lewis, A. D.; Fletcher, T. H., Prediction of sawdust pyrolysis yields from a flat-flame burner using the CPD model. *Energy & Fuels* **2013**, 27, 942-953.

5. Solum, M. S.; Mayne, C. L.; Orendt, A. M.; Pugmire, R. J.; Hall, T.; Fletcher, T. H., Characterization of macromolecular structure elements from a Green River oil shale, I. Extracts. *Energy and Fuels* **2014**, 28, 453-465.
6. Hillier, J. L. Pyrolysis kinetics and chemical structure considerations of a Green River oil shale and its derivatives. Ph.D. Dissertation, Chemical Engineering Department, Brigham Young University, Provo, UT, 2011.
7. Fletcher, T. H.; Gillis, R.; Adams, J.; Hall, T.; Mayne, C. L.; Solum, M. S.; Pugmire, R. J., Characterization of macromolecular structure elements from a Green River oil shale, ii. Characterization of pyrolysis products by <sup>13</sup>C NMR, GC/MS and FTIR. *Energy and Fuels* **2014**, 28, 2959-2970.
8. Solum, M. S.; Pugmire, R. J.; Grant, D. M., Carbon-13 solid-state NMR of Argonne premium coals. *Energy & Fuels* **1989**, 3, (2), 187-193.
9. Boucher, R. J.; Standen, G.; Eglinton, G., Molecular characterization of kerogens by mild selective chemical degradation -- ruthenium tetroxide oxidation. *Fuel* **1991**, 70, (6), 695-702.

## CHAPTER 6. ANALYSIS OF CHANGES IN CHAR AROMATICITY

In order to understand the pyrolysis of shale oil, we looked for a way to track the aromaticity of the char (or the organic material left behind after pyrolysis). Throughout pyrolysis, the aromaticity of the carbons in the char increased from 0.2 to 0.8.<sup>1</sup> A balance was performed assuming that no new aromatic carbons are produced during pyrolysis. A simple mass balance of the aromatic carbons can then be used to predict the final amount in the char. This approach allows us to see if there are any aliphatic carbons that become aromatic in the experiment. Table 6-1 shows the elemental analyses of unreacted kerogen, tar, and light gas from the kerogen retort. Note that the tar composition comes from the literature for a similar sample.

**Table 6-1. Elemental Compositions of Shale Oil and Pyrolysis Products.**

	Weight Fractions					Carbon Aromaticity
	Oxygen	Hydrogen	Carbon	Sulfur	Nitrogen	
Extracted Kerogen <sup>1</sup>	0.081	0.095	0.762	0.037	0.025	0.2
Tar <sup>2</sup>	0.013	0.114	0.851	0.007	0.018	0.19
Gas <sup>3</sup>	0.651	0.0478	0.273	0.0	0.0	0.0

1. The composition for the extracted kerogen comes from Fletcher et. al.<sup>2</sup>
2. The composition for the tar comes from Netzel and Miknis<sup>3</sup>
3. The composition of the gas comes from Fletcher et.al.<sup>1</sup> It is assumed that the “Other” portion of the light gases can be averaged as water.

We performed a carbon balance for the amount of carbon that is left in the char. We used the yields that were found by Fletcher et. al.<sup>1</sup> for Green River shale oil shown in Table 6-2.

**Table 6-2. Final Yields of the Pyrolysis of Shale Oil.**

	Char	Tar	Gas
Final Weight Fraction	0.2018	0.6557	0.1426

The carbon balance is shown in Equation (6-1):

$$C_{shale} = C_{tar} * f_{tar} + C_{gas} * f_{gas} + C_{char} * f_{char} \quad (6-1)$$

Everything in Equation (1) is known except for  $C_{char}$ . The value of  $C_{char}$  that was calculated from Equation (6-1) was 0.818. A similar balance on aromatic carbon is shown in Equation (6-2), assuming that aromatic carbons are not created or destroyed in the retort. The only unknown in Equation (6-2) is  $f_{a'char}$ .

$$C_{shale} * f_{a'shale} = C_{tar} * f_{a'tar} * f_{tar} + C_{char} * f_{a'char} * f_{char} \quad (6-2)$$

The calculated value of  $f_{a'char}$  was 0.281, but the measured value of  $f_{a'char}$  was 0.81 (GR2.9 in Table 4-4). This difference between the actual aromaticity and the calculated aromaticity shows that there are carbons that become aromatic as the reaction moves forward. We have several theories as to how this could happen. One, parts of the carbon matrix that have

broken off can be reattached through a ring addition (Figure 6-1a). Two, the hydrogen could be scavenged from the remaining matrix, forming new double bonds that then form into aromatic regions (Figure 6-1b).

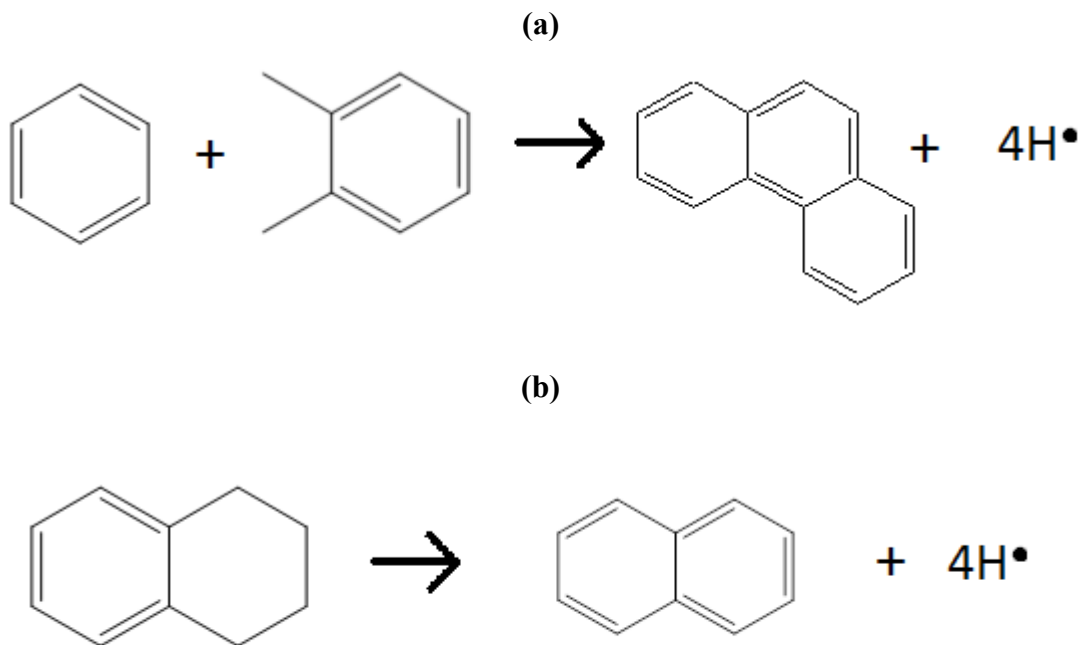


**Figure 6-1. Two possible path ways to increase the aromaticity of the shale oil char.**

We performed a thought experiment to verify the elemental composition of the tar. We assumed the tar was 19 wt% aromatic and 81 wt% aliphatic based on the data of Fletcher et al.<sup>1</sup> The aromatic fraction was assumed to have a carbon to hydrogen ratio of 1 (like benzene but close to most polyaromatics) and the aliphatic was assumed to have the same carbon to hydrogen ratio as C<sub>11</sub>H<sub>25</sub>.

The weight fraction of carbon in the aromatic fraction is calculated as follows:

$$\frac{\text{Weight of Carbons}}{\text{Molecular Weight}} = \frac{12.01}{12.01+1.008} = 0.923 \quad (6-4)$$

The weight fraction of carbon in the aliphatic fraction is calculated in a similar manner:

$$\frac{\text{Weight of Carbons}}{\text{Molecular Weight}} = \frac{11 \cdot 12.01}{11 \cdot 12.01 + 25 \cdot 1.008} = 0.84 \quad (6-5)$$

Therefore, a weighted average of the carbon content of the tar using these species as surrogates can be calculated as follows:

$$C_{tar} = f_{aromatic} * C_{aromatic} + f_{aliphatic} * C_{aliphatic} = .19 * .923 + .81 * .84 = 0.856 \quad (6-6)$$

The final carbon fraction of 0.856 is close to the carbon fraction determined by Netzel and Miknis<sup>3</sup> and listed in Table 6-1. Based on these results, the elemental compositions from the Netzel and Miknis paper are accurate enough for our model.

Our findings highlight the need to reconsider changes in the char structure that pyrolysis produces. The reaction is not the simple bridge-breaking mechanism that we have previously assumed to model pyrolysis of oil shale. Instead, pyrolysis contains many reactions that link the char and may contribute to which products are produced in the tar and the gas. We looked at the amount of crosslinking in the CPD model, but that amount was negligible and would not add aromatic carbons anyway. Further work is needed to elucidate the exact mechanism of the aromatic production and to model aromaticity so that we can predict the possible products of pyrolysis and the chemical structure changes in the char.

One of the questions that arose from this carbon aromaticity balance was the actual carbon content of the char samples from the experiments at BYU. The NMR samples were sent to Huffman Laboratories in Golden, Colorado for analysis using BYU funds external to the DOE grant. The results of the elemental char analyses were shown in Table 4-1.

Plots of carbon, hydrogen, and H to C ratio are shown in Figures 6-2 and 6-3. The final measured carbon content of the char is 83 to 85 wt%, which is similar to the value of 81.8% calculated above.

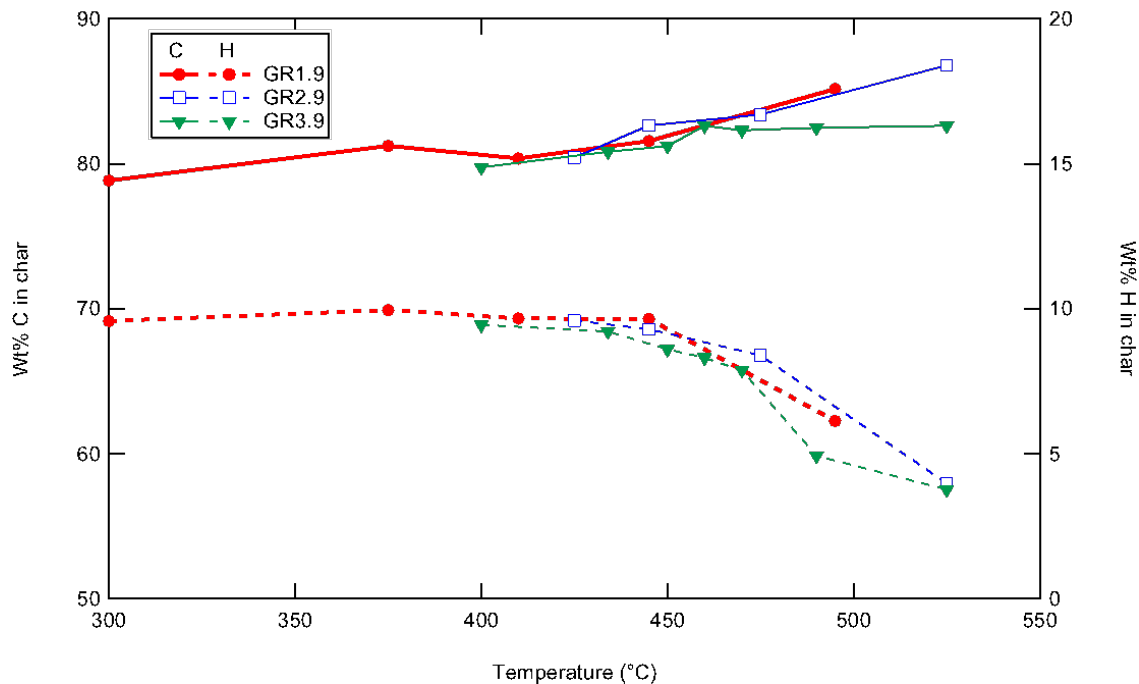


**Figure 6-2. Carbon and hydrogen contents of the chars from the kerogen retort collected at different temperatures. The heating rate was 10 K/min for these experiments.**

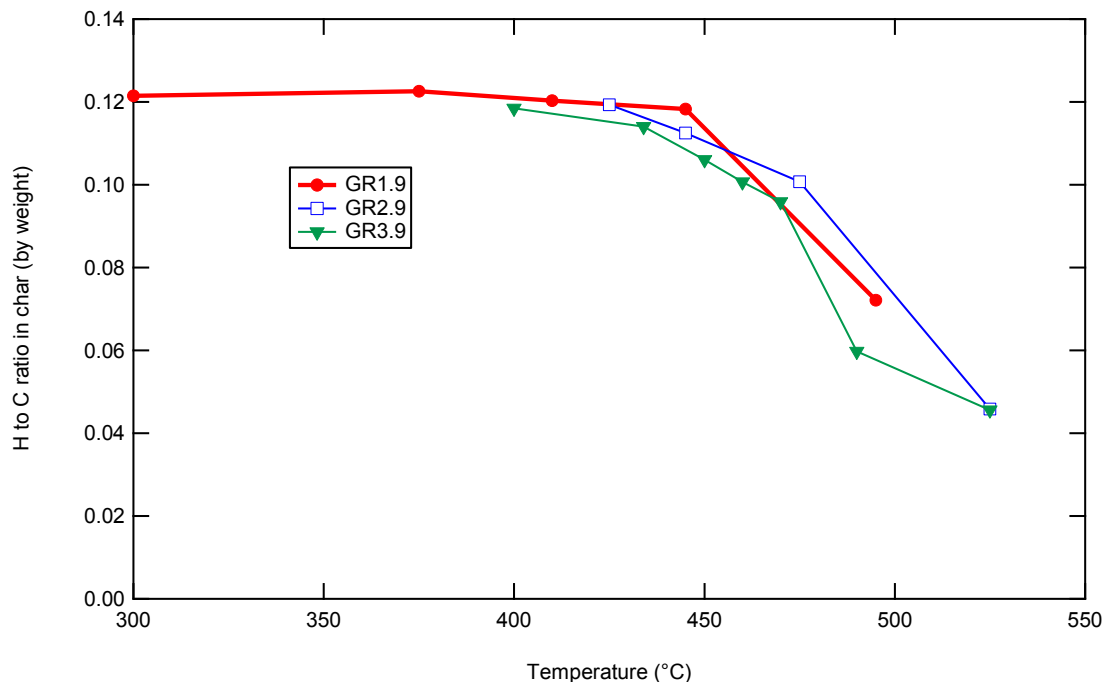


**Figure 6-3. Hydrogen to carbon ratios of the chars from the kerogen retort collected at different temperatures. The heating rate was 10 K/min for these experiments.**

## References

1. Fletcher, T. H.; Gillis, R.; Adams, J.; Hall, T.; Mayne, C. L.; Solum, M. S.; Pugmire, R. J., Characterization of macromolecular structure elements from a Green River oil shale, II. Characterization of pyrolysis products by  $^{13}\text{C}$  NMR, GC/MS, and FTIR. *Energy and Fuels* **2014**, 28, 2959-2970.
2. Mark S. Solum, C. L. M., Anita M. Orendt Ronald J. Pugmire, Jacob Adams, Thomas H. Fletcher, Characterization of macromolecular structure elements from a Green River oil shale, I. Extracts. *Energy & Fuels* **2014**, (28), 453-465.
3. Netzel, D. A.; Miknis, F. P., NMR study of US eastern and western shale oils produced by pyrolysis and hydrolysis. *Fuel* **1982**, 61, (11), 1101-1109.

## CHAPTER 7. SUMMARY AND CONCLUSIONS

---

A large set of experiments were performed on a single set of oil shale samples from the Utah Green River formation. Specific conclusions were included in each chapter. The shale was demineralized using a nine-step procedure to better perform subsequent chemical and thermal decomposition analyses. Bitumen was extracted during the demineralization process and analyzed with liquid-state  $^{13}\text{C}$  NMR. The kerogen remaining after the extraction and demineralization process was analyzed for elemental composition and for chemical structure using the latest techniques in  $^{13}\text{C}$  NMR spectroscopy. These analyses quantified the chemical structure of the bitumen and kerogen in a manner that has not before been available.

Crushed shale samples were pyrolyzed at several heating rates (0.5 to 10 K/min) in a TGA at ambient pressure and 40 atm, and rate coefficients were regressed for both the first-order model and the DAEM. The mass release due to the effect of pressure on the pyrolysis rate was shown to be small. Pyrolysis at higher heating rates was subject to mass and heat transfer effects. The  $\text{CO}_2$  formation from the shale pyrolysis at temperatures above  $575^\circ\text{C}$  was also fit with mass release kinetic models.

Kerogen was pyrolyzed in a novel kerogen retort at 10 K/min. Char, tar, and gas samples from this retort were analyzed by several methods, including  $^{13}\text{C}$  NMR, GC/MS, and FTIR. The tar was defined as the products that condensed after cooling to room temperature and corresponds to the oil produced. The tar was approximately 20% aromatic with long chain alkane structures prevalent. The aromaticity of the char increased to approximately 80% with large decreases in the side chain molecular weight.

The CPD model was used to model the pyrolysis rates of tar and light gas. New rate coefficients were generated for the CPD model to match the pyrolysis data from the kerogen retort, and it was necessary to model a light gas and a heavy gas. The heavy gas became part of the tar because of its high molecular weight.

A balance was performed on the aromatic carbon in the char, presuming that no new aromatic carbon was formed during pyrolysis. This aromaticity balance did not match the change in aromaticity in the char, meaning that there are mechanisms present that form substantial amounts of aromatic carbon in the late stages of pyrolysis.

## RECOMMENDATIONS

---

The rate coefficients regressed from the TGA data should be used for simulations of the pyrolysis of Utah Green River oil shale at pressures ranging from 1 to 40 atm and heating rates from 1 to 10 K/min. However, use of these coefficients at heating rates lower than 1 K/min is not recommended at this time. Additional research is needed to confidently determine pyrolysis rates at very slow heating rates. When heating rates of 1 K/day are desired, a piecewise approach with periods of constant temperature reaction might provide more reliable experimental measurements for modeling.

The CPD model calculations are based on the chemical structure of the kerogen. It would be interesting to see if this approach could be used to model the gas and tar release from kerogens from other oil shale deposits around the world.

The mechanism for char formation from the kerogen (i.e., coking) should be explored further based on the chemical structure information determined in this study.

## PUBLICATIONS AND PRESENTATIONS

---

### Publications based on this work

- Fletcher, T. H., R. Gillis, J. Adams, T. Hall, C. L. Mayne, M. S. Solum, and R. J. Pugmire, "Characterization of Macromolecular Structure Elements from a Green River Oil Shale, II. Characterization of Pyrolysis Products by  $^{13}\text{C}$  NMR, GC/MS, and FTIR," *Energy & Fuels*, **28**, 2959–2970 (2014). [dx.doi.org/10.1021/ef500095j](https://doi.org/10.1021/ef500095j)
- Solum, M. S., C. L. Mayne, A. M. Orendt, R. J. Pugmire, J. Adams, T. H. Fletcher, "Characterization of Macromolecular Structure Elements from a Green River Oil Shale, I. Extracts," *Energy and Fuels*, **28**, 453-465 (2014). [dx.doi.org/10.1021/ef401918u](https://doi.org/10.1021/ef401918u)

### Presentations based on this work

- Fletcher, T. H., A. M. Orendt, J. C. Facelli, M. S. Solum, C. L. Mayne, and M. Deo, "Oil Shale Pyrolysis Kinetics and Product Characterization," Unconventional Fuels Conference, University of Utah, Salt Lake City, UT (May 15, 2012).
- T. H. Fletcher, "Oil Shale 1: Chemical Structure and Pyrolysis," short course presentation to Statoil, Trondheim, Norway (October 8, 2012).
- Pugmire, R. J., T. H. Fletcher, J. Hillier, M. Solum, C. Mayne, and A. Orendt, "Detailed Characterization and Pyrolysis of Shale, Kerogen, Kerogen Chars, Bitumen, and Light Gases from a Green River Oil Shale Core," presented at the 33<sup>rd</sup> Oil Shale Symposium, Golden, CO (Oct 14-16, 2013).
- Fletcher, T. H., R. Gillis, J. Adams, T. Hall, C. L. Mayne, M. S. Solum, and R. J. Pugmire, "Characterization of Pyrolysis Products from a Utah Green River Oil Shale by  $^{13}\text{C}$  NMR, GC/MS, and FTIR," presented at the 33<sup>rd</sup> Oil Shale Symposium, Golden, CO (Oct 14-16, 2013).
- Fletcher, T. H., D. C. Barfuss, and R. J. Pugmire, "Modeling Oil Shale Pyrolysis using the Chemical Percolation Devolatilization Model," presented at the 34<sup>th</sup> Oil Shale Symposium, Golden, CO (October 13-15, 2014).

## **National Energy Technology Laboratory**

626 Cochrans Mill Road  
P.O. Box 10940  
Pittsburgh, PA 15236-0940

3610 Collins Ferry Road  
P.O. Box 880  
Morgantown, WV 26507-0880

13131 Dairy Ashford, Suite 225  
Sugarland, TX 77478

1450 Queen Avenue SW  
Albany, OR 97321-2198

2175 University Ave. South  
Suite 201  
Fairbanks, AK 99709

Visit the NETL website at:  
[www.netl.doe.gov](http://www.netl.doe.gov)

Customer Service:  
1-800-553-7681

